Reaching Grid Parity Using BP Solar Crystalline Silicon Technology
A Systems Class Application

DOE Award Number:
DE -FC36-07GO17049.006

Recipient:
Leon Fabick

Project Title:
Reaching Grid Parity Using BP Solar Crystalline Silicon Technology:
A Systems Class Application

Project Manager:
Daniel W. Cunningham

BP Solar team members
Anderson, W; Amin, D; Carlson, D E; Clark, R F; Creager, J; Cunningham, D W; Daniels, E; Garvison, P L; Gleaton, M; Griffin, L; Hering, M; Kelly, G; Kobayashi, M; Koval, T D; Lewis, M; Bennett, M; Meyer, J; Miller, J; Placer, N; Posbic, J P; Poulin, W C; Roncin, S P; Shaner, J; Stoddard, N; Warfield, D B; Wohlgemuth, J; Wu, B; Zahler, J; Zuretti, H A.

Consortium members
AGC Flat Glass NA, Arizona State University, BASF NA Corp, Ceradyne, Dow Corning Corp, Fat Spaniel Technologies, Florida Solar Energy Center, Georgia Institute of Technology, Komax Systems York, Recticel NA Inc., Sacramento Municipal Urban District, Specialized Technology Resources Inc., Zantrex.

Executive Summary
The primary target market for this program was the residential and commercial PV markets, drawing on BP Solar's premium product and service offerings, brand and marketing strength, and unique routes to market. These two markets were chosen because:

- in 2005 they represented more than 50% of the overall US PV market;
- they are the two markets that will likely meet grid parity first; and
- they are the two market segments in which product development can lead to the added value necessary to generate market growth before reaching grid parity.

Federal investment in this program resulted in substantial progress toward the DOE TPP target, providing significant advancements in the following areas:

- Lower component costs particularly the modules and inverters.
- Increased availability and lower cost of silicon feedstock.
- Product specifically developed for residential and commercial applications.
- Reducing the cost of installation through optimization of the products.
- Increased value of electricity in mid-term to drive volume increases, via the green grid technology.

- Large scale manufacture of PV products in the US, generating increased US employment in manufacturing and installation.

To achieve these goals BP Solar assembled a team that included suppliers of critical materials, automated equipment developers/manufacturers, inverter and other BOS manufacturers, a utility company, and University research groups. The program addressed all aspects of the crystalline silicon PV business from raw materials (particularly silicon feedstock) through installation of the system on the customers' site. By involving the material and equipment vendors, we ensured that supplies of silicon feedstock and other PV specific materials like encapsulation materials (EVA and cover glass) will be available in the quantities required to meet the DOE goals of 5 to 10 GW of installed US PV by 2015 and at the prices necessary for PV systems to reach grid parity in 2015.
This final technical report highlights the accomplishments of the BP Solar technical team from 2006 to the end of the project in February 2010. All the main contributors and team members are recognized for this accomplishment and their endeavors are recorded in the twelve main tasks described here.

Dr Daniel W. Cunningham. Frederick Maryland, November 2010.

Table of Contents

Task 1: Silicon Feedstock Development
Task 2: Casting
Task 3: Wafering
Task 4: Cells and Contacts
Task 5: Modules
Task 6: Manufacturing
Task 7: Inverter System Development
Task 8: Monitoring and BOS
Task 9: Systems Engineering
Task 10: Systems Installation and Maintenance
Task 11: Deployment
Task12: Collaboration

Appendices
Appendix 1: Patent Applications
Appendix 2: Publications

Task 1: Silicon Feedstock Development

The goal of this task is to create silicon from an arc furnace operation that provides a suitable starting material for subsequent refining into solar grade silicon through non-gaseous intermediates, typically a directional solidification. Principal requirements for solar grade silicon place limits on dopant impurities such as boron (B) and phosphorus (P), as well as metals within the silicon. A significant portion of the development work for this task was completed by our subcontractor, Dow Corning Corporation.

Approach

Dow Corning's approach to solar grade silicon under this program is to couple the use of higher purity feedstock in the arc furnace with select downstream processing to remove any residual impurities. Calculations using the mass balance models predict that the desired levels of purity can be achieved with the right combination of feedstock and processing steps. This approach requires not only the identification of materials with the appropriate level of purity and reactivity but also processing them into a form that allows them to be used at manufacturing scale in furnaces designed around conventional materials. This development process for each raw material consists of the following sequence of steps:

(1) Identification of a commercial source of the raw material or a process which can be used to make a material of requisite purity
(2) Forming the raw material into a suitable form via a briquetting process
(3) Testing the smelting characteristics of the feedstock in the small arc furnace
(4) Large scale production of the briquettes
(5) Evaluation of the briquettes in a commercial arc furnace

Arc Furnace Background and Development

Silicon metal is prepared by the carbothermic reduction of silica in an arc furnace. In this process a mixture of a carbon, quartz and wood chips (in larger arc furnaces) is continuously fed into the top of the furnace while silicon is removed from a tap hole at the bottom of the furnace. Limestone is also added to prevent slag buildup inside the furnace and make continuous tapping possible.

The key step in the carbothermic reduction of quartz is the conversion of carbon to silicon carbide according to the following reaction:

$$SiO + 2C \rightarrow SiC + CO$$

During the carbothermic reduction process trace impurities in the raw materials concentrate to various degrees in the silicon. In general most of the phosphorous and approximately 30-50% of the boron in the tapped silicon comes from the carbon source. The remainder of the boron, phosphorous and other impurities (trace metals, aluminum and calcium) comes from either the quartz or processing aids like limestone.

Mass balance curves have been developed for impurities introduced by the raw materials. In general only 10-20 % of the original phosphorous and 40-60 % of the boron content in the feedstocks are retained in the tapped silicon. The remainder of the boron and phosphorous are lost through the vent stacks. As a result, the impurity level of boron and

phosphorous in the tapped silicon can be predicted based on the level of boron and phosphorous in each feedstock, the retention factor of boron and phosphorous for each feedstock and the quantity of each feedstock used in the furnace.

An empirical model was developed which allows us to predict boron and phosphorous concentrations in the silicon directly tapped from the arc furnace based on the mass and purity of each feedstock, and the retention factor of boron and phosphorous in the furnace for each starting material. Assuming that no external contamination occurs, the model predicts that we should be able to make a material with less than 1.0 ppmw of boron and phosphorous if the boron concentration in the starting materials are less than 0.3 ppmw and the phosphorous concentration is less than 5 ppmw in the carbon source and less than 0.5 ppmw in the silica source.

Materials

Synthetic Carbon and Silica sources: Initial tests completed by Dow Corning had successfully produced high purity silicon using 100% briquettes at a small pilot scale. The boron (B) and phosphorous (P) levels were higher than expected in the silicon and traced to a root cause of higher B and P in the silica briquette binder. Based on raw material to product ratios and determined retention factors, we have defined the need to have Si source (natural or briquette) with 0.2ppmw B and 1.5ppmw P.

In a typical arc furnace, the reductant (carbon) sources include use of coal/charcoal, wood chips, and erosion of the graphite arc electrodes, contributing carbon to the reaction in the approximate ratio of 70:20:10 weight percent, respectively. Evidence collected suggests reductant (carbon) source should focus on removal of alkali metals from the forming binders of these synthetic carbon sources.

A synthetic silica formulation with specific briquette geometry was developed with reasonable properties for briquette formation and finished briquette strength, critical to proper application within the arc furnace. This formulation was modified from initial silica briquette formulations and from carbon briquette formulation in order to provide lowered B and P while retaining mechanical properties.

The Dow Corning chosen carbon sources for the briquetting work have very low levels of boron and according to our models do not significantly contribute boron to the tapped silicon. As a result, most of our efforts have focused on the purification of quartz. In addition to the quartz beneficiation studies, we have also evaluated a project on the digestion and re-precipitation of various silica sources with a reasonable degree of success, as shown in Figure 1.1.

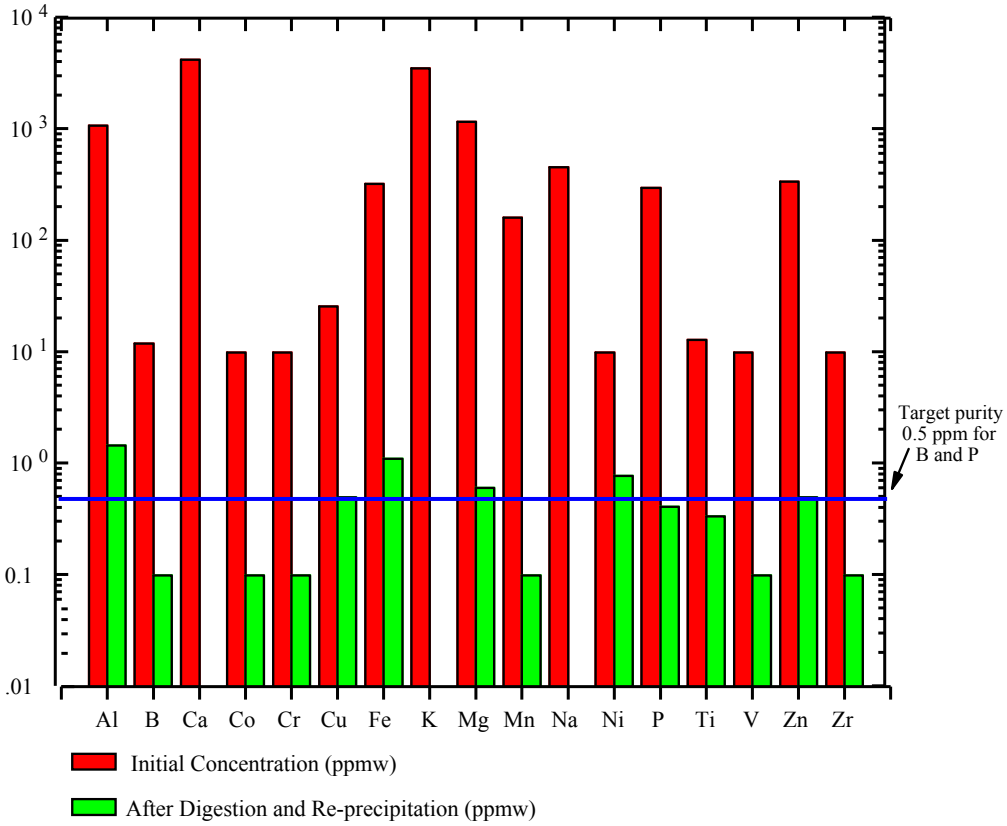

Figure 1.1: Impurity content before and after processing

Analytical Methods: Development of analytical methods that allows fast turnaround and analysis of low levels of impurities are important for commercial scale production of these materials. An initial investigation of Laser Assisted Microwave Plasma Spectroscopy (LAMPS) and Laser Ablation ICP-MS as potential techniques for rapid analysis of raw materials was performed. It appears that LAMPS technology is still in the early stages of development so emphasis shifted to further evaluate Laser Ablation ICP-MS. Preliminary studies with Laser Ablation ICPMS are encouraging. The technique proved capable of detecting B and P concentrations in quartz above 0.5 ppmw.

Limestone Sources: In commercial arc furnaces, limestone is used as an additive to stabilize the tap hole and minimize the build-up of slag inside the furnace during normal operation. Although this improves the stability of the arc furnace, metals and other impurities in the limestone are transferred to the tapped silicon. To eliminate this source of contamination, samples of calcium carbonate were obtained from various sources and analyzed for their boron, phosphorous and iron content. In general, the precipitated calcium carbonates were purer than the ground materials which in turn, were much purer than bulk limestone. Based on this survey we have identified several sources of high purity calcium carbonate which can be used in a briquetting process to replace bulk limestone and its inherent impurities.

Methods of making briquettes: A feasibility study on using vibratory compaction molding to make shaped carbon and/or silica briquettes was completed. Vibratory compaction molding is often used in place of extrusion to make concrete block and other decorative moldings. In vibratory compaction molding the mold is vibrated at a high frequency before and/or during the compaction process. As a result, it is possible to make high green strength moldings at low water content.
Using a Dow Corning local sub-contractor set up to make 8" concrete blocks, we were able to manually process a lower water version of our carbon briquette formulation through their equipment and molds. We were also able to process an "all-in-one" formulation containing both carbon and quartz. Although the molded blocks were too large to be tested in an arc furnace, the trial was sufficiently promising that we have scheduled a follow-up trial, using a custom die that will make briquettes more suitable for use in an arc furnace.

Trial with shaped briquettes: 130 MT of extruded carbon briquettes were produced to support the first trial with shaped briquettes. However, the first trial had to be postponed until changes could be made to the furnace's feed handling system. The first attempt to feed the shaped briquettes into the furnace using the same procedure that was used with pillow shaped briquettes was unsuccessful. During the test, approximately 90 % of the briquettes were broken. A root cause analysis is currently being performed to see if a feeding system can be developed that will allow us to use the briquettes.

Processes

Directional solidification: For further refining through directional solidification, Dow Corning has demonstrated the ability to control the solidification rate for a given crucible design and silicon mass. Ongoing solidification interface velocity studies suggest that the optimal velocity for high throughput with effective segregation will be between 0.5 and 1.2 mm per minute. By varying the operating conditions and configuration of the directional solidification furnace, Dow Corning has been able to vary the solidification rate between 0.25 mm/minute to over 2.95 mm/minute. However, at rates greater than approximately 1.2 mm/minute effective segregation of boron and phosphorous is compromised. At solidification rates below 0.7 mm/minute the segregation ratios for boron and phosphorous are near theoretical and can be used in an overall manufacturing scheme for controlling the final boron and phosphorous content. Figure 1.2 shows the solidification process for different growth rates.

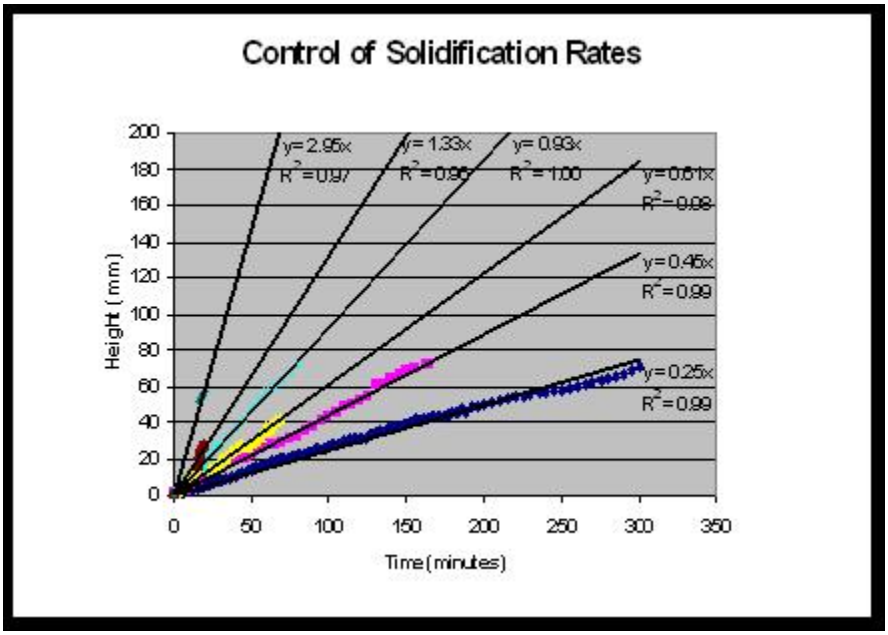

Figure 1.2: Control of Solidification Rate

The Unit Cost of crucibles for directional solidification is one key factor contributing to this route as a viable solution for purification. A test series on crucible materials of construction suggest that crucible liners of both quartz and graphite can be reused. Significant work was completed to evaluate many potential crucible lining materials in an effort to optimize the molten silicon release, minimize silicon contamination, and maximize the number of re-uses.

Use of slags for refining: Dow Corning has also evaluated the use of slags to remove boron and phosphorous. Through our contacts in the solar industry, Dow Corning have become aware of some small scale slagging studies which reduced boron and phosphorous levels to below 1 ppmw from starting levels of 5.5 and 14 ppmw, respectively. We are in the process of initiating a sub-contract to do trials to assess the viability of this technology in a manufacturing process. We have also been investigating the use of Alkaline-SiO_2 slags to remove boron. In one experiment the boron concentration was reduced by 35% after treating the silicon for one hour at 1540 °C with the slag. The concentration of other metals such as Ca, Al, Fe and Ti were also reduced.

Commercial smelting trials: A smelting trial with carbon briquettes has been completed in a commercial arc furnace. In normal operation, a combination of charcoal and wood chips is used as the carbon sources. During the trial, part of the charcoal was replaced with carbon briquettes. At replacement levels up to 80%, the furnace could be operated although there were some issues around the tap hole. Attempts to run the furnace at higher replacement levels (100%) were unsuccessful even for short periods of time. On the other hand, at a replacement level of 50% the furnace operated close to normal. Boron levels in the tapped silicon dropped from an average of 3.3 ppmw with standard raw materials to 2.3 ppmw when 80% of the charcoal was replaced with carbon

briquettes. The drop was consistent with the predictions from mass balance models. See Figure 1.3.

During the same trial, the concentration of phosphorous in the tapped silicon was also followed. However, no correlation was seen between the percent of carbon briquettes in the feed and the phosphorous concentration in the tap. A drop in the phosphorous concentration was observed when the feedstock was initially switched to 50% carbon briquettes but the concentration slowly increased until the phosphorous level was similar to the levels seen using only charcoal. At this point, the phosphorous content leveled off and was more or less independent of the carbon briquette composition in the feedstock. We believe the phosphorous results can be explained by changes in the bed porosity (density). Since the briquettes are much smaller (1-2 inches) and uniform in shape compared to the other materials (~ 4 inches), the furnace charge packs more tightly and the gas flow through the bed is altered. During the trial, the bulk density of the feedstock changed from 450 kg/m^3 (baseline) to 735 kg/m^3 as the charge changed from 100% charcoal to 100% briquettes.

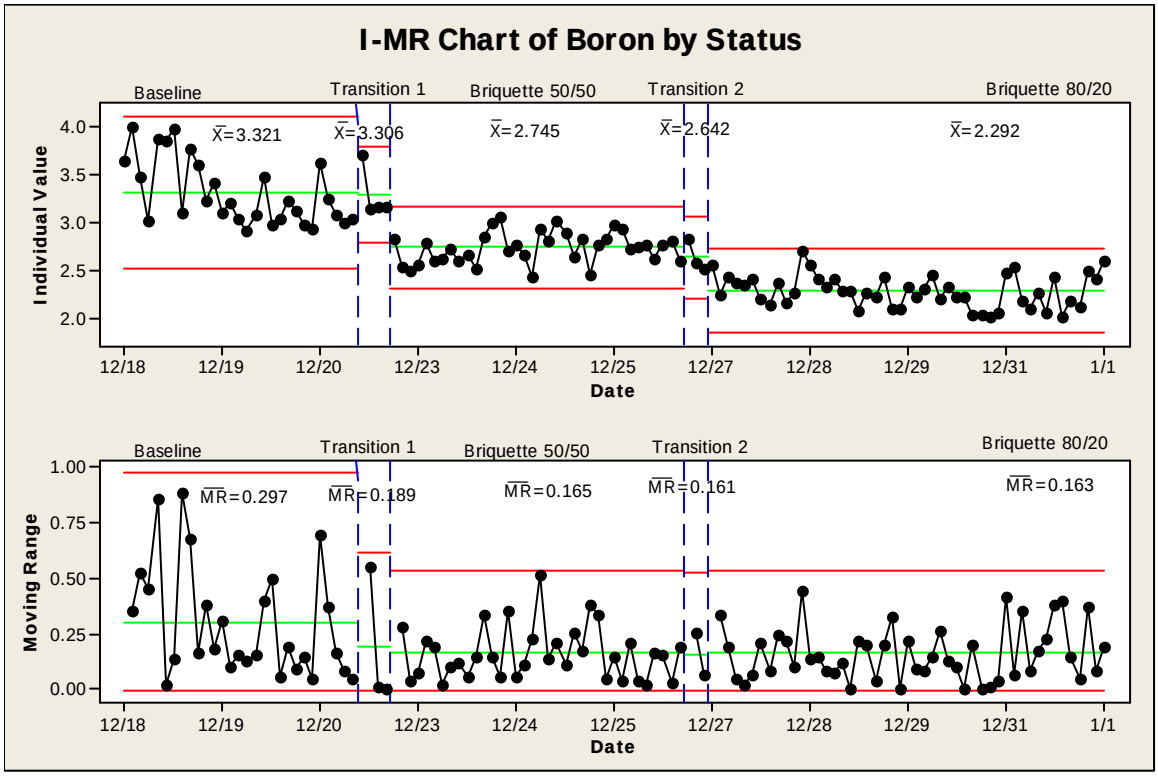

Figure 1.3: Boron Level during arc furnace run

Dow Corning completed a twelve day smelting trial with uncured carbon briquettes. Prior to running the uncured briquettes, the furnace was burned out and run for three days with cured briquettes at a charcoal replacement level of 54 %. The cured briquettes were then replaced with an equivalent weight of uncured briquettes and the furnace run for an additional nine days. During the course of the trial 160 MT of uncured carbon briquettes were consumed. Overall the run was very successful. Power consumption was slightly lower and the tonnage of tapped silicon was slightly higher with the uncured briquettes.

On the other hand, the electrode consumption was slightly higher as were the boron and phosphorous levels in the tapped silicon. (See Figures 1.4 and 5) We believe most of these variations were due to the higher level of fines (broken briquettes) in the uncured briquette charges.

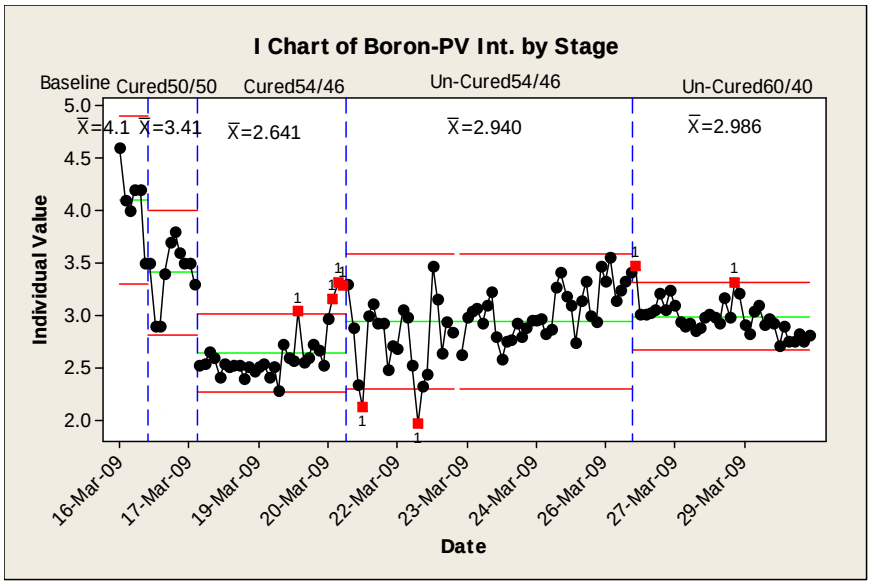

Figure 1.4: Boron concentration during the smelting trial

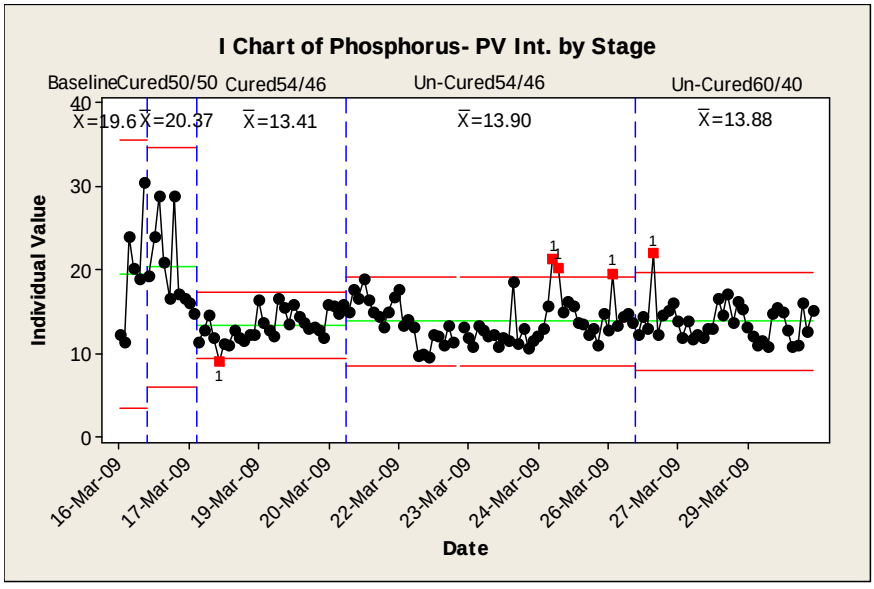

Figure 1.5: Phosphorous concentration during the smelting trial

Testing of Materials at BP Solar

Though BP Solar conducted some initial testing of Dow Corning solar grade materials, none were deemed suitable to process to solar cells in the contract period. In light of this, BP Solar procured solar grade silicon from two other sources to mitigate the schedule delays from Dow Corning. In casting trials, two main results have been achieved:

First, a three-dopant system has been devised that has been proven to widen the process window for solar grade silicon. The results of this development are shown in Figure 1.6. Without the process change, we would expect the casting yield to be limited due to a switch to n-type material. The new doping method eliminated most of this yield loss.

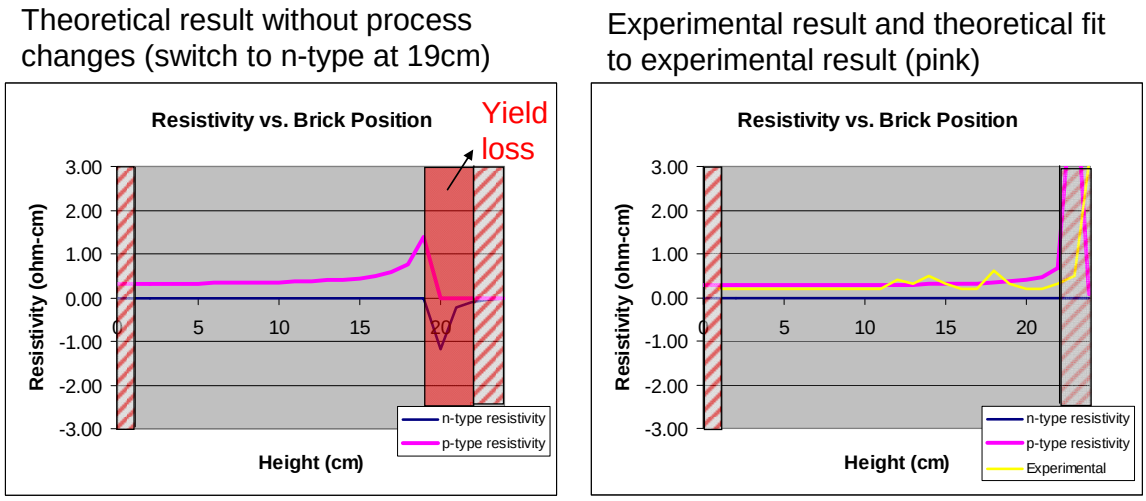

Figure 1.6: Theoretical and experimental results using low resistivity SOG feedstock

Second, solar grade silicon was mixed at 50% and cast to a 0.6 ohm-cm target. The target was met with <1% yield loss due to a switch from n-type to p-type at the ingot corners (see Figure 1.7).

Figure 1.7: Side plates (left) and corner bricks (right) showing p/n transition at the very top of the ingot

Ingots made using 43% SGS mixed with intrinsic polysilicon were cast and processed into cells. The cell efficiency was somewhat lower than average (see Figure 1.8).

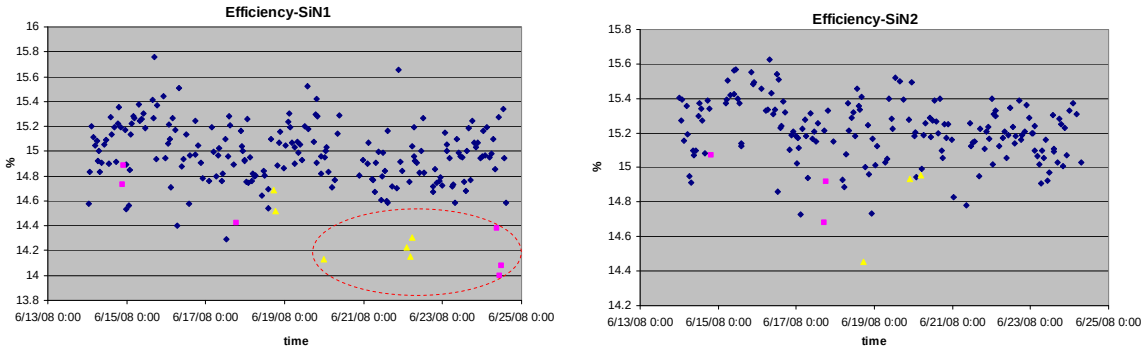

Figure 1.8: Cell efficiency on normal production (blue) and for lots coming from solar grade silicon ingots (pink and yellow), normal cell process (left), varied cell process (right)

Results approached 15% but did not quite achieve it. Analysis of cells indicate higher recombination than normal at structural defects (grain boundaries and dislocation) which resulted in lower current and fill factor than usual. Efforts to measure dissolved metals by DLTS have turned up no traces in finished cells, indicating that any metal concentration is in precipitated form.

As part of metals analysis and contaminant reduction when working with solar grade silicon materials, testing of alternative no-fire release coatings resulted in some improvement of typical crucible induced "red-zone" low lifetime regions on the border of the ingot as shown in Figure 1.9.

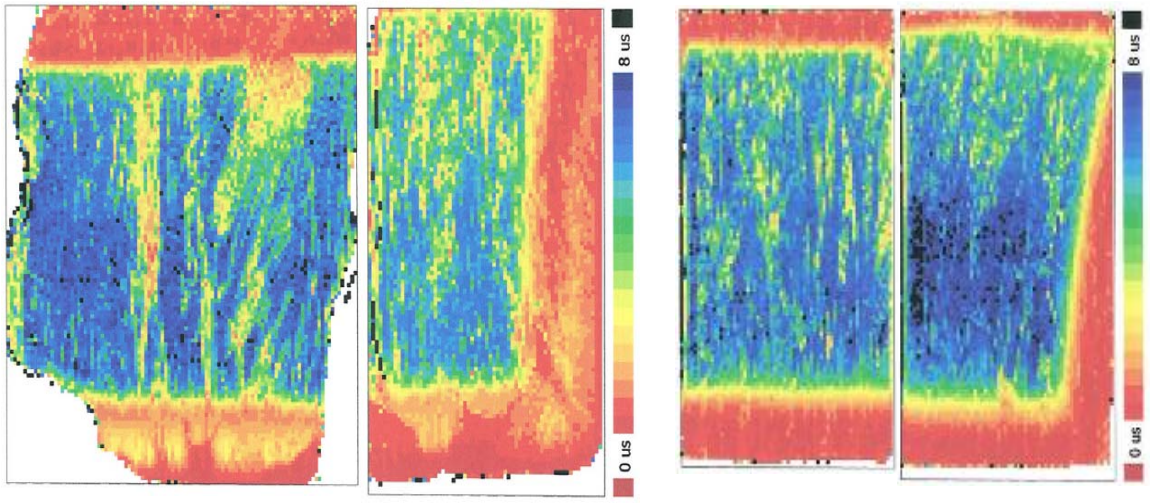

Figure 1.9: Brick lifetime maps: An ingot with lowered contamination (left) and average contamination (right). The lifetime increase indicates a halving of the iron concentration, just by eliminating crucible process-induced contamination.

An additional ingot with 50% solar grade silicon has been cast using the Mono^{2} ^{TM} casting technique. The wafers from this ingot were processed using our latest advances in screen print to meet the second year stage gate deliverable of 16% cell efficiency on a 50% SGS wafer. Initial concentrations of impurities in the SGS feedstock were measured

to be: 2.1 ppmw phosphorus, 0.4 ppmw boron. Additional dopant was added for precise control of the resistivity profile.

Part way through the second contact year, the subcontract with Dow Corning for solar grade silicon was terminated by mutual agreement. We elected not to issue another subcontract for solar grade silicon at this time, but instead to use commercially available materials from other suppliers that meet the requirements set forth in our goals.

The first ingot cast utilizing one supplier's solar grade silicon had lower lifetime at the brick level than expected and was not processed further.

A second ingot was cast with a second supplier's material, having starting dopant concentrations of 0.3 ppmw B, 0.7 ppmw P. The target resistivity at 50% mixing was 1.1 ohm-cm, with a p-type yield of > 90%. In addition, multi crystalline ingots have been cast using 100% of this solar grade material. The resistivity was in-spec through the usable height of the ingot, as shown in Figure 1.10.

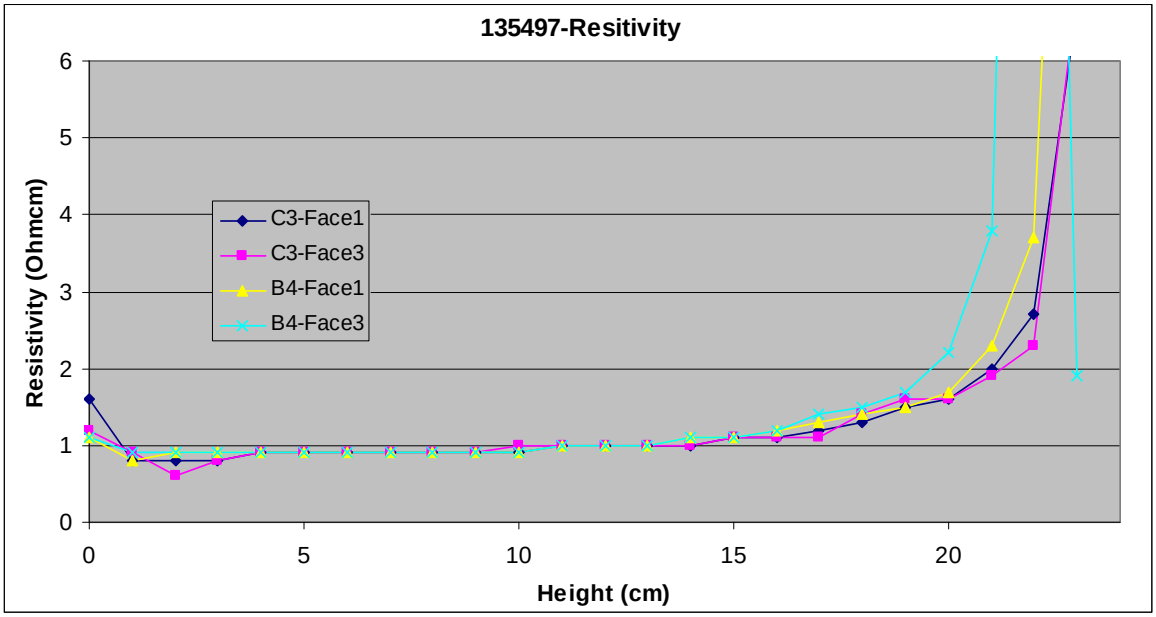

Figure 1.10: Resistivity of the ingot as a function of vertical position

The yield of good silicon from the ingot was lower than usual, with a 5% increase in inclusion-reject material, evaluated to be due to a higher level of carbon and nitrogen in the solar grade feedstock versus standard silicon. The cutting yield at wire saw was within normal ranges for seven of eight cuts. The other cut had lower yield, without a clear attributable cause. In the cell line, mechanical yield for 17 of 18 lots was in normal ranges, with one lot below average. In cell efficiency, there was a high level of rejects from shunts, averaging 6.7%, compared with normal values around 1%, which we attribute again to the presence of a higher level of carbon and nitrogen that formed many micron-scale inclusions within the solar cell device junction region. The remainder of the cells had good distributions, as shown in Table 1.1.

	Efficiency	Isc	Voc	Fill Factor
Normal Production	1	1	1	1
Trial lots	0.9718	0.9839	0.9906	0.9804
Trial lots after shunts removed	1.0026	0.9899	1.0053	1.0089

Table 1.1: Cell performance of solar grade silicon multi lots normalized relative to production averages

Task 2: Casting

The goal of this task is to develop, optimize and commercialize the Mono^{2}™ process, with focus on casting furnace improvements, next generation furnace designs, production improvement of enabling materials (crucibles and coatings) through our subcontractor Ceradyne, and defect analysis through our subcontractor North Carolina State University.

Background

The Mono^{2} ™ process is a patent pending method and set of tools to produce near CZ-quality mono crystalline silicon utilizing traditional directional solidification process equipment with some modifications. Mono^{2} ™ has the multi crystalline casting benefits of:

- high throughput
- lowered oxygen content and subsequent lowered light-induced degradation (LID) at the module level
- improved packing fraction in the module for improved power (no pseudo square loss of active area as with CZ)

Approach

Delivering Mono^{2} ™ as a new commercial product has required innovation and development not only in casting, but cell production, module processing, systems and marketing at BP Solar. Because it has had such a wide-ranging impact, the delivery was scheduled in a phased approach. The first commercial demonstration of the process was conducted in late 2007 with a total of 210 kW of modules produced and delivered to a customer. The array was instrumented to report on energy collection from the Mono^{2}™ array in comparison to a multi crystalline array installed adjacent. During the demonstration the following performance parameters were achieved:

- Cell efficiency of 15.7% versus a goal of 16%, although the demonstration cells were not texture etched.
- Module maximum STC output power of 178 W versus a production goal of 180 W.
- The module yield matched the production goal.
- The cell yield was 4% lower than the production goal indicating the need to improve in line wafer and cell handling.

Second year production of 1.2MW of Mono$^{2\ TM}$ product was installed as a single standalone array at Colorado State University at Pueblo in November 2008, see Figure 2.1. All production of these cells and modules were completed at Frederick, MD, but resulted in suboptimal efficiency that will be discussed later in this section.

Figure 2.1: Installation as of 12 November 2008 at CSU-Pueblo

Third year production in October of 2009 produced 1.5MW of Mono$^{2\ TM}$ ingots and wafers in Frederick, MD, that was converted to cells and modules by some of our manufacturing partners with more advanced cell production capabilities. As of writing, cell production was complete with Mono$^{2\ TM}$ achieving median cell efficiency of 16.7%, with modules destined to end up in a European project before close of 2010.

Process

BP Solar has developed a new measurement system for production of Mono$^{2\ TM}$ that has been integrated with the casting stations, both in hardware and most recently in software. The system is now fully operational and capable of operating without human intervention. At least eight ingots have been cast in 'hands-free' mode to produce a Mono$^{2\ TM}$ or seeded multi ingot. Numerous improvements have been made with timing elements and settings of the program, and the interface designed and documented for full for production operation.

As part of scale-up and process development, a cleaning and handling system to enable the Mono$^{2\ TM}$ casting operations was designed and installed into the raw materials processing portion of the casting facility. This allows for efficient processing and loading of both Gen4 (265kg) and Gen5 (400kg) ingots.

In mid-2008, we converted ten casting stations to Mono$^{2\ TM}$ operation. In order to be qualified on the new process, each station produced three Mono$^{2\ TM}$ ingots successfully without intervention. Nine of the ten stations were qualified immediately, with some

hardware delays before the 10th was certified. The qualification process transitioned to a pre-production trial run whose aim was the production of 1.2MW of Mono$^{2\ TM}$ modules. Through pre-production piloting, BP Solar confirmed the capability to run a process that allows more than 12 ingots to be grown from a single original seed layer. This is important to keep operational costs down in the overall economic model.

Early 2009, extensive work was completed on the investigation into the poor performance of Mono$^{2\ TM}$ cells made in late 2008. After a series of casting experiments that rolled back various changes to the casting process from 2007 and analyzed wafer and cell properties, it was determined that the cast ingot quality was not the driving factor for the low performance. Instead, a change in the cutting slurry and wafer cleaning operations at the beginning of 2008 was identified as the most likely culprit for the low performance. The performance effect was seen as low fill factors, with the structural defect appearing to be small areas of under-etched material from surface debris etch-masking (wire saw grit and kerf) that allowed higher than normal junction leakage currents. This was exacerbated by the (100) oriented crystal that allowed pyramids to form under these etch-mask initiators.

Subsequent to production trials, our development work has focused on how to further improve the quality and consistency of Mono$^{2\ TM}$ material. Analysis from our subcontract with NCSU showed there is not a significant build-up of metallic impurities in the seed material over the several casts of the recycling process, but that the crystalline quality of the seed material can degrade from an undercutting process that sometimes occurs. This information has been used to change the slab recycling process to maintain higher quality. We have also worked to decrease the prevalence of inclusions and the dislocation cascades that they create in the ingots. In one case, we cast two ingots using our low carbon technology to decrease inclusion-rich material. In another case, we analyzed our current growth profile and found the thermal gradient to exceed normal values. A new growth recipe was developed to maintain the current growth rate but decrease the gradient, as shown in Figure 2.2.

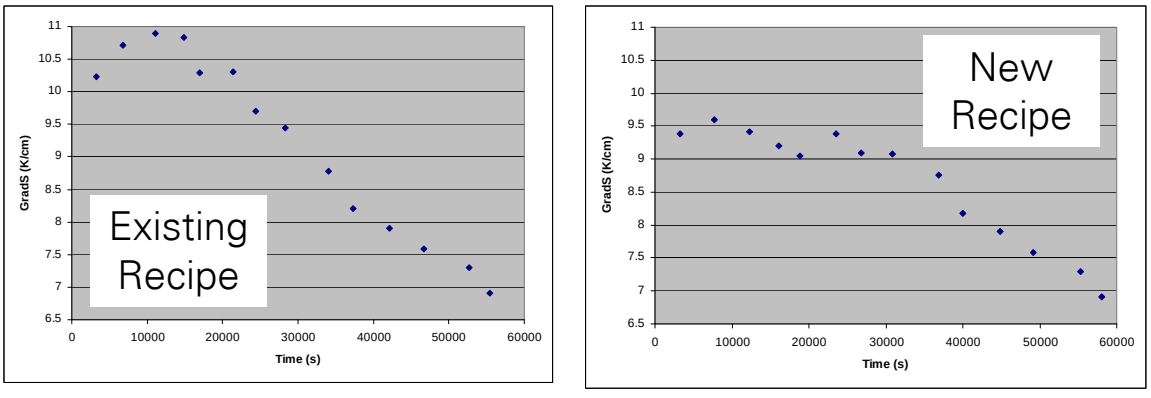

Figure 2.2: Thermal gradients as simulated in our 3D casting simulation package for the current Mono^2 recipe (left) and a newly developed one (right)

Production furnace work and Simulation

Significant work centered on development of capability at the 400kg (Gen5) ingot size, and a new casting station was purchased and installed as a comparison to the current underperforming Gen5 station. To better understand thermal and fluid flow issues inside the furnace, a 3D simulation model was set up. The preliminary results of temperature and velocity are shown in Figures 2.3 and 2.4 below. Since it is a symmetric system, only one quarter was calculated.

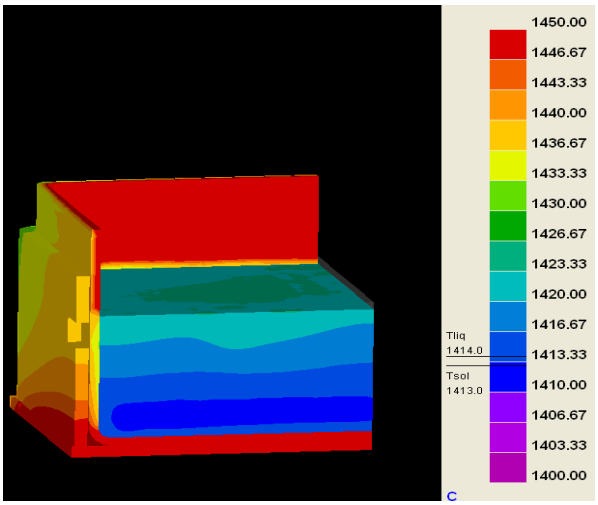

Figure 2.3: Temperature distribution in the furnace

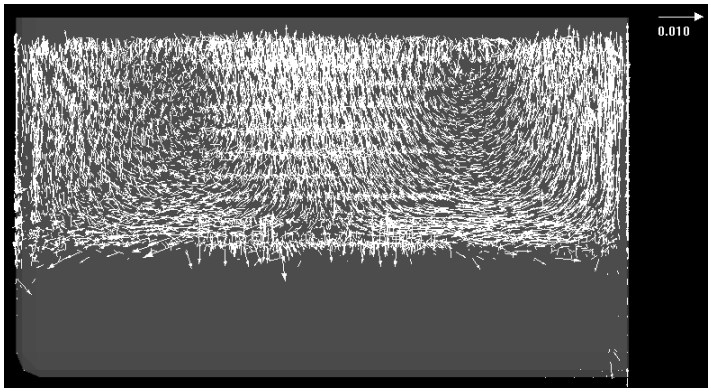

Figure 2.4: Velocity vector in the molten silicon

Through the development period, a total of 22 ingots have been cast in the Gen5 casting stations. One vendor's station has consistently performed poorly, mostly because of inclusion yield losses. The other vendor's station has performed better, but still yields below standard material due primarily to small crystal structure, identified in some cases as inclusions. To understand some of the crystallization issues, we studied the interaction of gas flow dynamics with the temperature profile of the furnace and its effect on crystallization. In Figure 2.5 the gas flow has been simulated with ten nozzles deploying high velocity argon into the furnace with a vacuum exhaust down below.

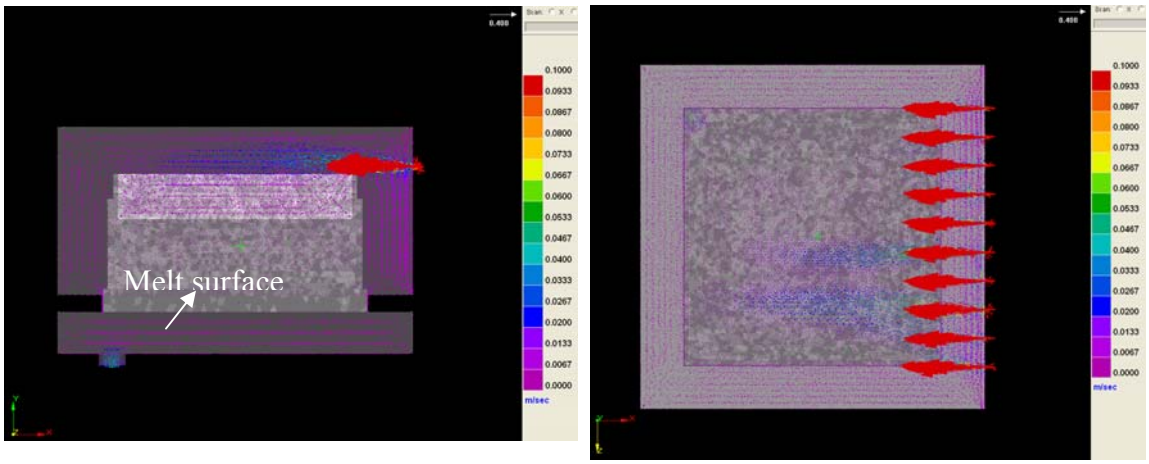

Figure 2.5: Simulation of Gas Flow

Although significant argon flow comes from the nozzles, the flow velocity drops dramatically outside of the jet area, and only modest flow velocities are found at the surface of the silicon melt. Lack of clean argon flow at the melt surface can significantly increase the carbon and nitrogen concentration in an ingot.
The thermal profile in an ingot just after solidification is shown in Figure 2.6 with a time series of the growth process used to simulate crystallization of the ingot using the CAFE methodology. The isotherms are generally flat, especially at the top, while near the bottom there is a slightly convex curvature.

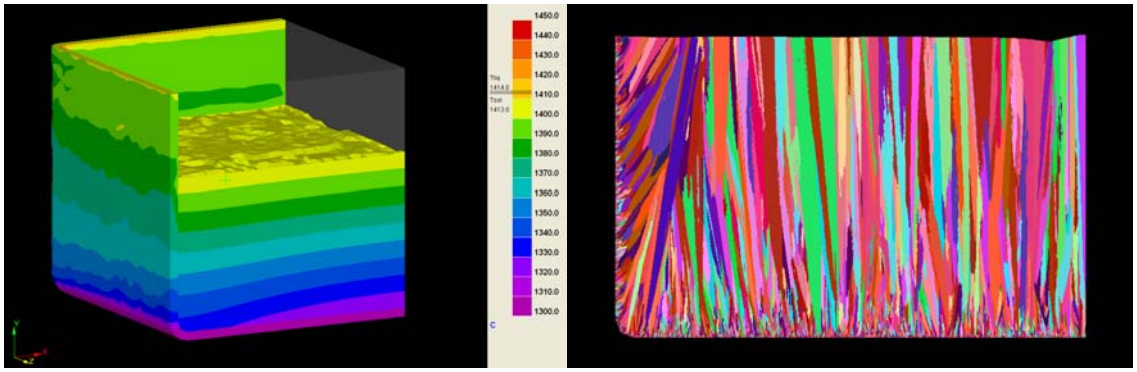

Figure 2.6: Simulation of Thermal Profile and Crystallization

Even though the simulation package assumes dendritic crystal growth, the results for the crystallization pattern are remarkably good. The nucleation conditions still require fine tuning to match the behavior in some parts of the ingot, but the combination of thermal modeling with crystallization has proved fruitful so far. Significant future work is planned to optimize the grain structure with application to Mono$^{2\,TM}$.

Next generation furnace design

To further improve casting and Mono^{2} ^{TM} economics, the capital expenditure requirements per unit produced and process intensity as measured by equipment vessels per unit produced were identified as major factors to true large scale commercialization of silicon based PV and Mono^{2} ^{TM} product. A comprehensive design package was commissioned by BP Solar to detail a new integrated design for and advanced casting system. Through the design process and BP safety reviews, nearly 1000 man-hours have been devoted to ensure process safety in scale-up and intensification through PHA (Process Hazard Assessment) and FMEA (Failure Mode and Effects Analysis) tools. A HAZOP (Hazard and Operability Study) and LOPA (Layers of Protection Analysis) have not yet been completed pending the final tool layout.

Project risk assessment also identified twelve critical technical items and plans were developed to address each one, including:

- Ability to fabricate large ceramic parts (>1m^3 volume, >3m total length)
- Viability of melter transfer tray concept
- Need for pre-heat chamber in melter design
- Ability to fabricate large C-C (carbon-carbon) composite parts and validate structural strength
- Identification and qualification of material of construction for melter charging tray
- Prototype validation of graphite heat exchanger concept
- Prototype validation of graphite cartridge heat concept
- Determination of dissolution rate of silica exposed to liquid silicon at elevated temperature
- Durability of C-C composite materials under proposed use conditions
- Determination of extent of reaction between C-C composite material and silica under proposed use conditions
- Modeling and identification of expected thermal profiles within vessels

Progress in each of these areas has included:

- Work with subcontractor Ceradyne resulted in successful fabrication of parts meeting both size criteria
- Vendors capable of manufacturing large C-C parts were identified and mechanical test completed
- Testing and modeling indicates no need for pre-heat chamber prior to introduction of silicon to melt chamber
- Prototyping of melter charging apparatus validated transfer concept
- Graphite heat exchanger mock-up completed and pressure-flows validated with cold test
- Graphite cartridge heater testing completed with peak temperature, power output, and longevity test validated
- 895 hours silicon contained in silica test validates correlation of silica dissolution rate with temperature and that the measured rate should be compatible with ceramic part lifetime assumptions

- Thermal modeling of the system identified some critical issues that had to be addressed and redesigned, particularly around thermal uniformity and cold spots that could allow silicon to solidify in unintended areas

Large ceramics and improved release coatings

Testing of "hard coat" crucibles and have seen generally good release properties, with isolated sticking points. After additional feedback, Ceradyne continued working to perfect the Si_3N_4 hard coat system. Numerous parts were supplied to BP Solar to determine the minimal coating layer thickness required, verify Ceradyne kiln firing parameters, and qualify first and second sources of Si_3N_4 raw materials. Parts were supplied in both standard crucible sizes (Gen4, 720 x 720 x 420 mm) and in jumbo (Gen5, 877 x 877 x 420 mm) sizes. In casting nearly 30 ingots, lowered inclusions and higher minority carrier lifetime results were seen. It was discovered that one of the materials used in the "hard coat" formulation had potentially excessive levels of phosphorus that was modifying the resistivity of the ingot and producing the falsely increased minority carrier lifetimes. Alternative vendors were identified for this binder and qualified. An example of ingot cast using the Ceradyne release coating is shown in Figure 2.7.

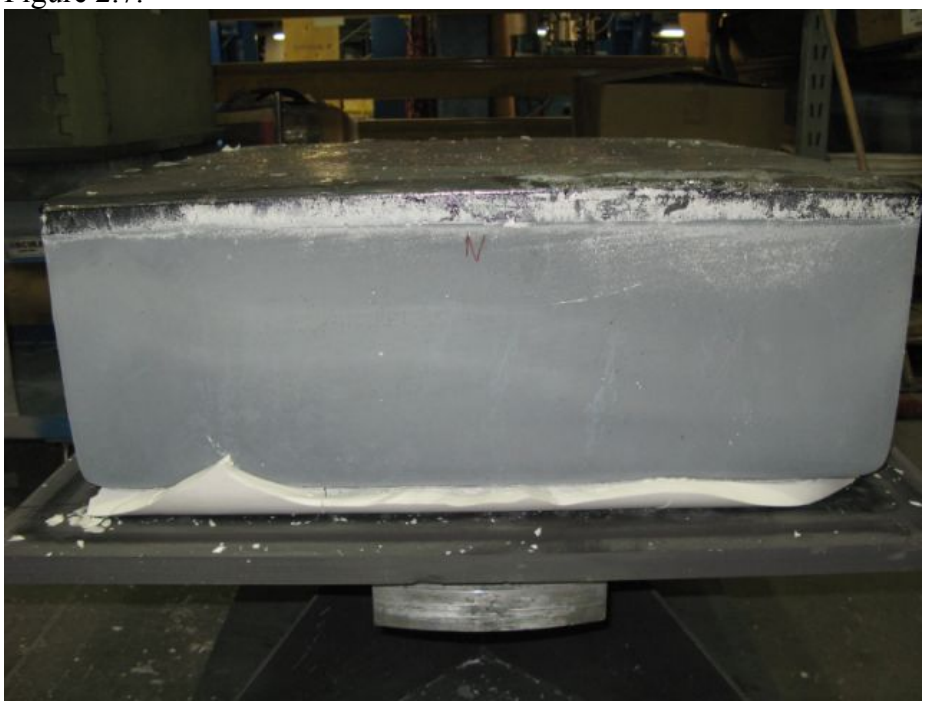

Figure 2.7: Ingot cast using Ceradyne "hard coat" system

In addition to coating developments with our subcontractor Ceradyne, over the course of the contract have developed our own automatic spraying process for applying a BP Solar developed coating. With the reduction of operator intensity and increased consistency of coating it is estimated to have a investment payback of under one year.

Ceradyne delivered both high purity crucibles and crucibles manufactured by a novel casting process not yet disclosed. Both sets of crucibles performed well in casting trials.

Defect Analysis - North Carolina State University

NCSU performed analysis on an edge cross-sectional slice of a Mono$^{2\ TM}$ ingot to evaluate microwave photoconductive decay minority carrier lifetime and to determine whether the lower performance areas were due to structural or chemical defects. At the base of the ingot, small localized low lifetime regions are caused by what appears to be a liquid under fill during the casting process with additional evidence of small gas pockets within the crystal. During initial growth phases, etch pits lining up on (100) planes are evidence that an interstitial-rich growth region is causing dislocation loops, most possibly due to slow initial growth rates or higher than equilibrium thermal gradients.
Deep-level transient spectroscopy (DLTS) of the base low lifetime regions confirmed results similar to other cast materials, that is the influence on lifetime and presence of iron, as Fe-B pairs, from the crucible. The distribution (shown in Figure 2.8) is influenced by at least one other characteristic of the silicon than distance from the crucible wall.

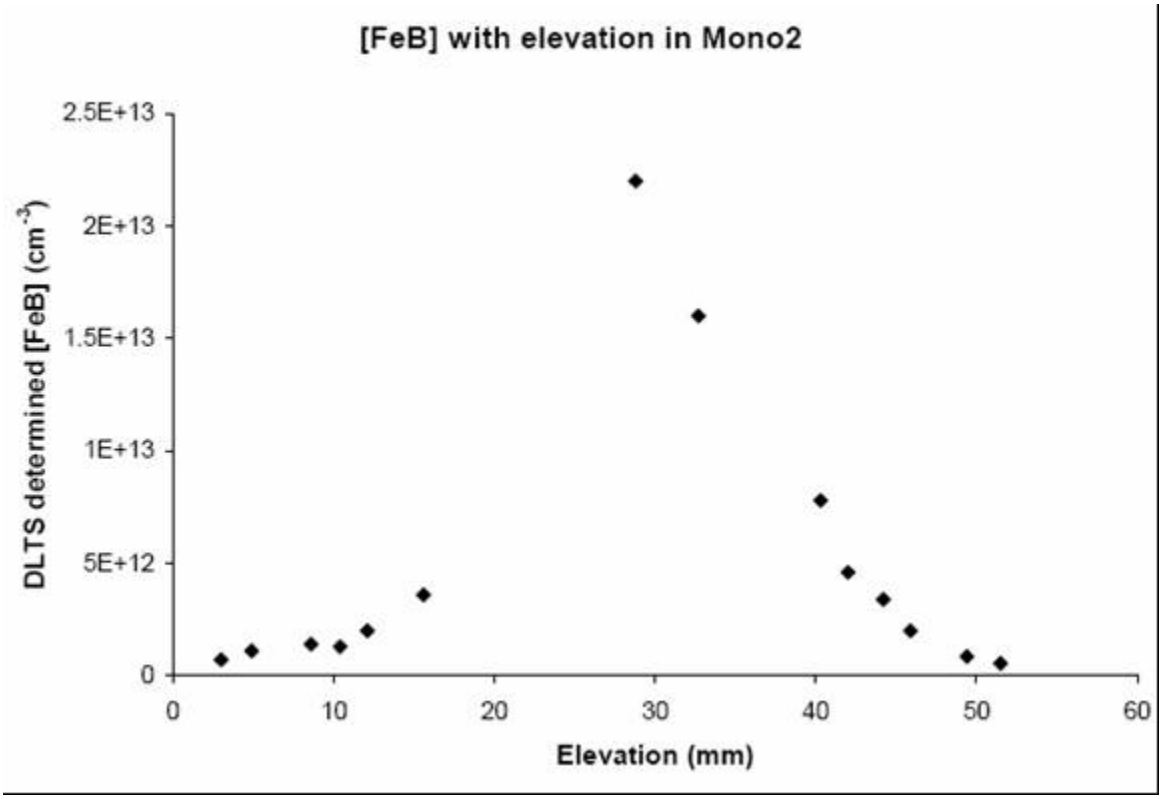

Figure 2.8: Concentration of FeB complex with elevation above the crucible base

Further defect study also showed that particle defects typical of mc-Si casting, silicon carbide and silicon nitride, are present in the material and most likely the cause of the majority of dislocation cascades. Dislocation branching can be seen to occur in several distinct forms, acute and abrupt are shown in Figure 2.9, which will require further study to determine their exact cause.

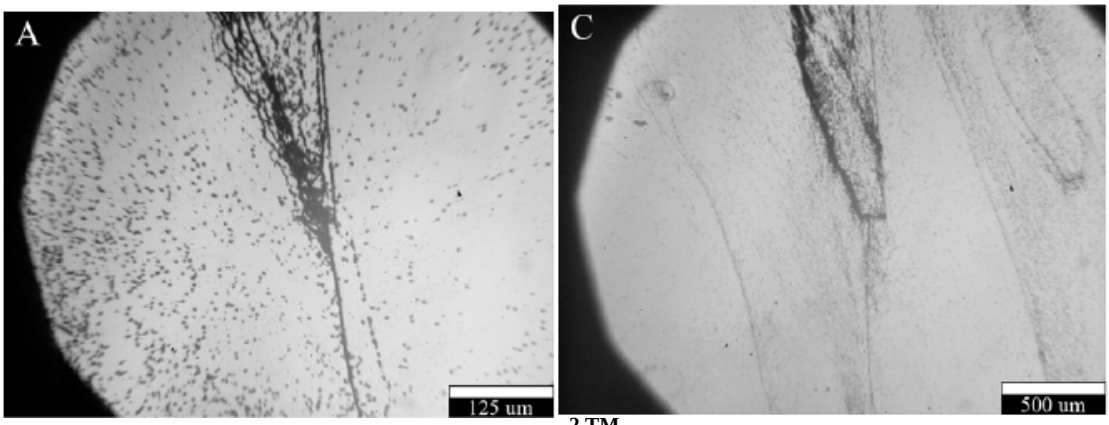

Figure 2.9: Dislocation Cascades in Mono$^{2\ TM}$ Silicon

By FTIR, it has been shown that Mono$^{2\ TM}$ ingots have a higher concentration of oxygen by up to a factor of two in the lower half of the ingot compared with ingots cast using multi-crystalline silicon (Figure 2.10). While higher, the absolute values are still low relative to typical CZ concentrations. Lateral profiles of carbon and oxygen have shown a slight increase in oxygen in the first 2 cm from the side wall of the crucible, while carbon profiles remain flat.

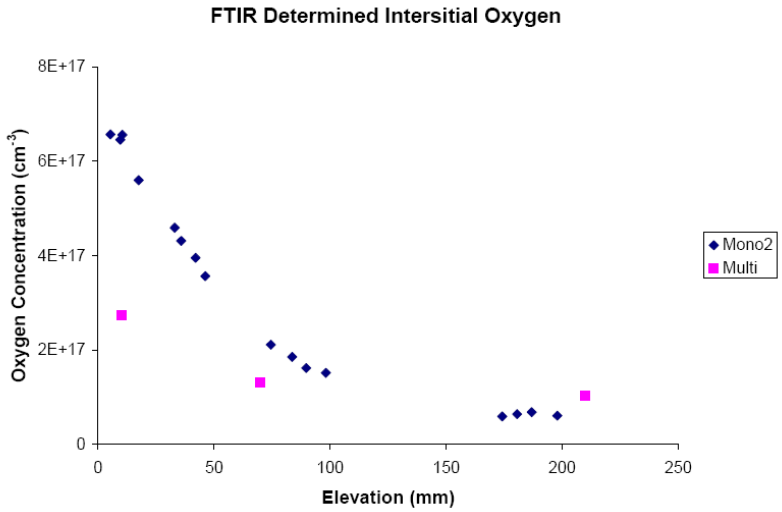

Figure 2.10: Oxygen profiles from the bottom to the top of bricks from Mono$^{2\ TM}$ and multi ingots. The elevated oxygen is believed to be due to a lack of settling time at lower temperatures

There is a low lifetime region that extends some 3-4 cm from the side wall, but this is not related to oxygen concentration. Instead, Deep Level Transient Spectroscopy has shown a good match between the iron-boron pair concentration and the lifetime (see Figure 2.11), indicating that metallic contamination is the root cause.

An analysis for sources for iron focused on the crucible firing furnaces, where Kanthal (Fe-Cr) type heaters are used to sinter the release coating at 1100 ºC for two hours. To test the contamination in the furnace, we took two high purity CZ wafers and set them in the furnace for a normal cycle. Afterwards, the wafers were tested by SIMS at NCSU for

metal contamination. The results are shown in Figure 2.12, with extremely high concentrations (up to 20 ppma) of metals found extending deep into the wafer. This contamination source is significant, and potential ways to address it are being considered.

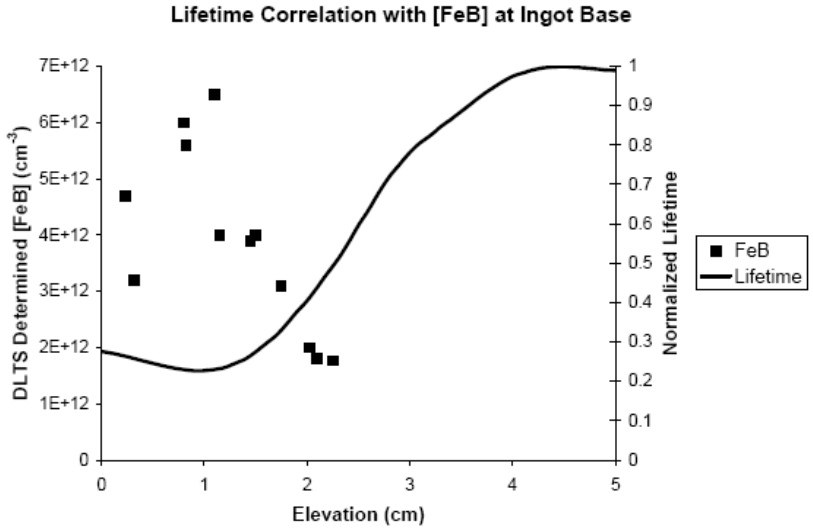

Figure 2.11: Scaled Minority carrier lifetime superposed with DLTS measurements of FeB pair concentration

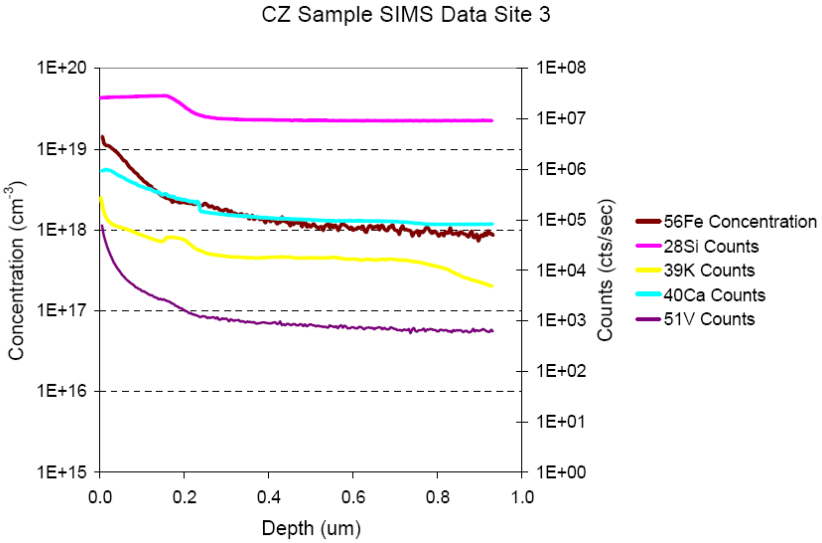

Figure 2.12: SIMS metal depth profiles in a contaminated CZ wafer. Only the iron is calibrated to be quantitative

Two samples were received from BP Solar that had been contaminated in the furnaces used for casting. One sample was a feedstock piece from an aborted casting that was partially melted in the process. A dark gray coating was present on the surface. EDS was only able to detect carbon in this coating. A second sample was a chunk from a multi crystalline brick that was exposed to the casting furnace environment. EDS previously

detected oxygen, carbon, and iron within this coating. Since the sensitivity of EDS is relatively low (~1 atomic %), SIMS was performed on both samples. Figure 2.13 is the quantitative iron SIMS analysis of the surface coating on the feedstock piece exposed to the casting furnace environment. The iron concentration varies with depth, being as high as 10^{19} cm^{-3} near the surface and dropping to 10^{18} cm^{-3} just beneath the surface. The mass spectroscopy data shown in Figure 2.14 indicates that other elements are present as well. The largest peaks have been labeled up to a mass of 100 a.m.u. since higher masses are likely due to combinations of elements. The primary contaminants detected are C, S, Na, Fe, and Cr. Most peaks stay approximately the same height to at least a depth of six microns with the exception of slight drops in the C, Na, and Cr peaks.

Shown in Figure 2.15 is the quantitative iron concentration profile taken from the surface of the multi crystalline chunk which was originally part of a brick exposed to the casting furnace environment. Iron was detected at concentrations reaching 10^{21} cm^{-3} in this coating which is about 2 atomic %. The same elements are present in this sample's coating as were in the feedstock piece's coating. There are slight drops visible in the C related peaks with increased depth.

The concentration of iron in these surface coatings is incredibly high ranging from 10^{19} to 10^{21} cm^{-3}. Iron has been identified in previous reports as the primary lifetime reducing impurity in BP Solar cast silicon, and the furnaces used during casting are significant sources of this contamination. The coating thickness on both samples has not been determined so it is difficult to say just how much total iron is present on the surface. It is at least 2 microns thick on both samples.

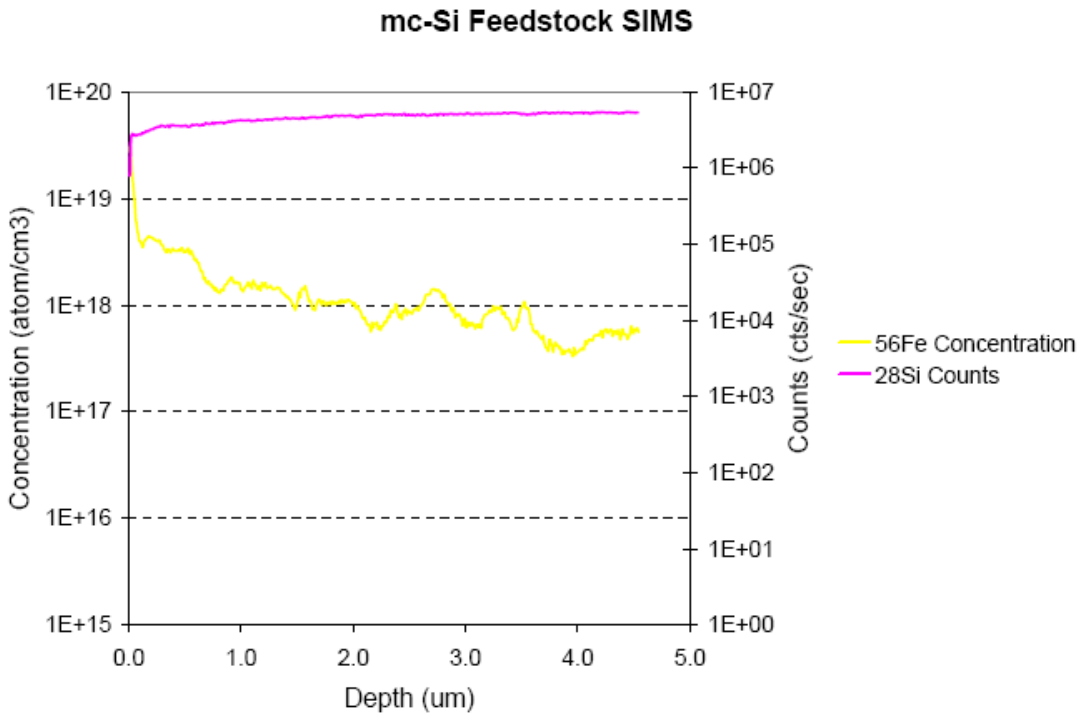

Figure 2.13: Quantitative Fe concentration data from SIMS on the surface of the partially melted feedstock piece.

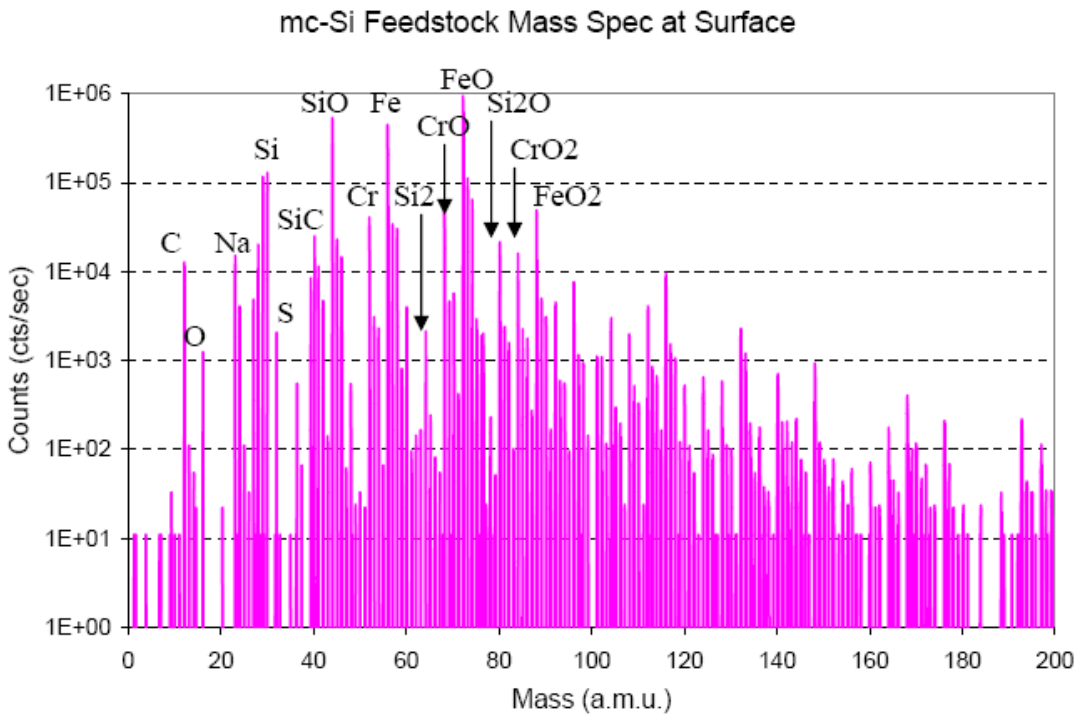

Figure 2.14: SIMS mass spectra from surface of feedstock piece

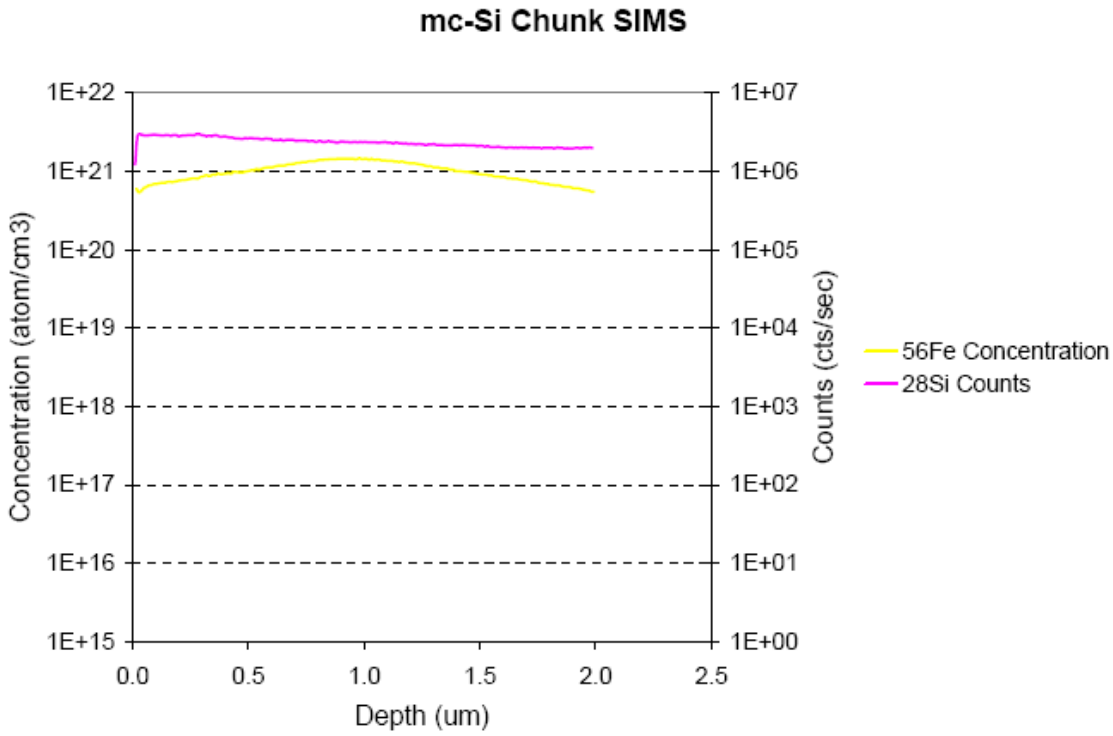

Figure 2.15: Iron concentration SIMS data in mc-Si chunk surface layer

Task 3: Wafering

The goal of this task are to develop a process for cutting 180 μm thick wafers using thinner (< 130 μm thick) wire and develop an integrated demounting and cleaning process.

Approach

After initial testing, it was determined the primary limiting factor for the use of thin wire is the wire wear and survivability after transit through the cutting area of the saw. Thinner diameter wire allows a greater number of cuts per centimeter of mounted block, creating additional wire passes, contact, and wear on the wire. Most double table and double mount saws contain too much silicon to cut at high feed rates with thin wire, with the additional complication that thinner wire can transmit any cutting defects to adjacent mounts increasing saw defects. Initial test cutting performance on current equipment is unacceptable at 160 μm wafer thickness. The saw manufacturer recommends lowering the temperature and density of the slurry, as well as lower table speed, which would impact production speed and costs. The cleaning performance of 160 μm thick wafers is also unacceptable on our present equipment, with a significantly higher breakage rate. Therefore, we opted to purchase and install a new generation single table saw designed for cutting thin wafers using thin wire, Meyer Burger DS264, and examine alternate cleaning tools.

Also, slurry and its cutting performance to reduce wire wear was examined through testing of a water based slurry (as opposed to polyethylene glycol, PEG, based slurries), where heat removal, viscosity, and lubricity can be tailored independently of one another.

Cutting with 120 μm thick wire

An initial twenty-three cuts were completed using 120 μm wire to produce 200 μm thick wafers. We also completed 9 cuts using 120 μm wire to produce 180 μm thick wafers. The initial wafering yields with the 120 μm diameter wire were poor as a result of an adhesive problem. Once this was solved the results (for both 200 and 180 μm thicknesses) were encouraging with most performance parameters (yield, thickness variation, etc.) statistically equivalent to the production yields for 200 μm thick wafers using 140 μm thick wire.

The Meyer Burger DS264 trial was compared with an HCT E500 SD-B and a Meyer Burger DS262C. The results of that comparison are shown in Table 3.1 below. The saw performance may have been better in the production trial had the slurry quality been controlled better. Several slurry samples taken during the trial showed elevated levels of fine particles in the slurry.

A trial of ten cuts was conducted using 120 μm diameter wire, cutting 160 μm wafers. The Average Total Thickness Variation (TTV), deviation of thickness, standard deviation of TTV, and number of broken wafers after cleaning was higher than normal when compared to cuts done at 180 μm and 200 μm thicknesses on the same saw.

Item	DS 264
Yield	0
% Thick	++
% Thin	++
% Saw mark groove	--
% Saw mark step	--
% TTV	++
% Chips	0
% Cracks	--
% Holes	0
% Breakage	++
% Glue	0
% Wire break	0
% Cassette broken	--
% Cassette thick	0
% Missing	0
Thickness st. dev.	++
TTV	--
TTV st. dev.	++

Table 3.1: Meyer Burger DS264 wire saw performance vs. HCT E500SD-B and Meyer Burger DS262C (++ favorable, -- unfavorable, 0 no statistical significance)

Four cuts were completed using slurry containing silicon carbide with an average particle size of 8 μm in an effort to decrease kerf loss. No benefit was observed using the smaller particle size slurry. Cutting efficiency appears to be reduced with higher cutting temperatures and increased bow in the web during the cuts.

In an effort to reduce silicon waste across the saw room and with the inability for older saws to handle 120 μm wire, 130 μm wire from Tokusen USA was tested with three different elongation specifications – 2.3, 2.5, 2.7%. Testing indicated a decreased likelihood of wire breaks with the higher elongation specification. A complete conversion of the saw room took place during the period of this contract. Additional testing was carried out to certify wire production from two different Bekaert plants for 120 μm wire.

After setup of new recipes in the sizing saws, brick grinders, and wire saws, ten development cuts have been completed on 156mm square wafers at 180μm thickness. Results are mixed with yields ~12% lower than the baseline production yield for 125mm square, 200 μm thick wafers. During development, a preliminary wire saw recipe was determined along with a non-alkaline, ICT-compatible cleaning process. Key process inputs affecting wafer cleaning have been identified, and control of these inputs is being established.

Brick grinding to improve wafer strength and reduce breakage yields

Experimentation indicated that both wafering and cell line mechanical yields can be improved by machining the brick faces to remove block cutting damage before wire sawing. We were able to improve the wafer strength (as determined by a 4-beam bending test) from ~7N for non-ground bricks to ~12N for the finely ground bricks.

A focused improvement effort continued to reduce wafer chip defects and increase the wafer strength. Specific items included:

- Improvements in wafer quality in regards to wafer total thickness variation (TTV) and thickness
- Purging of all damaged cassettes and the establishment of a cassette management system
- Modifying the demounting acid bath temperature and concentration to improve separation of wafers from mount and reduce breakage

Destructive wafer strength tests were performed on wafers cleaned in the Lab (low alkaline clean), Elma (NaOH clean), RENA (ultrasonic + detergent clean), and RENA-ICT (acid based etch) for comparison (See Table 3.2). The acid etched wafers were weaker than the wafers cleaned through ELMA (NaOH). This can be partially explained by the damage removal and micro crack tip widening in the NaOH-based ELMA process. We did not see any significant difference in wafer strength between those cleaned in RENA versus Lab cleaned. As expected, the thinner wafers deflected more than the thicker wafers, but also broke at lower loads. No conclusions can be made about the strength of Mono$^{2\ TM}$ vs. multi in this test.

Table 3.2: Mechanical results of cleaning experiment

Test Date	Lot #	Wafer Thk	Cleaning	Multi/Mono^2	Deflection (mm)	Breaking Load(N)
5/22/2008	104665	200µm	Not Cleaned	Multi	7.46±1.6	8.0±2.0
5/15/2008	104429	200µm	Acid Clean	Multi	8.1 ± 0.7	8.7 ± 1.5
5/15/2008	104429	200µm	ELMA	Mutli	9.7 ± 1.1	10.8 ± 2.6
5/15/2008	RQ1	160µm	RENA	Mono^2	10.9 ± 1.4	5.7 ± 1.3
5/15/2008	103857L	160µm	Lab	Mono^2	10.3 ± 1.4	5.2 ± 1.0
5/15/2008	108357L	160µm	ICT*	Mono^2	15.3 ± 3.0	5.9 ± 0.9

Integrated demounting and cleaning

After initial tests indicated tank and cassette based washing was not capable of high yield with thin wafers, BP Solar procured new automated equipment for pre-washing, in-line washing, and wafer separation. Several development periods were needed to establish proper cleaning and demounting chemistry, proper setup, operation, and maintenance periods for the wafer separator, and process cleaning conditions for in-line cleaning.

BP Solar originally used a steel recoverable wire saw mounting plate but opted to a single use glass-filled epoxy plate for ease of operation, decreased labor requirements, and high reproducibility and consistency of mounting. With further thin wafer testing, the wire

saw manufacturers recommended a retest of steel mounting plates versus epoxy. A test of these steel beams resulted in a 1% improvement in wafer and cell yield, but required significant development of the demounting, cleaning, and recovery process for these steel beams to eliminate previous problems and operator hazards. An improved recovery process was developed during the course of this contract.

A low foaming detergent is under test as an ICT compatible wafer cleaning process. Laboratory testing had been successful, so a month-long cleaning trial was undertaken to evaluate the cleaning process in a production environment. The cell line efficiency, breakage and number of stained wafers did not show any significant difference between the two processes. The foaming issue was successfully eliminated. However, after a relatively short bath life there were certain lots that this detergent had trouble cleaning. With this reduced bath life, the cost per wafer is about four times the cost of the caustic process, but required to produce ICT-compatible wafers.

Water based slurry cutting trials

Initial water-based slurry cutting trial was completed in three cuts performed with three different viscosities:

- The first cut used low viscosity slurry, during which wafers were sliced in half and fell from partially cut bricks at 61 mm into the cut, indicative of severe wire skips. The bowing of the wire web appeared high, indicating inefficient cutting. Many wafers fell at the end of the cut, and the end wafers cracked off.
- In the second cut with intermediate viscosity, wire bow appeared lower, but many wafers fell near the end of the cut, except where an endplate remained.
- The third cut had high viscosity and end plates on #1 and # 2 side. Unfortunately, there was a wire break at 104 mm into cut. Many wire skips were observed at this point, with bow in the web at ~5 mm. At 116 mm many wafers were observed falling down due to wire skips. Many wafers fell at the end of the cut. Wafers near the end plates and small gaps between bricks did not fall.

Altogether, the experiment was not successful and indicated both the mounting adhesive needed to be altered (wafers falling at end of cut) and the slurry reformulated to increase cutting efficiency. It was also noticed that a significant force to the wafers falling off the mount during cutting was due to hydrogen bubbles created between the wafers bowing them apart. The hydrogen forms in a reaction with the water-based carrier and the silicon swarf generated during cutting.

A second trial was run with water-based slurry, aimed at suppressing hydrogen formation during the cut. Two cuts resulted in the following conclusions:

- Need to determine how much surfactant is required for proper formulation
- Epoxy of sufficient bond strength and water-tolerance that survive under these cutting conditions
- The water-silicon reaction to generate hydrogen creates over-the-road transport issues for slurry recovery, the current method of freezing slurry is not time or cost effective
- A lower level of hydrogen suppressant reduced premature detachment of wafers for the mounting beam
- A carrier formulation to tolerate a higher kerf loading

Task 4: Cells and Contacts

The goals of Task 4 were directed toward improvements in cell fabrication to utilize our Mono$^{2\ TM}$ wafer technology while driving performance improvement and cost reduction through thin cell processing, emitter improvement, advanced metallization, back contact cells, and device modeling and optimization. Each of these focus areas comprise subtasks and our efforts and results are described below. Finally, a section is added focusing on characterization of Mono$^{2\ TM}$ as this occupied significant resources during the second year of the program.

Thin Cell Processing

The aim objective to develop cell processes and materials required to move from the industry standard 200um wafer thickness toward 100um wafer thicknesses. Specific areas of focus at BP Solar were on iso-chemical texturing to improve light collection and minimize thickness reduction during the saw-damage removal process and qualification of low-bow Al-BSF paste materials and processes to minimize wafer deformation and yield loss after co-firing. Taken together these process changes would enable transition from 125mm, 200um wafers to 156mm, 180um wafers.

Iso-chemical Texturing

Iso-chemical texturing (ICT) process development was performed using our Frederick, MD, production facility with a RENA InTex prototype process tool. Activities focused on three principle areas efforts;

1. Process window definition around key parameters;
2. Cosmetic and reliability performance of modules with ICT cells;
3. Pilot production to validate performance of cells with ICT in our Frederick, MD, production facility.

Additionally, high yield of 99.5% was demonstrated at small volumes for 160um thick wafers.

Process window definition focused on assessing the impact of etch depth, etch process temperature, and wafer manufacturer on the cosmetic and electrical performance of ICT cells completed in our production facility. Results for the impact of etch depth is shown in Table 4.1. The 4.2um etch depth is consistent with Rena's recommended process target.

Table 4.1. Cell performance as a function of ICT etch depth

Etch Depth (µm)	L-a-b Color (a-scale)	Efficiency (%)	Isc (A)	Voc	FF	n-factor
3.5	16.8	14.41	5.17	0.601	0.725	1.26
4.2	16.1	14.47	5.16	0.600	0.730	1.22
4.9	13.4	14.41	5.17	0.601	0.725	1.23
5.3	12.8	14.47	5.20	0.601	0.724	1.25
6.3	12.1	14.33	5.15	0.600	0.725	1.28

In Table 4.2 the impact of bath temperature on etch rate and performance is shown.

Table 4.2. Cell performance as a function of ICT etch temperature

ICT Temp (C)	Etch Rate (µm/min)	L-a-b Color (a-scale)	Efficiency (%)	Isc (A)	Voc (mV)	FF	n-factor
5.5	0.95	14.7	14.74	5.21	599	73.9	1.25
7.5	1.11	11.9	14.76	5.22	600	73.7	1.22
9.5	1.30	8.6	14.17	5.19	598	71.2	1.26
12.0	1.48	9.8	14.43	5.21	599	72.3	1.25
15.0	1.97	7.4	14.63	5.18	599	73.6	1.25

Because ICT relies on the residual wire saw damage to form texture in the wafer surface, the wafer source and associated sawing and cleaning process is assumed to impact the ICT process. Table 4.3 summarizes these results.

Table 4.3. Cell performance as a function of wafer supplier

	Etch Depth (microns)	L-a-b Color (a-scale)	Efficiency (%)	Isc (A)	Voc	FF	n-factor
BP Solar	4.0	13.4	14.23	5.145	0.598	0.723	1.28
Supplier 1	4.0	14.6	14.28	5.133	0.599	0.726	1.26
Supplier 2	4.0	14.9	14.44	5.173	0.602	0.724	1.26
Supplier 3	4.2	17.0	14.08	5.149	0.596	0.716	1.39
Supplier 4	4.0	15.1	13.97	5.106	0.594	0.720	1.35
Supplier 5	4.1	18.1	14.56	5.243	0.603	0.720	1.26

The ICT process was generally found to be robust with regard to the tested parameters and wide process windows were identified for the start of production.

Before transitioning to ICT texturing in production in our Frederick facility, a pilot of ~6,000 cells was conducted to determine the impact of ICT on module power (Figure 4.4).

- Prior to running the pilot, the co-optimization of diffusion and co-fire settings showed a 0.4% absolute efficiency improvement at cell test for ICT relative to cells featuring BP Solar's standard planar NaOH-etch. This gain was due to an increase in Isc while Voc and FF showed decreases.
- When applying these conditions to the pilot run an efficiency increase of only 0.2% was seen relative to the NaOH-etch control. This was largely due to problems with front print and with replicating optimal temperature profile for co-fire and was primarily seen as decreased FF relative to the co-optimization results.
- Modules built in the pilot trial had an average of ~3W lower power than the Na-etch control. The key factor in this underperformance a relative gain of Isc for the NaOH-etched cells upon encapsulating.

Table 4.4. Cell and module performance for ICT cells vs. NaOH planar etched baseline

Group	Bin	Module				Bare Cell		
		Pmax	FF	Voc	Isc	FF	Voc	Isc
ICT	Bin 5	168.5	0.718	43.45	5.40	0.751	0.6015	5.324
	Bin 6	173.0	0.726	43.61	5.46	0.7621	0.6053	5.3677
	Bin 7	177.0	0.731	43.98	5.51	0.7683	0.6099	5.414
NaOH	Bin 5	173.4	0.733	43.70	5.41	0.7687	0.6046	5.167
	Bin 6	177.3	0.742	44.00	5.43	0.7787	0.6094	5.211
	Bin 7	180.0	0.746	44.31	5.44	0.785	0.6137	5.249
ICT vs. NaOH %diff	Bin 5	-2.83%	-2.05%	-0.57%	-0.18%	-2.30%	-0.51%	3.04%
	Bin 6	-2.43%	-2.16%	-0.89%	0.55%	-2.13%	-0.67%	3.01%
	Bin 7	-1.67%	-2.01%	-0.74%	1.29%	-2.13%	-0.62%	3.14%

On the basis of ICT performance with our Frederick process flow along with the change in BP Solar's business plans, the decision was made not to implement ICT in production.

Low-Bow Al-BSF Paste

Assessment of low-bow paste offerings from two major manufacturers, including Ferro, was completed at both the laboratory scale and pre-production pilot scale. Verification of module stability using cells made with each low-bow paste was completed through BP Solar's Q6100 reliability test with each successfully passing the accelerated aging testing. In a pre-production pilot run in Frederick, MD, excessive cell breakage was observed during module assembly for cells made using the Ferro low bow paste resulting in lower than expected yield. Additionally, slight performance reduction was observed relative to the baseline process. Ultimately, because of the change in BP Solar's business plans along with not making a conversion to thinner cells, low-bow paste was not implemented in BP Solar's Frederick facility.

Advanced Emitter

The objective of this subtask was to develop design and process modifications for emitter formation and contacting to improve "blue response" and open circuit voltage. This effort focused on two approaches – shallow emitter and selective emitter.

Shallow Emitter

Work initially focused on the improvement of emitter performance by forming a "shallow" emitter with a higher sheet resistance than our standard 45 ohms per square. This effort would consist of diffusion process definition, contact redesign, and Ag paste and co-fire modification. Work at BP Solar principally focused on modification of our existing belt-diffusion process to adjust the emitter sheet resistance target while working with paste vendors to identify pastes that would contact 80 ohms per square emitters. The principal challenge for the paste was to avoid shunting while not sacrificing contact resistance. In the course of the work several candidate pastes were identified. However, the belt diffusion equipment in our Frederick facility was found to have inadequate process control to form a uniform, high quality shallow emitter. Figure 4.5 shows sheet resistance for our standard 45 ohms per square emitter (a) and for 75 ohms per square emitter (b). These are representative of the change in emitter sheet resistance uniformity encountered with transitioning to a higher sheet resistance. For this reason, selective emitter was pursued as a backup option.

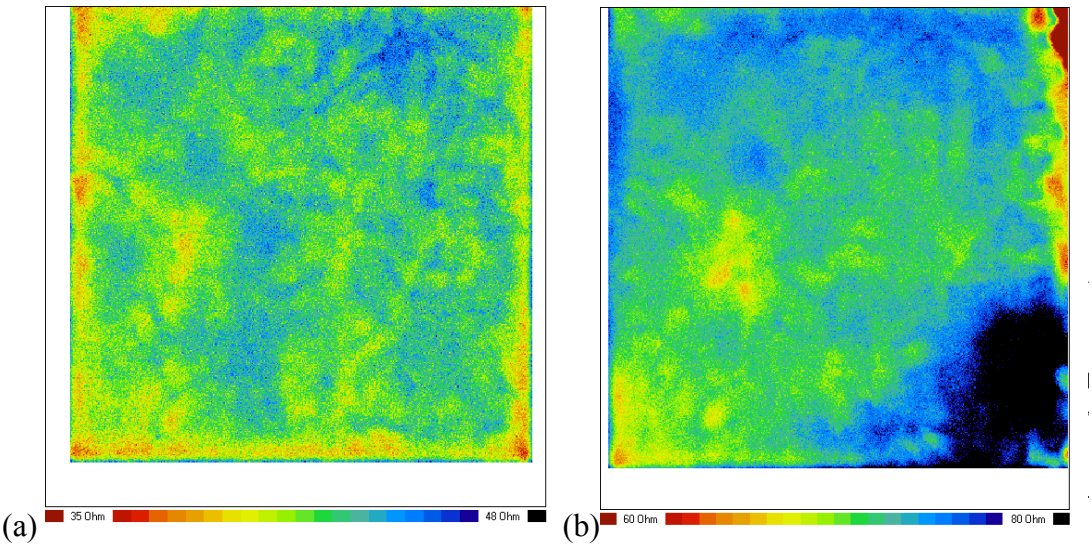

Figure 4.5. Sheet resistance uniformity for belt-diffused cells with 45 ohms per square (a) and 75 ohms per square (b) sheet resistance targets

Selective Emitter

A dopant-ink based selective emitter formation process was evaluated for possible licensing from a technology developer. The results were promising for application to a baseline mono cell process with >0.5% absolute efficiency improvement demonstrated.

Advanced Metallization

The objective of the advanced metallization subtask was to evaluate and select for further development non-screen print metallization techniques that are capable of printing narrow, high aspect ratio lines in a non-contact manner. In the course of the investigation four deposition techniques were evaluated – extrusion, aerosol jet, inkjet, and laser transfer. Most of these options were evaluated under non-disclosure agreements, so the partner identity can not be revealed. Co-extrusion was evaluated with our subcontractor, PARC. Of these options aerosol and inkjet printing suffered from an inability to rapidly deposit thick materials. Laser transfer printing was at a very early stage of development and its principle advantage was being non-contact. Line width and aspect ratio were not obviously superior to advanced screen-print. Only PARC's co-extrusion technology was compelling for near- to medium-term applications.

Over the course of the program PARC independently optimized their extrusion nozzle and materials, enabling the printing of fine lines with exceptional geometry. At the conclusion of year 2 activities, 50um wide and 50 um tall lines were demonstrated. Additionally, an efficiency increase of 1% absolute was demonstrated relative to our baseline process in a controlled experiment. The performance improvement was achieved principally through improved Isc and fill factor with an attendant improvement in Voc.

Back Contact Cells

Laser-Fired Back Contacts

Fraunhofer ISE has demonstrated silicon solar cell conversion efficiencies as high as 21.8% by laser-firing localized aluminum rear contacts through a dielectric layer of thermally grown silicon dioxide. In a series of experiments, we formed localized contacts to p-type Si wafers (1.5 Ω-cm) by laser-firing aluminum through a dielectric passivation layer of intrinsic amorphous silicon (a-Si:H). In these experiments, the thickness of the aluminum was varied from 0.5 to 3.3 µm, and the aluminum was laser-fired through 80 nm of intrinsic a-Si:H using a Nd:YAG laser with the power varying from 0.8 to 2.4 Watts.

As shown in the contour plot of Figure 4.6, a low series resistance was obtained over a wide range of aluminum thicknesses and laser powers. For the lowest laser power, the series resistance increased rapidly as the aluminum thickness increased since the energy density of the laser beam was insufficient to melt the thick aluminum film and fuse it through the a-Si:H into the Si wafer. Other experiments have shown that it is easier to form aluminum laser-fired contacts through a-Si:H than through other dielectrics such as silicon dioxide and silicon nitride. Moreover, a-Si:H has been shown to be an excellent passivation layer that can be deposited at relatively low temperatures (< 200°C).

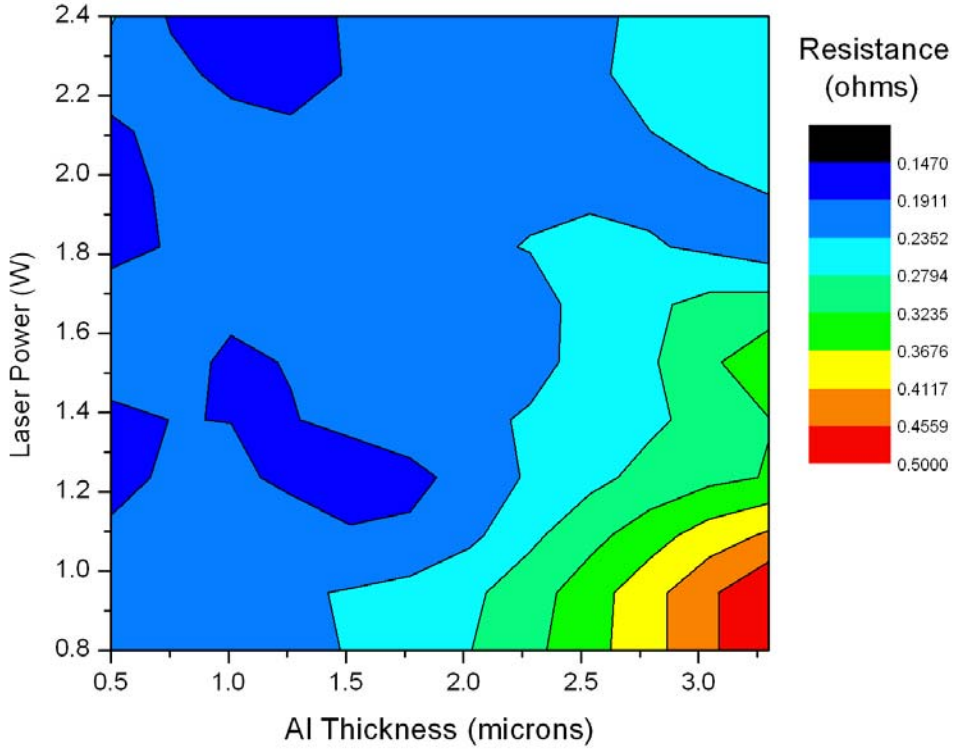

Figure 4.6. Contour plot of laser power vs. Al thickness for laser firing Al contacts through a-Si:H on a p-type Si wafer.

In some cases a high resistance contact can result after laser firing of aluminum through a dielectric due to the removal of all the metal in an annular region near the outer periphery of the laser-fired region. By probing the electrical resistance from the front of the sample to an ohmic contact on the rear, we observe that the central region of the laser-fired region can make a good ohmic contact to the silicon wafer, but the presence of the metal-depleted annular region creates a high resistance path to the metal surrounding central region of the laser-fired region. A good low-resistance contact can often be obtained by depositing a 2nd layer of the metal.

When high resistance laser-fired contacts are examined under a microscope, one often observes a blue dielectric ring just outside a crater formed by the ablation of silicon (see Figure 4.7). In this case a laser pulse was incident on a silver film (~ 1 μm thick) that was deposited on top of a doped silicon wafer coated with a layer of silicon nitride (~ 80 nm thick). There are three distinct regions apparent in the figure. In the central region one can see a crater (~ 2 μm deep) formed by laser ablation of the silicon. Just outside the crater, an annular bluish region is evident where the silicon nitride layer is exposed by laser ablation of the silver layer. Just outside this blue dielectric ring, one can see evidence of splattered silver streaking out from the laser-fired region. Thus, the contact exhibits a very high resistance since there is no conductive path from the surrounding silver film to the doped silicon in the crater.

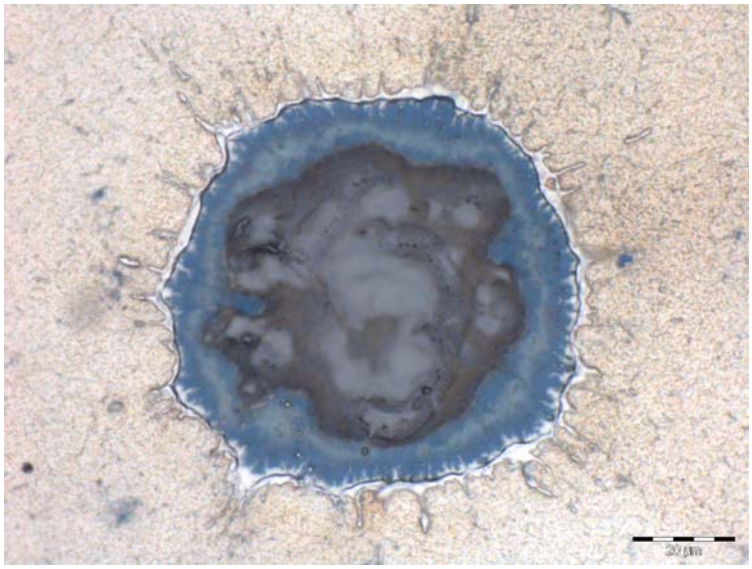

Figure 4.7. A photograph of a laser-fired contact for a silver film deposited on a silicon wafer coated with silicon nitride.

However, under some laser firing conditions, it is possible to obtain high quality, low resistance contacts. The photograph in Figure 4.8 shows a type of laser-fired contact that can exhibit a low resistance. In this case one observes a significant amount of material splattered across the dielectric ring region. Since this splattered material is a mixture of silver and doped silicon, it is very conductive and forms a number of conductive paths for current to flow between the doped silicon crater and the surrounding silver film. Splattering can occur due to phase explosion when the laser beam superheats the molten

silicon, and it becomes more energy efficient to explosively eject large molten clusters rather than evaporate atoms.

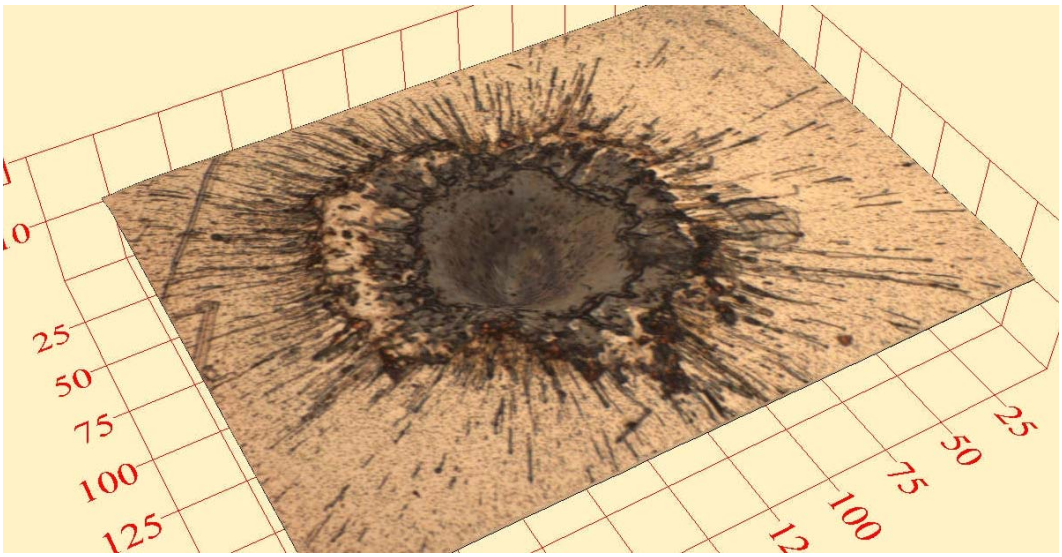

Figure 4.8. A photograph of a laser-fired silver contact where significant spattering of material occurred. The silver was deposited on a silicon wafer coated with silicon nitride

It is also possible to choose laser firing conditions where a low-resistance contact can be formed where the molten rim of the crater is pushed over the annular dielectric region (see Figure 4.9). In this photograph one can see that a portion of the crater rim covers the blue dielectric ring allowing the doped silicon to make a low resistance contact to the surrounding silver film.

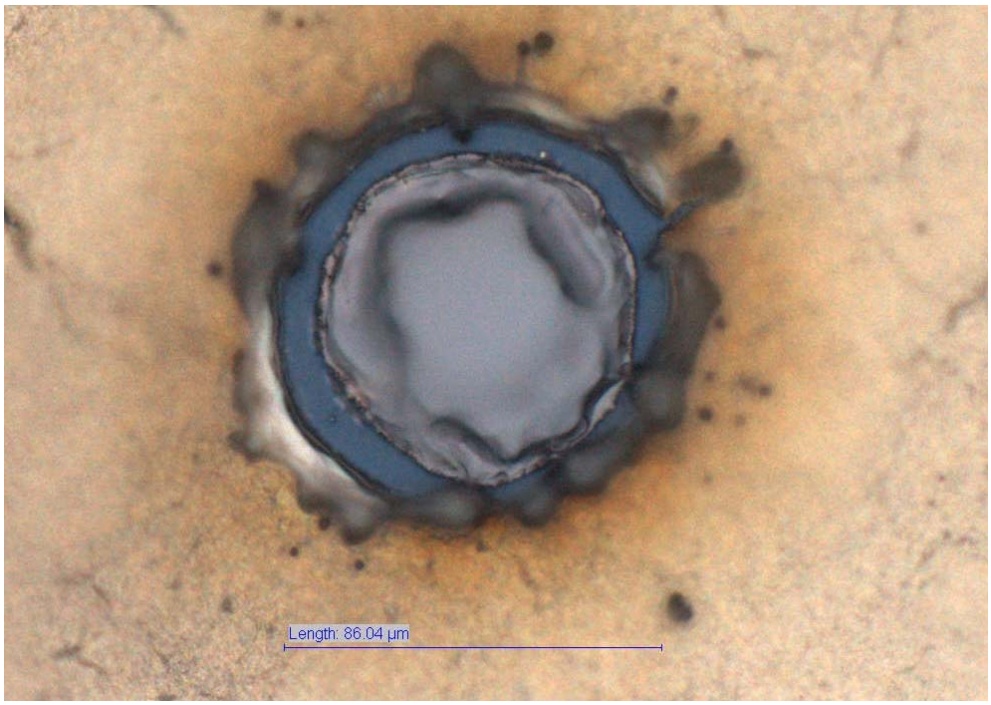

Figure 4.9: Photograph of a laser fired contact where the rim of the crater has been pushed across the blue dielectric ring (near the bottom right of the contact).

The Evans Analytical Group has analyzed the region under a laser-fired crater. The sample was prepared with the structure Ag/Al/SiN_x/c-Si, and the laser ablated almost all the Ag/Al/SiN_x from the surface leaving a crater about 1 - 2 microns deep and ~ 100 µm in diameter. There is clear evidence that the silicon melted to a depth of ~ 0.5 – 2.0 microns under the crater bottom and a number of filaments are evident extending to the bottom of the molten zone (see Figure 4.10). The filaments are rich in both Ag and Al indicating that the metals melted and were mixed together before penetrating the silicon. The filaments may be due to the accumulation of metals at grain boundaries within a re-crystallized region. Metal precipitates are also evident at the bottom of the molten zone.

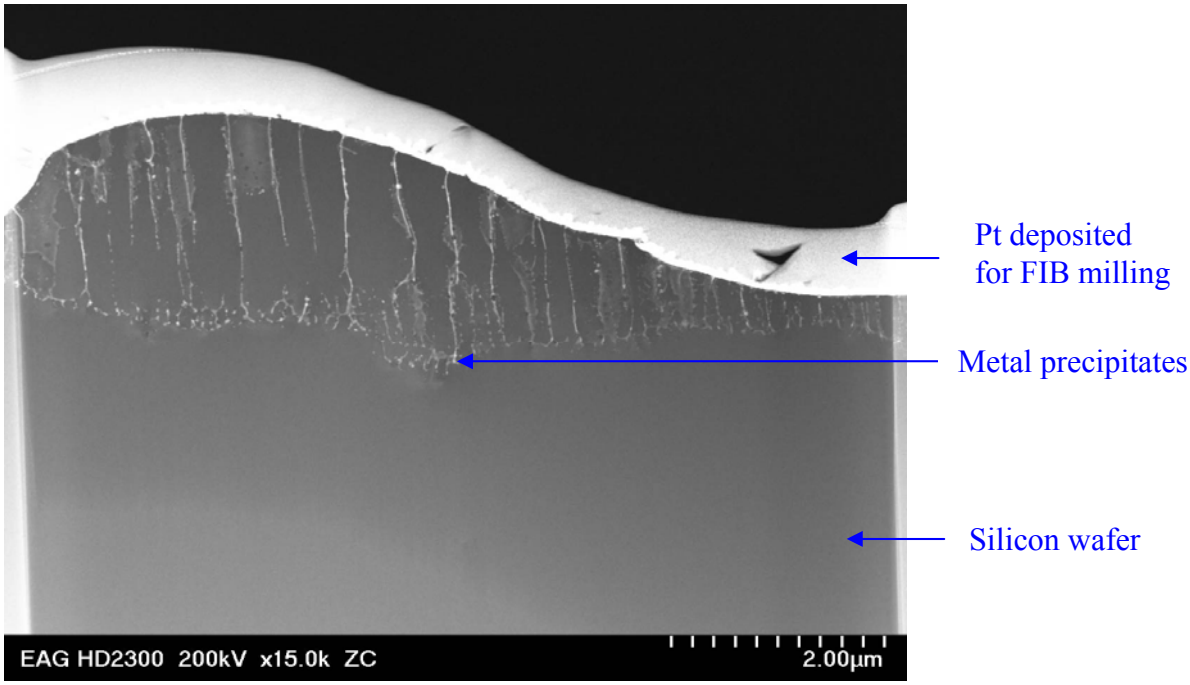

Figure 4.10. STEM image of the crater region at the bottom of a laser-fired contact

Modeling of Back-Contact Solar Cells

Georgia Tech has been performing some modeling for us on back contact cells where we assume that most of the rear surface is coated with a shallow emitter and the base and emitter rear contacts are made through localized n^+ and p^+ regions. The modeling shows that an efficiency of 24% can be obtained with p-type Si (1 ohm-cm, bulk lifetime = 1 ms) if the spacing of the localized contact regions (each 100 microns in diameter) is about 0.5 mm (see Figure 4.11). The model also assumes that the front surface is textured and is coated with a well-passivated (S_{eff} = 3 cm/s) silicon nitride antireflection coating.

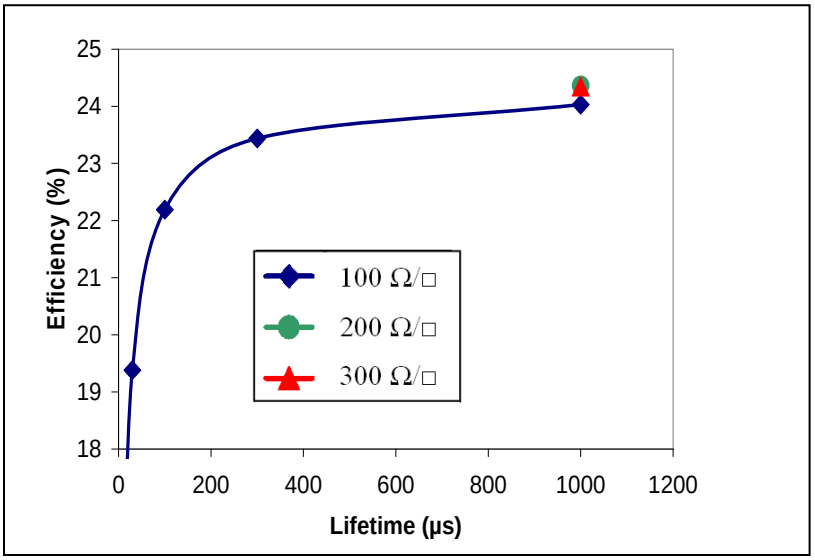

Figure 4.11. Efficiency vs. lifetime for a back contact solar cell (when the lifetime was 1000 µs, the sheet resistance of the rear shallow emitter was varied from 100 to 300 Ω/□)

The modeling by Georgia Tech also shows that an efficiency of ~ 22.3% is possible for a cell made with 1 ohm-cm, p-type Mono^2 silicon where the shallow rear surface emitter has a sheet resistance of ~ 100 Ω/□. The Mono^2 wafer is assumed to be 150 µm thick with a high quality silicon nitride antireflection coating on the front surface.
In addition, the modeling shows that for all other parameters being equal, the lifetime for n-type Si must be about 2.4 times larger than that for p-type Si for comparable device performance (see Figure 4.12).

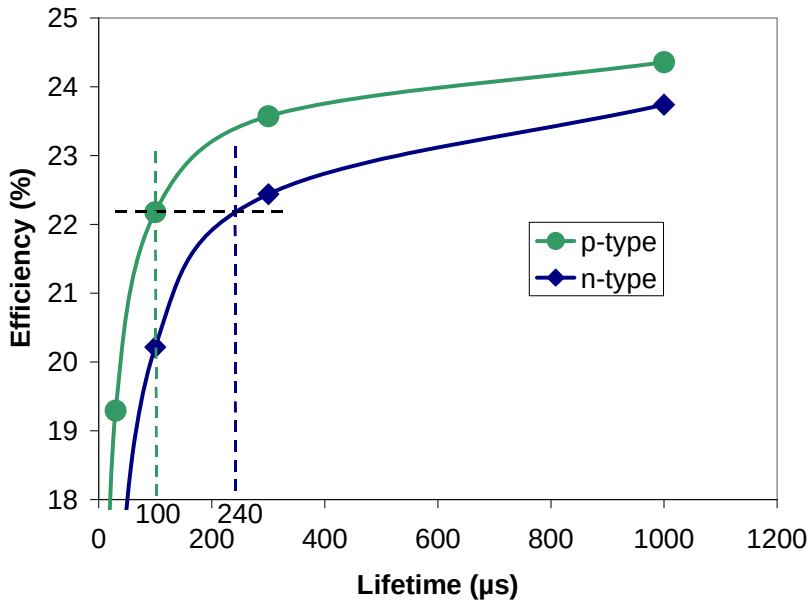

Figure 4.12: Efficiency vs. lifetime for back-contact cells made with p- or n-type Si wafers.

Device Modeling and Optimization
The objectives of the device modeling and optimization subtask are to use modeling capabilities developed at Georgia Tech along with process splits to identify areas for potential improvement of BP Solar's screen-print cell performance. Additionally, areas for performance improvement through device or process modification were explored.

Georgia Tech Co-Processing Work
The aim of this experiment was to compare and contrast the different BP multi-crystalline solar cell process steps to GT's process steps. The different processing steps compared were (i) damage removal etch, (ii) diffusion, (iii) isolation (iv) anti-reflection deposition and (iv) contact firing. For each of the first five groups of wafers, GT-processing began at different stages. The first process step at GT for each group is indicated in Table 4.5. Each process step performed at GT was monitored using data collected after each stage of the process. The data collected after each stage is shown in Table 4.6. Performance of the finished cell is evaluated using the light IV data collected at the end of the processing sequence. The average performance parameters of the best three finished cells in each of the five groups are listed in Table 4.7.

Table 4.5. Starting wafers for Georgia Tech experiment

Description of wafers from BP	Number of Wafers	GT process beginning step	Code Name Used for the group of wafers
As Cut wafers	11	Saw Damage Removal step	BPAC
Saw Damage removed wafers	11	Emitter Diffusion step	BPSD
Diffused wafers	11	Edge Isolation & Post Diffusion Cleaning step	BPD
Plasma etched wafers	11	Silicon Nitride ARC deposition step	BPPE
Silicon nitride coated wafers	11	Contact screen printing step	BPSiN
Finished solar cells	11	-	BPSP

Table 4.6. Measurements made after each process step

Process	Post Process Data Collected
Sawed Wafers (As Cut)	Thickness, Effective bulk lifetime in Iodine
Saw Damage Removal	Thickness, Resistivity, Effective bulk lifetime in Iodine
Clean	-
Emitter Diffusion	Sheet Resistance, Implied Voc, Effective bulk lifetime in Iodine
Isolation, Post Diffusion Clean	-
Silicon Nitride Deposition	Reflectance
Contact Firing	Light IV, Spectral Response, IQE, Effective bulk lifetime in Iodine

Table 4.7. Ave. performance parameters of the best three finished cells in each group

Group	Voc(mV)	Jsc(mA/cm^2)	Fill Factor	Efficiency (%)
BPAC	627	31.7	0.739	14.7
BPSD	626	31.9	0.749	15.0
BPD	623	31.8	0.736	14.6
BPPE	621	31.5	0.722	14.1
BPSiN	620	31.7	0.743	14.6

It is clear from the IV data that the open circuit voltage is higher in the wafers that were diffused at GT using the $POCL_3$ process(Average 625 mV), compared to BP diffusion (Average 621 mV). In addition the Voc drops further with the BP Silicon nitride process (Average 619 mV). The overall efficiency difference between the GT and BP processed cells is not very large in spite of the higher Voc for the GT cells. This is due to the less than optimal contact firing done at GT. Further studies will be aimed at improving the diffusion and silicon nitride processes in combination with an optimized firing condition to achieve higher efficiencies.

Back-Print Optimization

A simple but effective means of improving cost and performance was to redesign the back contact pattern. The new contact structure minimized the bus bar area, reducing the Ag consumed per cell, and maximized the Al coverage, increasing the extent of the BSF. The combined effect of these changes was a relative performance improvement of 0.6% at the cell level and 1.0% at the module level. Additionally, a cost of conversion reduction of $0.04/Wp was achieved.

Mono^{2TM} Characterization

Significant effort was devoted to characterization and cell process definition for Mono^{2TM}. A sampling protocol was devised in collaboration with our Silicon Technology group to fully sample the material quality across the lateral and vertical dimensions of a cast ingot. This entailed selecting six unique brick positions from each ingot and scribing a V-shaped structure on the brick edge to identify vertical position of wafers along with a brick identification mark. These bricks were then wafered and samples selected to characterize material performance across the ingot.

Material quality in Mono^{2TM} is a function of the vertical position of the wafer in the ingot. This is apparently due to the presence of a high concentration of sub-grain boundaries in the upper regions of the casting. This can be seen in the Figure 4.13 showing cell efficiency for BP Solar's standard screen-print cell as a function of brick location and height in the brick. Each plot shows the efficiency of cells made from a given brick – A1, B4, C2, C3, D5, and E3, from left to right top row then bottom row. Each plot shows cell efficiency from the bottom to top of the ingot from left to right on the x-axis. Silicon Technology is currently working on casting process changes to improve performance through the height of the ingot.

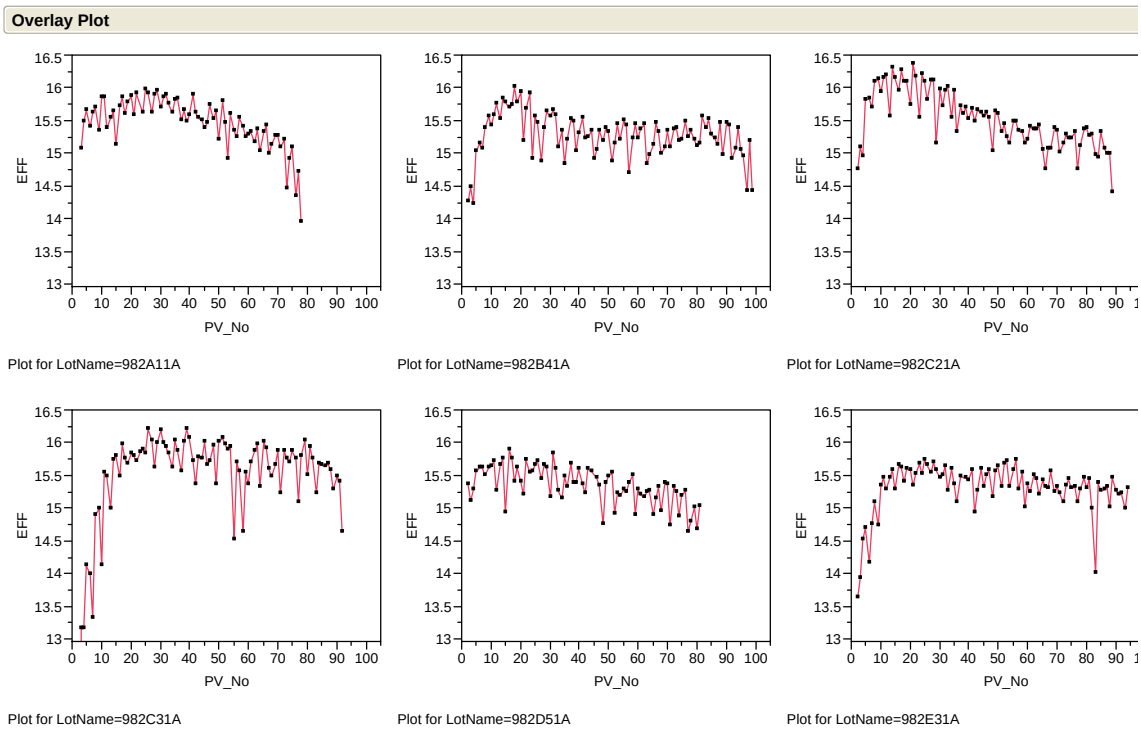

Figure 4.13. Efficiency as a function of position in Cast Silicon using standard cell process

In addition to using BP Solar's standard cell process to diagnose material performance, alternative process flows were explored. The two main alternatives explored were ICT texture with a tube-diffused emitter and pyramid texture with a tube-diffused emitter. The efficiency distribution plots are shown in Figure 4.14. In this trial two textures were used – alkaline or pyramid and ICT. Two brick positions were processed: A1 – a corner brick – and C2 – an interior brick that is almost entirely mono-crystalline (100)-oriented material. Four different casting conditions were evaluated. 139, 301, and 762 are Mono^{2TM} ingots cast with varying conditions. Ingot 159 is a multi-crystalline reference ingot. In this trial the upper portion of the ingots were ICT textured and the lower portions were pyramid textured. It is clear from the data, along with other tests that the preferred cell process incorporates pyramid texturing and tube diffusion for the mono-crystalline interior bricks. Exterior bricks should be processed using an ICT texture.

The next steps for Mono^{2TM} will center on continued testing of pyramid and ICT textured cell processes, including full ingot characterization and tests in modules to determine if the cell-level efficiency improvements shown here are carried through to the module.

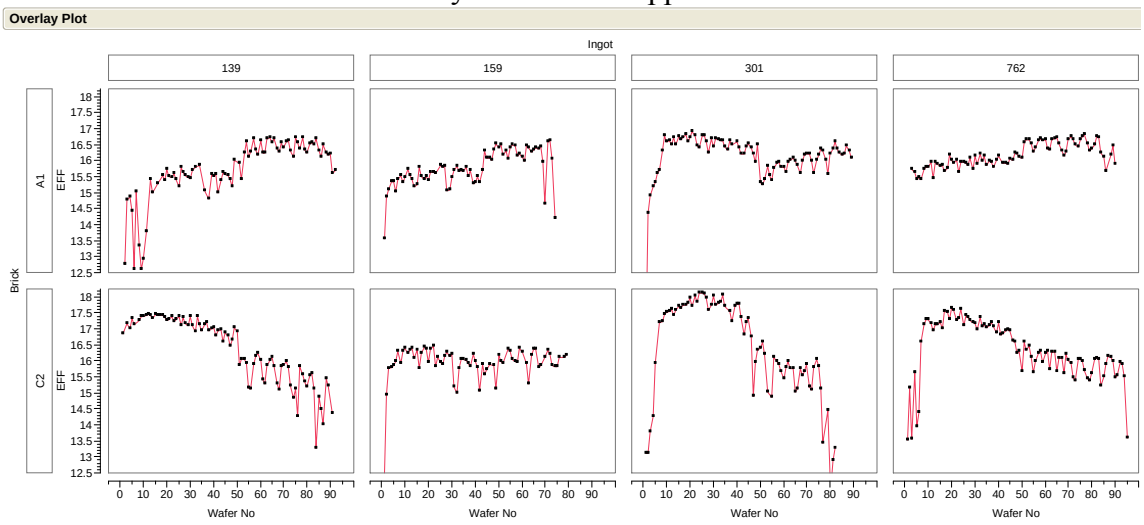

Figure 4.14. Efficiency as a function of position in Cast Silicon for two different cell processes.

A larger trial with Mono^{2TM} wafers was conducted during the last quarter at our cell manufacturing partner under supervision of Frederick-based BP Solar silicon and cell technologists. These trials yielded very impressive top cells with efficiencies of 18.35% demonstrated on 125mm x 125mm wafers using a pyramid texture. However, consistent with prior trials, the spread of efficiencies was larger than achieved with standard multi material processed with a similar cell process flow using ICT texture.

Table 4.8 summarizes the results for the pre-pilot optimization splits (averages and standard deviations over all tested conditions), along with averages and standard deviations for the "mini"-pilot. The Mono^{2TM} HP (for high-performance) refers to interior bricks with (100) single-crystal material and processed with a pyramid texture and nominally mono cell process; Mono^{2TM} refers to the perimeter bricks processed with an ICT textured standard multi cell process. Several unexpected and as yet unexplained observations are under investigation. Particularly, the reduced Voc and FF for Mono^{2TM} HP with the pyramid mono process relative to the Mono^{2TM} processed with a standard ICT multi process. Also, between the optimization splits and the pilot, there was an unexplained increase in the series resistance (Rs) value for Mono^{2TM} HP.

Table 4.8. Mono^{2TM} Cell process Trial

		Optimization Splits		Mini-Pilot Trial	
		Mono^{2TM} HP	Mono^{2TM}	Mono^{2TM} HP	Mono^{2TM}
Efficiency (%)	Avg.	16.30	16.05	16.49	16.28
	Std. Dev.	1.01	0.57	1.04	0.47
Voc (mV)	Avg.	613	619	615	621
	Std. Dev.	12.0	5.5	13.0	4.9
Isc (A)	Avg.	5.46	5.24	5.53	5.29
	Std. Dev.	0.18	0.10	0.20	0.09
FF	Avg.	76.0	77.3	75.7	77.3
	Std. Dev.	1.7	1.6	1.1	0.8
Rs (mOhms)	Avg.	2.6	3.1	3.5	3.0
	Std. Dev.	0.6	0.5	0.4	0.4

These cells have been made into modules to correlate module performance to cell efficiency bin. Initial tests of the module power have been made, but reporting will wait for confirmation of calibration via outdoor measurements in Frederick, MD.

Task 5: Modules

Energy enhancement, Optical : Anti-reflection coating for module cover glass

In Task 5, BP Solar looked at reducing reflection losses from the glass surface by collaborating with subcontractor AGC Flat Glass North America to evaluate a highly durable antireflection coating to the outside surface of the module glass. The work over the period of the project investigated the total gain the glass produced for various weather conditions. BP Solar also reported on the gain at the solar simulator in a production environment plus the evolution of the glass coating. The production QC tool, HazeGuard Plus if also described. The following reviews these various aspects of the development.

AGC ARC glass was implemented for most of BP Solar large product types (95% of production) during the first quarter of the program (during H1-2007). Different options were evaluated to optimize the trade off of Transmission / Cosmetics / Durability are being investigated for quality control. AGC focused on developing a gradient index coating to achieve a grayish / neutral residual color in reflection with a visible and solar transmission above 94%. Evaluation of the efficiency gain from early versions of the glass indicated that it was not achieving the 2% gain originally measured during the qualification trials. AGC undertook several short term efforts to improve the coating quality and uniformity while BP Solar and AGC worked on development of a methodology to measure the transmission of the incoming glass. Both BP Solar and AGC have purchased a HazeGuard Plus in order to measure the visible transmission through the glass. While there were small off-set differences between the AGC and BP Solar units, they proved invaluable in determining transmission of the AR coated glass. BP is now using the unit as an incoming QA tool to check the transmission of the AR coated glass.

Film uniformity and pilot run

AGC's development efforts to improve the silicon based AR coating quality included three components:

1. Adjustment of the SiO_2 mixing ratio to improve the transmission gain.
2. Improve the temperature control of the incoming glass by adding a cooling area between the glass washer and the coating area.
3. Addition of a third head to the spray system to improve the uniformity.

The mixing ratio was altered and AGC produced 12 racks (160 pieces each) for BP Solar. Using the HazeGuard we verified that the new process glass had an average transmission of 93.9% versus 93.2% for the "older" process. This 0.77% gain should return our AR glass gain back to the +2% range. An interesting lesson gained from this exercise was that even with the improved process there was an overlap in the distribution of transmission from the tow groups as shown in Figure 5.1. So just measuring an

occasional piece of glass is not going to provide sufficient data to determine the distribution. This glass was then put through BP Solar module. The results are shown in Table 5.1. The 66% increase in output power is in good agreement with the 0.77% increase in transmission measured by the HazeGuard Plus.

Samples from the temperature control group have now been received in Frederick. They will be processed in the next quarter. Addition of the third spray head is also scheduled for the next quarter.

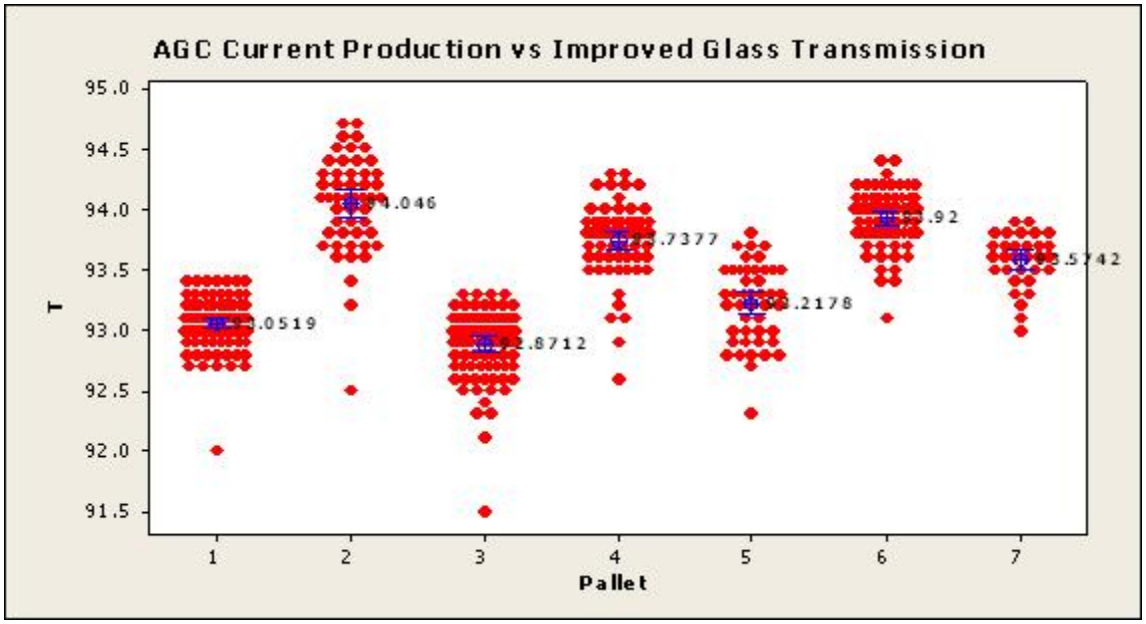

Figure 5.1: Values of glass transmission as measured by the HazeGuard Plus.
Pallets 1, 3, 5 and 7 are from the old process
Pallets 2, 4 and 6 are from the improved process

Table 5.1: Module results using improved AR Glass

June 18 Trial	Normal	Improved	% Delta
Pmax	172.3	173.3	0.61%
Isc	5.271	5.282	0.21%
FF	0.747	0.747	0.05%

AGC also worked on a longer term improvement project underway. This is a new coating process which provides very uniform AR coatings with higher transmission (2-2.5%). Figure 5.2 shows a plot of the increased transmission obtained using the new process. This process was called Gen 2 and was due to be ready for production in 2010.

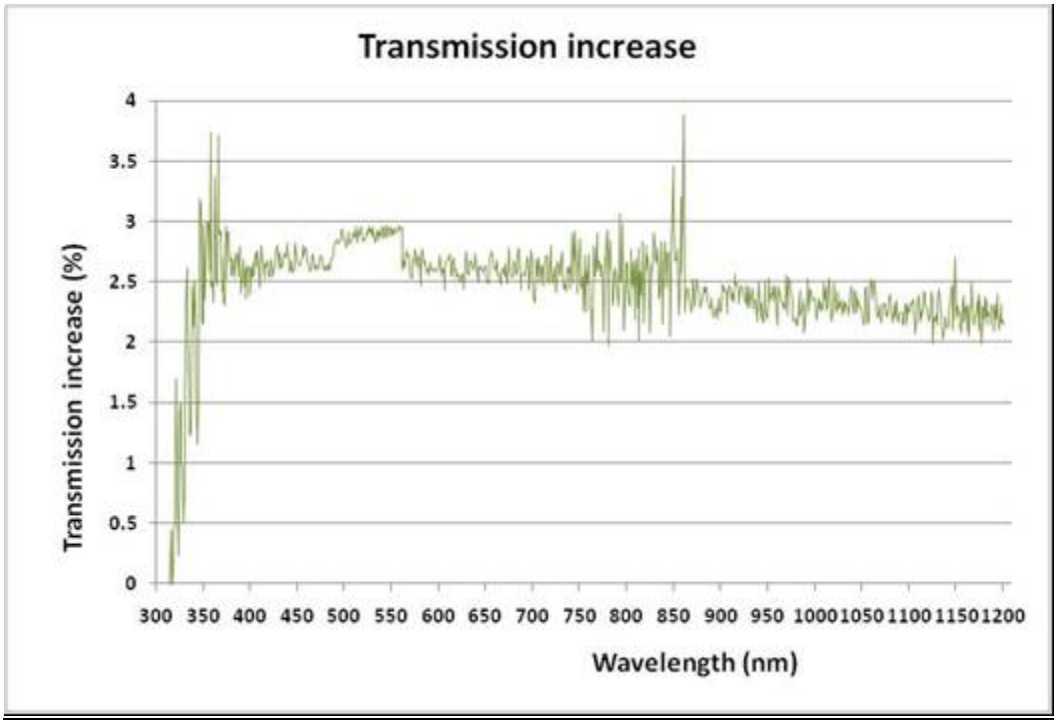

Figure 5.2: Transmission increase vs. wavelength for improved AR coating process

Outdoor performance of AGC ARC glass at BP Solar.
A sample module with ARC glass was deployed outdoors along side a module made with un-coated AGC module made with equivalent cells. The performance of the two modules and the gain observed for the ARC module can be described below in 2 scenarios:

1. *At normal (perpendicular) angles of incidence:* A gain of 2% to 2.5% over a un-coated module under STC or at noon, when the sun is directly overhead. This light would normally be reflected away but with the ARC it is directed into the module to be absorbed in the solar cell.
2. *Improved performance at glancing angles of incidence at early and late times of the day:* An additional 1% to 2% energy gain is obtained using ARC modules when the sun is low in the sky. The reflectivity of un-coated glass is not the same for all angles of incidence. As the angle gets shallower in the morning and evening, the percentage of light reflected gets even larger. This is where the impact of ARC glass is the highest. Figure 5.3 below shows the gain of ARC glass over un-coated glass through a whole day. The total gain over the un-coated glass is as high as 7% in the morning and evening averaged over a day; the total gain is 4%.

As this is a normalized graph (to module power at STC), the gain at noon over an un-coated glass sample is zero. However, note the improved performance at early and late times of the day when the incident angle becomes glancing and the anti-reflective effect is highest. This illustrates the additional energy that is obtained at illumination conditions that are not defined in standard test conditions but only in the field.

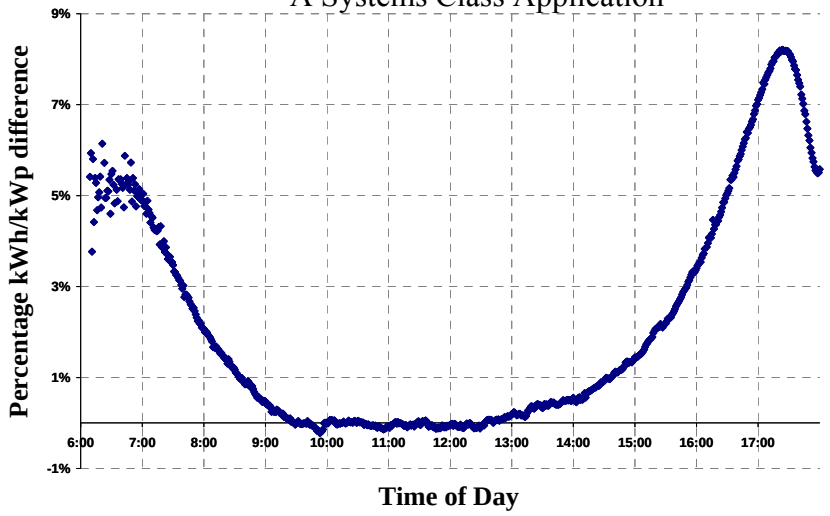

Figure 5.3: Percentage difference energy generation for an ARC module versus a control module with no coating

Energy enhancement, Electrical: Loss reduction by cell cleaving.

The total series resistance loss in a PV module is made up of numerous elements. These elements are shown in the schematic, Figure 5.4. The sum of these components represents the total series resistance of the module. Minimizing these components will reduce overall series resistance and increase fill factor, therefore, increasing the power of a module.

The magnitude of these losses is directly proportional to the square of the current (from Ohms law; Power $_{loss} = I^2R$). For this reason, resistive losses in a module made with *125mm cells* are lower than losses in one made with *156mm cells.* This is due to the higher current in the 156mm case. At BP Solar, we have investigated methods to utilize the larger cell format yet reduce the electrical losses within the module. Moreover, a module has been designed where the cell size is optimized to reduce these losses and boost performance and increase shade tolerance over a traditional assembly.

In laser cutting the large 156mm multi crystalline cells, the series resistance losses in the interconnect ribbon is greatly reduced. As a result, the performance of the module increases in the following ways:

- Better performance at high light levels. This is shown from the power distribution in Figure 5.5
- Improved cell encapsulated STC cell efficiency by 0.5% absolute
- Better power density in the field
- Twice the shade tolerance of a standard module due to a higher level of by-pass diode protection. This is enabled by leveraging BP Solars intellectual property, the Integra Bus™
- Improved handling and assembly robustness

Figure 4 shows the extent of encapsulated cell efficiency improvement as a result of reducing series resistance in the interconnect ribbon. In this example, the standard module contains 60, 243.4cm^2 (156mm) multi-crystalline silicon cells. Table 5.2 shows

the corresponding electrical results for the 400 module run.

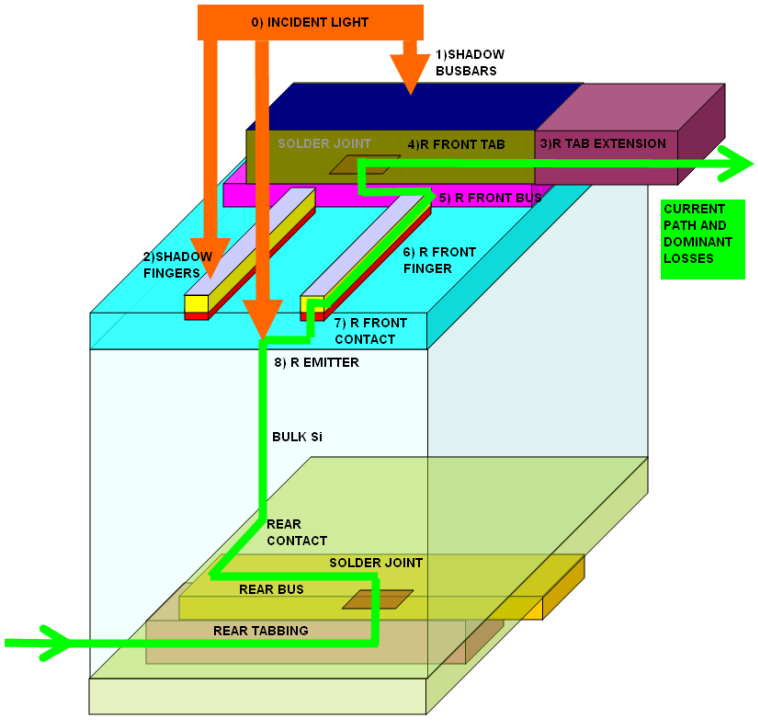

Figure 5.4: Resistive elements of an encapsulated cell

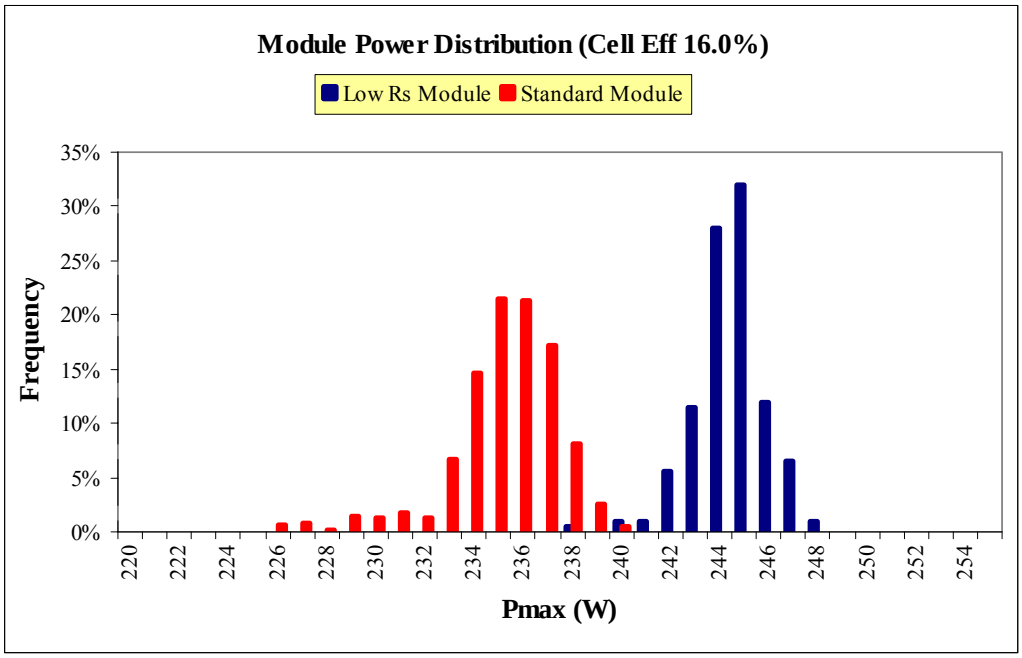

Figure 5.5: Standard module vs. Low Resistance, ½ cell version

Table 5.2: Electrical results for 400 modules made with the low series resistance design.

Module Type	Cell EFF	Pmax (W)	FF	Voc (V)	Isc (A)
Low Res Design	16.00-16.25%	245.0	0.745	37.4	8.78
Standard Design	16.00-16.25%	235.8	0.724	37.4	8.72
Diff Absolute		9.3	0.021	0.1	0.07
Diff Percent		3.9%	3.0%	0.2%	0.8%

The average power of the low resistance module distribution was 245W versus 235.8W for the standard module configuration. The primary factor that improved for the low resistance module was fill factor. In this case the average fill factor value for the low resistance module was 0.745 compared to 0.724 for the standard module. The reduced series resistance is also a key to improve performance in high irradiance locations where modules operate for extended periods at 1000W/m^2 and higher where maximum power point current is highest. Moreover, this design optimizes energy generation for these large cell products in sunny locations.

Outdoor performance and reliability of ½ cell module concept

The half cell module designed under this program has the following additional safety features.

- More circuits protected by-pass diodes. This increase the shade tolerance
- Lower current on the cell (1/2 that of a full size cell) gives better resilience to point shunt defects.

BP Solar built an array that contains sub-arrays with following type modules:

- 60 cell module sub-array (full cell)
- ½ cell HVM (that is all 120 cells in series) module sub-array
- ½ cell HPM (that is 60 cells in series with 2 parallel strings) module sub-array

In each case we shaded an area of 243 cm^2, the area of one full sized cell in each sub-array. The ac power output of each sub-array is shown in Figure 5.6 for a week in January, 2009. The shaded HVM sub-array produced 52% more kilowatt-hours than the shaded control – full cell sub-array. The shaded HPM sub-array produced 23% more kilowatt-hours than the shaded control – full cell sub-array.

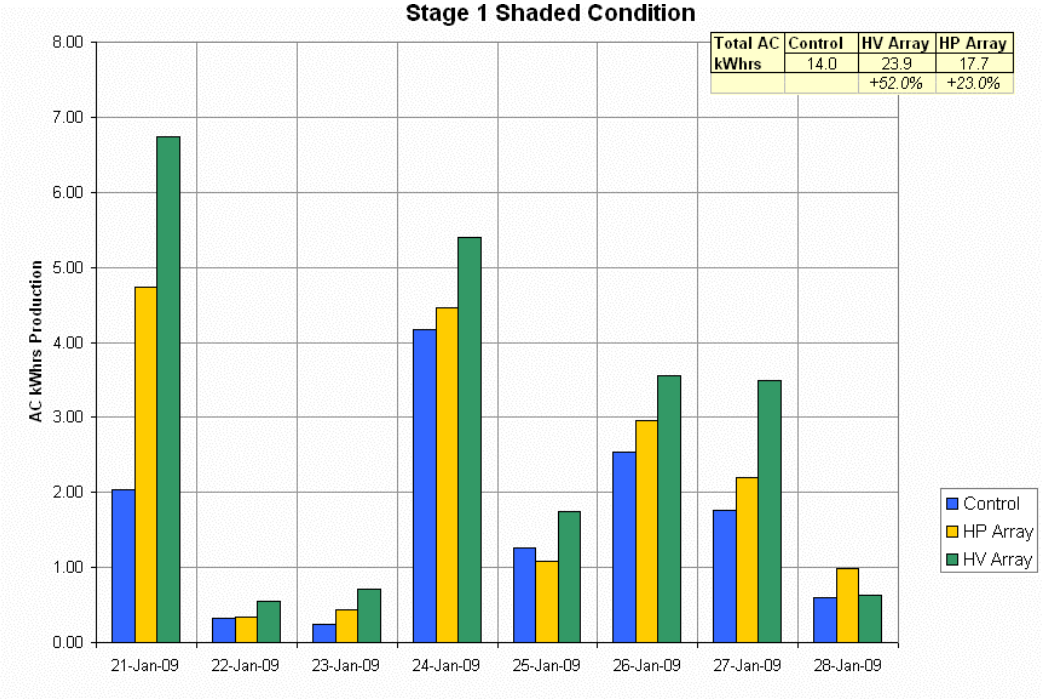

Figure 5.6: The daily power output of each sub array with an area of 243 cm^2 shaded in each sub array

This design innovation is planned to be rolled out in BP Solar Utility size modules in 2010.

Energy Enhancement, Thermal: Reduced module operating temperature

One of the major contributing factors to reduced module performance in the field is heat generation. Because solar cells are not 100% efficient at converting sunlight to electrons, a high percentage of the light that is absorbed is converted to heat energy which raises the temperature of the cell. In the module, the actual operating temperature of the cell can be higher than ambient temperature by 30^oC or more. Due to physical properties of solar cells, this reduces the cell voltage and reduces cell efficiency. While some semiconductors have less reduction than others, all solar cell efficiencies are reduced by increased temperature. For crystalline silicon solar cells, there is approximately 0.45% power reduction for every 1^oC increase in temperature.

The schematic in Figure 5.7 shows the simple thermal model used to calculate the influence of thermally conductive encapsulants on module temperature. In this figure, T1, T2, and T3 are the interface temperatures of the cell/EVA, EVA/back sheet, and back sheet to air respectively. K1 and K2 are the thermal conductivity coefficients of the EVA encapsulants and back sheet respectively while L1 and L2 are the corresponding thicknesses of these components. Figure 5.8 shows how these components come together as a mathematical expression to illustrate the total thermal resistance in a solar module.

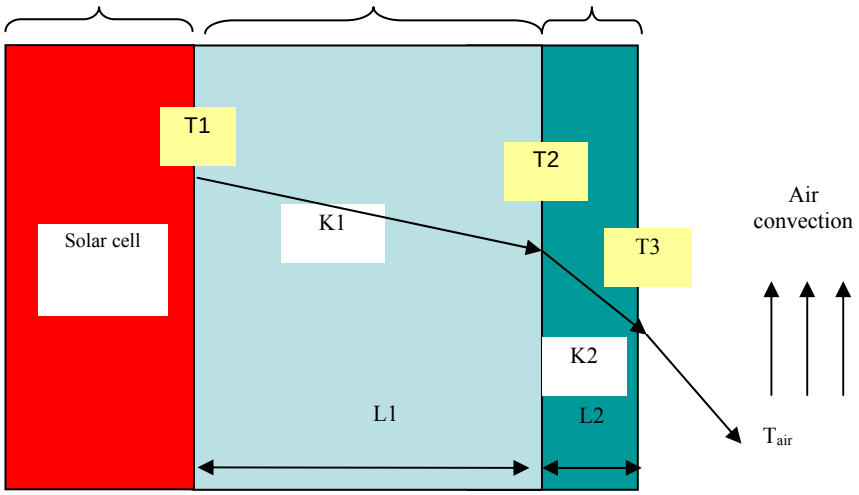

Figure 5.7: Schematic of Solar Module and respective components that affect cell junction temperature.

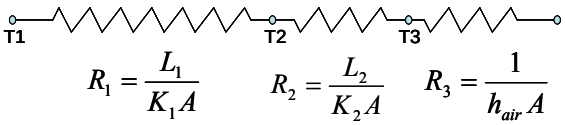

Figure 5.8: Thermal resistance equation

At BP Solar under the TPP project, we have been investigating the effect of improving thermal conductivity of encapsulants on the deployed performance of solar modules. With this type of encapsulant, it is important to have a high thermal conductivity and a low electrical conductivity so that the modules retain their insulation properties. BP Solar has been investigating a number of potential compounds and has been modeling the thermal properties before compounding these materials. To prove performance in the field, BP Solar initially made modules with these materials made incorporated into mini and determined their outdoor performance under various conditions.
An example of the gain, from one of the first trials where samples were made by casting the EVA encapsulant is shown below in figure 5.9.

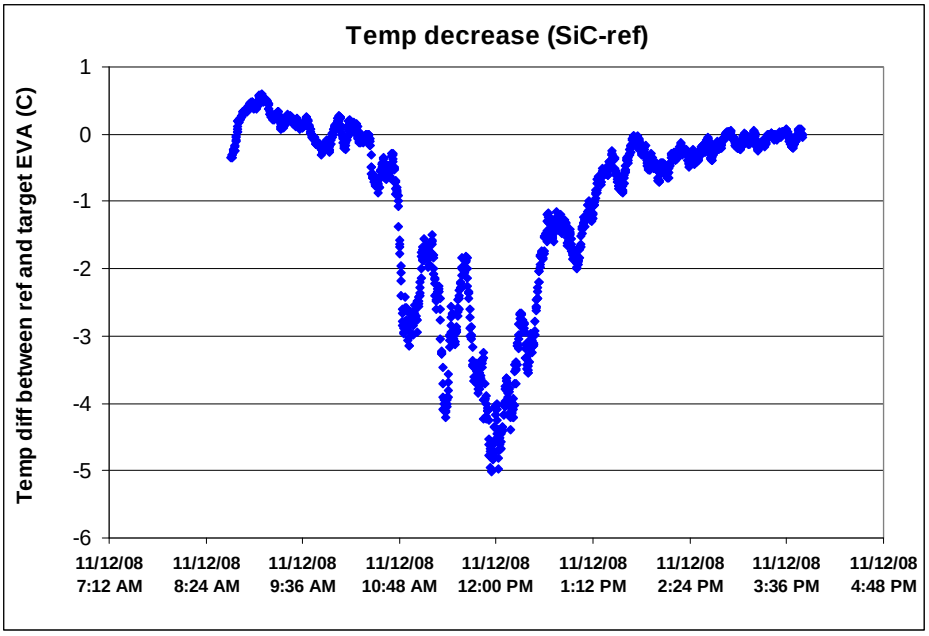

Figure 5.9. Mini-module temperature compared to a standard EVA control.

In order to prove the mathematical model, module samples were fabricated with various formulations of thermally conductive encapsulants. These modules were made along side control modules using our standard encapsulant. The modules were deployed at BP Solar in Frederick, Maryland and measured using a DayStar maximum power point tracker and data acquisition system. Along with the module electrical data, irradiance, ambient and module temperature plus wind speed were also measured. The modules maximum power was recorded every 1 minute. From this, the total daily energy was calculated and normalized by their STC power to generate Performance Factor. The difference in the modules performance factor is plotted as a function of time of day in Figure 5.10.

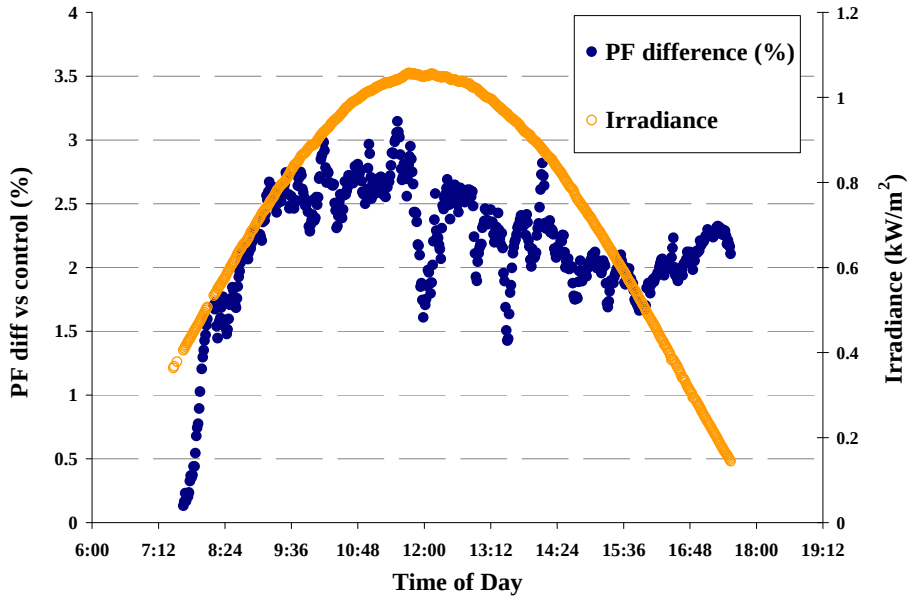

Figure 5.10: PF percentage difference for module made with thermally conductive encapsulant compared to a control module versus time of day.

The optimal formulation (combination of additives) was established using a number of comparative outdoor trials using the BP Solar DayStar system. At BP Solar, we have also made 72 cell (125mm multi-crystalline silicon) modules with improved EVA formulations. Samples with these formulations have been made and outdoor test results showed a 1-3% energy gain over controls. Figure 5.11 shows the energy gains for these different formulations below and the range associated with the different compositions.

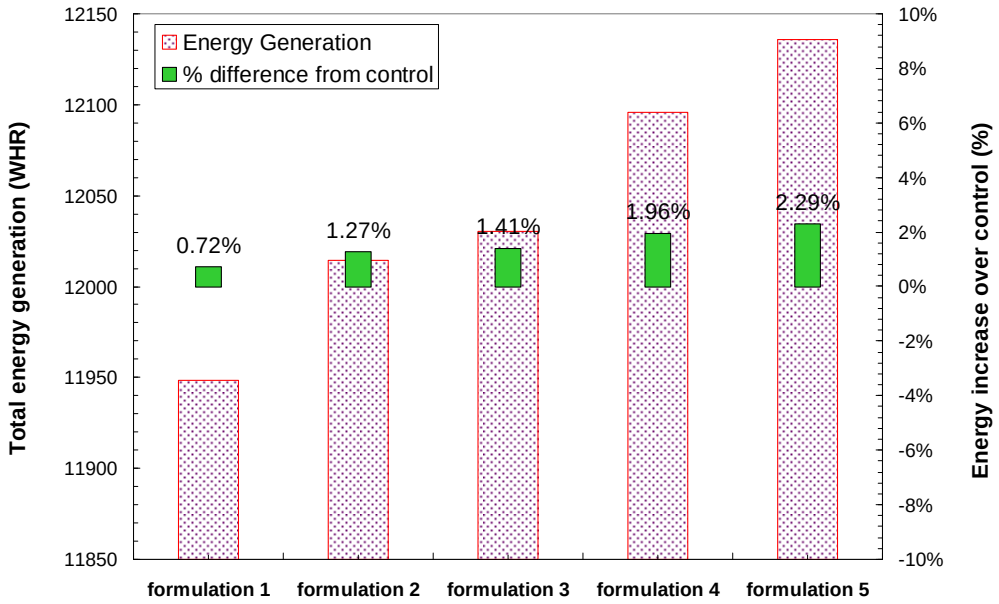

Figure 5.11: outdoor energy for filled EVA formulation vs. control modules

Modules with these filled EVA also have passed the internal BP Solar accelerated testing (BP Solar test name, Q6000).

The commercialization plan for this important new innovation will commence in 2010.

Module Reliability.

EVA and back sheet stability and longevity: Reaction rate modeling.

In order to better understand the relationship between material degradation and stress conditions, we have been undertaking a series of accelerated stress tests. Materials evaluated during the study are EVA and PET back sheet. We have evaluated the performance of the material alone as well as that of 4 cell mini-modules. Aging conditions evaluated to date were: 85°C/85%RH, 85°C/95%RH, 124°C/20psi and UV aging perform at 90°C black panel temperature with irradiance of 0.7W/m^2. The degradation rate for each condition was compared with that at the standard 85°C/85%RH condition. The parameters used to measure the degree of degradation include percent

light transmission and change in crystallinity. For the mini-modules, degradation of maximum power (Pmax) was monitored.

The results are shown in Figure 5.12. For the loss in light transmission, the most severe condition was 124°C/20psi when compared with 85°C/95%RH and 85°C/85%RH. After 1000hr, light transmission of EVA decreased about 2.7% under 85°C/85%RH and 2.4% under 85°C/95%RH. The same amount of light transmission loss occurred after only 56 hours at 124°C/20psi condition. Chemical and thermal analysis showed most of the light loss was due to the increase in the crystallinity in EVA and the increase in yellowness. Of course care must be taken when interpreting the results as the increase in crystallinity and yellowing may not occur at all under normal operating conditions.

For the aging of PET based back sheet, we used crystallinity as a measure. For semi-crystalline polymers, crystallinity increases with aging. With the increase in crystallinity, the volume of polymer decreases and ultimately surface cracking will occur. Figure 5.13 shows the crystallinity of PET based back sheet versus time under different aging conditions. The most severe aging condition was 124°C/20psi, followed by 85°C/85%RH and 85°C/95%RH. UV aging had the least impact on crystallinity.

Using 85°C/85%RH as a reference condition, aging acceleration factor (AA) for each condition can be calculated by comparing the slope of each condition in Figure 5.13. The values are listed below:

1) AA=37 for 124°C/20psi;
2) AA=0.85 for 85°C/95%RH;
3) AA=0.46 for UV aging;

Based on this work, to reach the same amount of final crystallinity in PET aged at 85°C/85%RH for 1000hr, one would only need 34hours at 124°C/20psi.

Figure 5.14 shows the correlation between power loss and different aging conditions. The most severe condition was once again124°C/20psi followed by 85°C/95%RH and 85°C/85%RH. The AA for 124°C/20psi was 120 and 85°C/95%RH was 3. Based on this analysis, at 85°C, for 10% increase in relative humidity, the module power degradation rate was tripled. In other words, for 85°C/85%RH 1000hr, the equivalent aging time at 85°C/95%RH was 330hr.

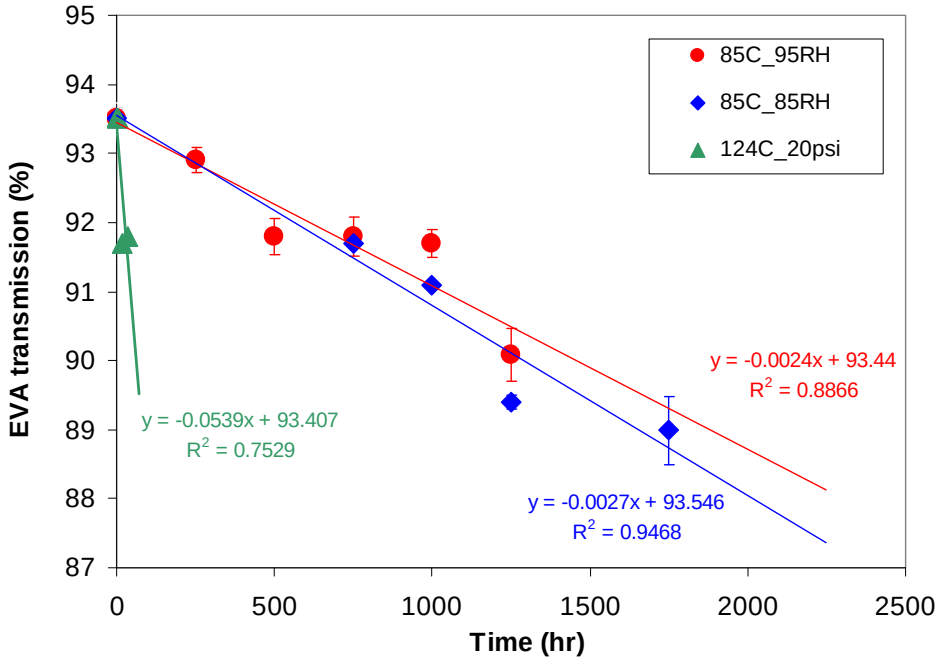

Figure 5.12: Light transmission rate of EVA aged under different conditions.

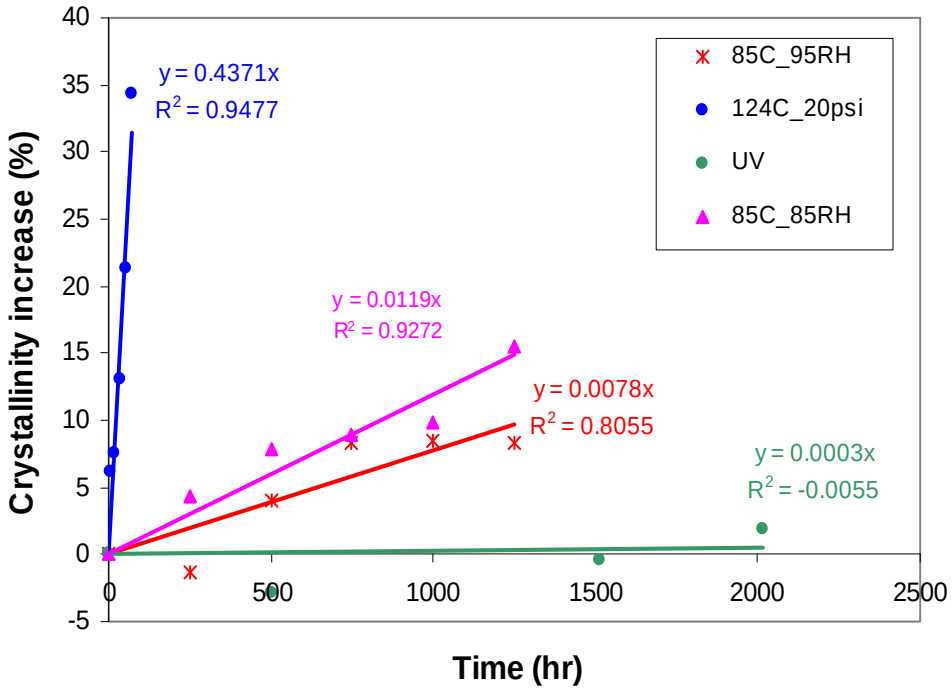

Figure 5.13: Increase in crystallinity under different aging conditions (first heat)

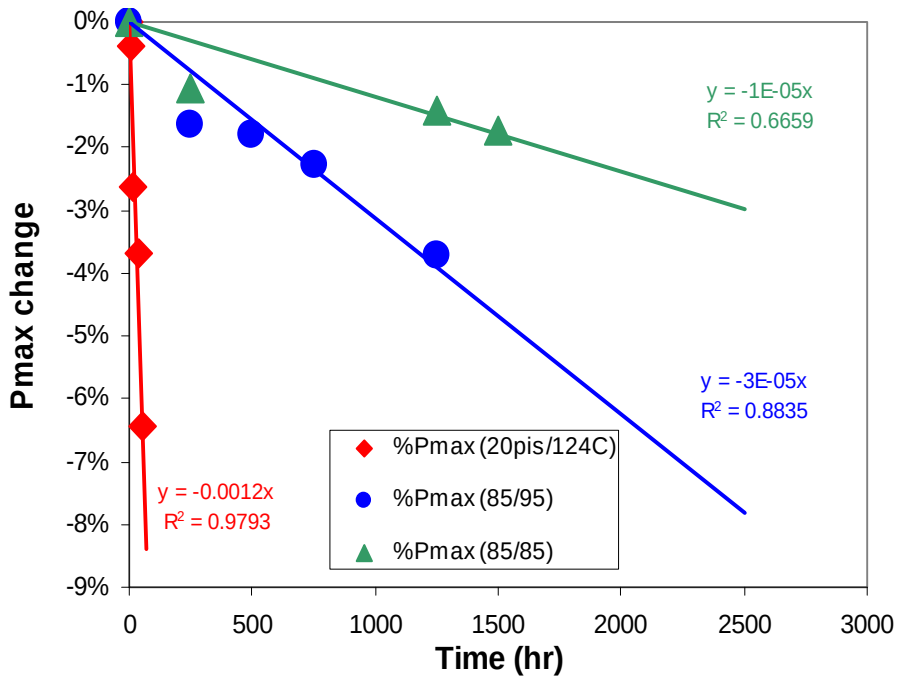

Figure 5.14: Maximum power loss at different accelerating conditions

We evaluated both the William Landers Ferry (WLF) theory and the Arrhenius theory for their applicability to EVA and polyester degradation. The Arrhenius theory appears to work better. Using the literature values of activation energy for EVA and polyester yields the curves in Figure 5.15. According to this analysis our 1250 hour damp heat test is equivalent to approximately 17 years of exposure of EVA and 24 years of exposure of polyester at 65°C. Since polyester has a glass transition of 80°C, 85°C will tremendously accelerate the aging of PET. More accurate measurement of the aging activation energy is needed. We plan to determine these using a laboratory environmental chamber.

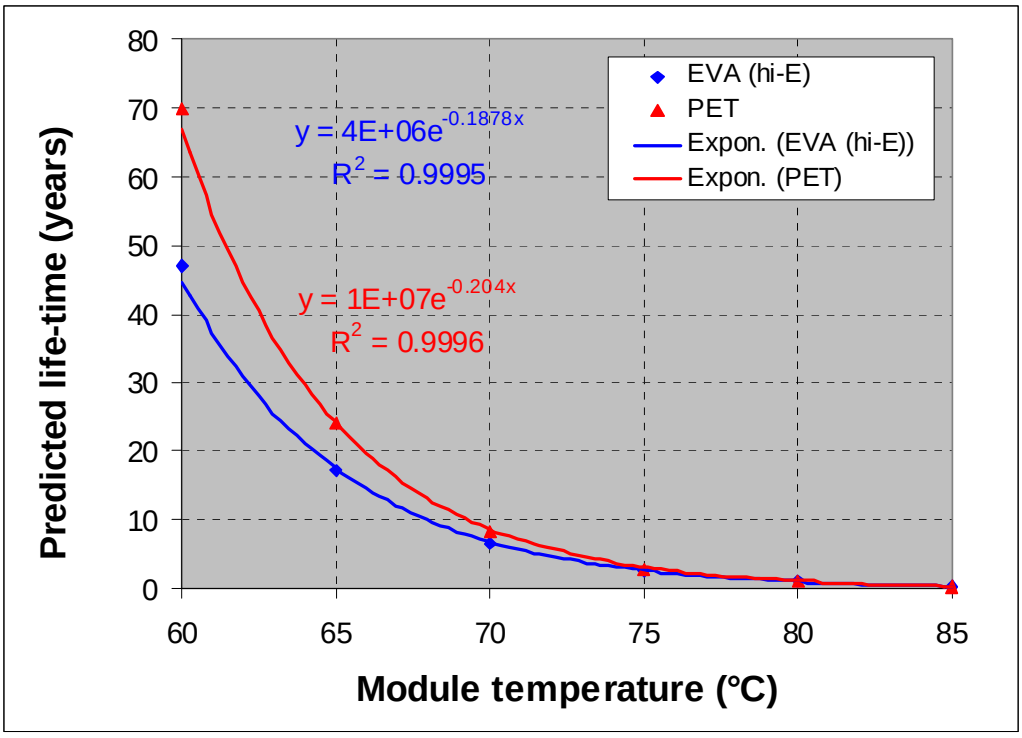

Figure 5.15: Predicted material lifetime for EVA and polyester

Influence of reduced solder joint quantity on long term reliability

Studies were performed at the Frederick development center to understand the effect of reducing solar cell solder joints on the long term reliability of the module. This work was performed in collaboration with the Module technology team and the Process Engineering team in Frederick.

For this study, an experiment was designed where cells strings were fabricated and solder joints were intentionally left out. Two cell designs were used, 125mm x 125mm cells with an Isc of 5.4A and 156mm x 156mm cells with an Isc of 8.4A.

For the 125mm cells, BP Solar make 5 solder joints on the front surface and 3 solder joints on the back. For the 156mm cells, BP Solar uses 6 solder joints on the front and 3 on the back.

The following combination of string designs was used:

- 12 cell strings, 125mm cells:
  - Front bus bars: 3, 2, and 1 solder joint per bus bar.
  - Back bus bars: 3, 2, and 1 solder joint per bus bar.
- 10 cell strings, 156mm cells.
  - Back bus bars: 3, 2, and 1 solder joint per bus bar.

Initial IV measurements were made using a Spire IV flash tester. After this, the laminates were placed in accelerated test chambers and exposed to thermal cycling (-40C to -85C) for a total of 500 thermal cycles. As per IEC requirements, all strings were held at a current equivalent to Isc for all temperatures above 25C. This is in line with IEC61215 edition 2.

At the end of this test, the strings were IV tested and reviewed for any change in performance.

The results for the test are shown in the graph below (Figure 5.16). The following points describe the features reported in the graphs.

- B = back. F = front
- B 3 (3 functioning joints) to B 1 (1 functioning joint).

Some preliminary conclusions from the study are as follows.

- Left hand data points (stars) show a small effect in reducing the number of solder contacts for **125mm cells**.
- Maximum fill factor drop is about **-5%** for these cells.
- For the **156mm cells** the sensitivity to losing active solder joints is much larger.
- In this case the FF losses progress from **-10% to -25% and -30%**
- **This indicates the stress generated for current densities is much higher for 156mm than 125mm**

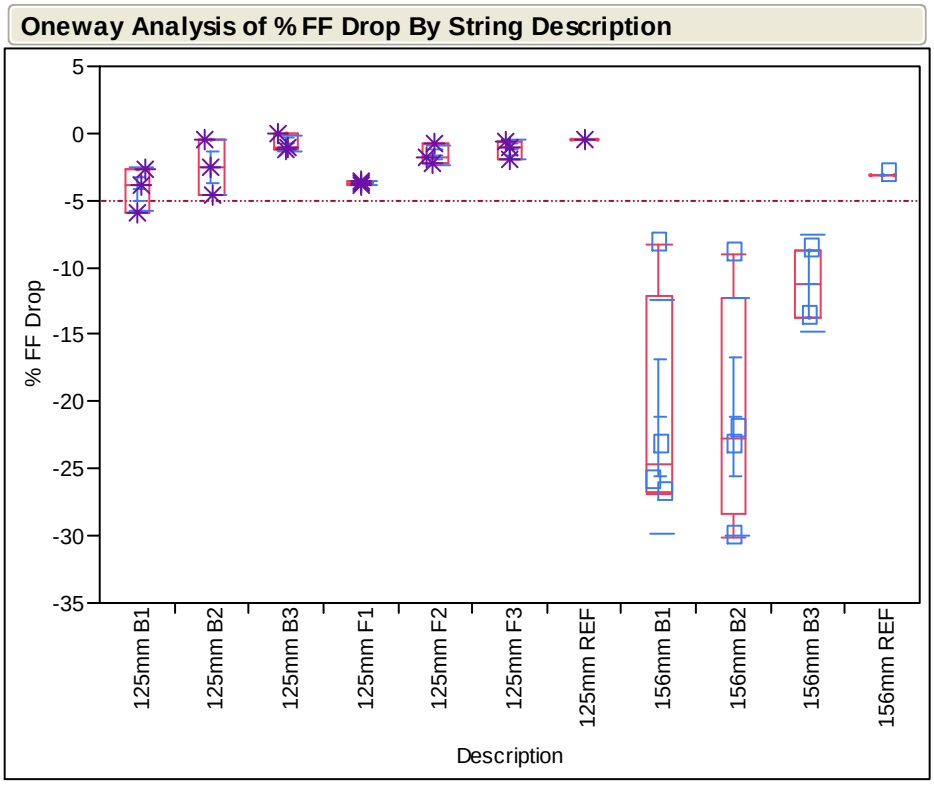

Means and Std Deviations

Level	Number	Mean	Std Dev	Std Err Mean	Lower 95%	Upper 95%
125mm B1	3	-4.143	1.64610	0.9504	-8.23	-0.0542
125mm B2	3	-2.527	2.11013	1.2183	-7.77	2.72
125mm B3	3	-0.757	0.64065	0.3699	-2.35	0.83
125mm F1	3	-3.717	0.17616	0.1017	-4.15	-3.28
125mm F2	3	-1.587	0.73105	0.4221	-3.40	0.23
125mm F3	3	-1.203	0.71178	0.4109	-2.97	0.56
125mm REF	1	-0.390	.	.	.	.
156mm B1	4	-21.165	8.67933	4.3397	-34.98	-7.35
156mm B2	4	-21.145	8.83462	4.4173	-35.20	-7.09
156mm B3	2	-11.215	3.59917	2.5450	-43.55	21.12
156mm REF	1	-3.140	.	.	.	.

Figure 5.16: Fill Factor change after 500 thermal cycles: 156mm and 125mm cell strings.

The images in Figure 5.17 show the 156mm cell laminates after 500 thermal cycles while Figure 5.18 shows the 125mm cell laminate after 500 thermal cycles. The image on the left is generated using standard thermal IR photography. This looks at differences in (heat) temperature within the cell strings under forward bias at short circuit current levels. The image on the right shows the same cells strings but viewing the cell electroluminescence under the same forward bias conditions.
The thermal infra red shows significant non uniformities in temperature for the single solder joint strings.

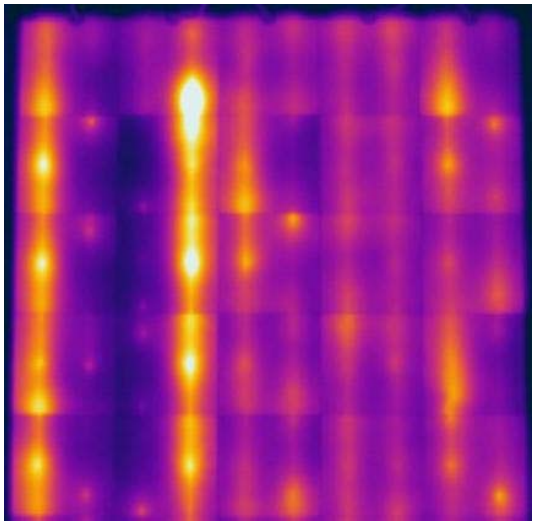

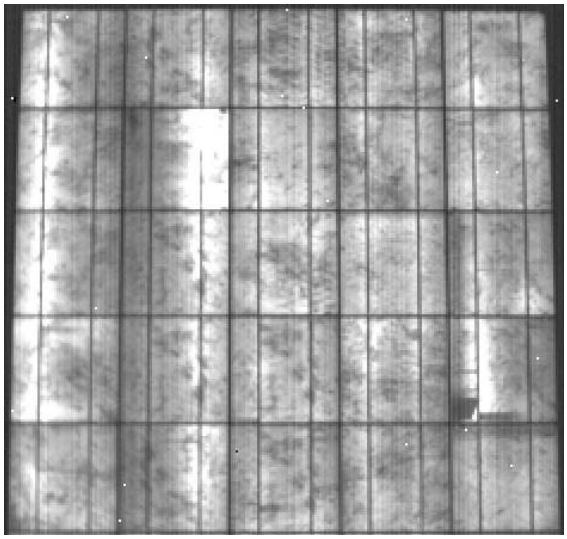

Note: Both images are post 500 thermal cycles.

Figure 5.17a: Thermal IR for 156 mm cells.

Figure 5.17b: EL image for 156 mm cells.

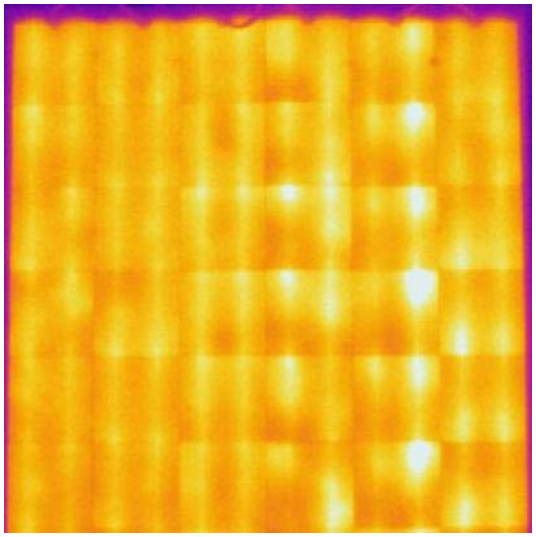

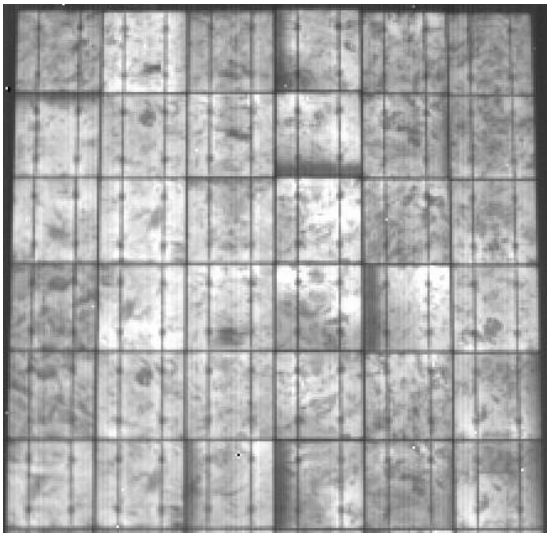

Figure 5.18a: Thermal IR for 125mm.

Figure 5.18b: EL image for 125mm.

Crack tolerance in modules using conventional front/rear contacted solar cells.
The question of whether you can build cells and modules on thin wafers is mostly a yield issue as models show that 100 μm of Si is enough material to absorb adequate sunlight to achieve high conversion efficiencies. So the question becomes, "Do thin cells have a greater likelihood of cracking during production, transport, installation or use", and if so "Does this result in long term degradation of the power"? The present qualification test

sequence, IEC 61215 does not adequately address this issue. The only mechanical test in IEC 61215 is a mechanical load test consisting of only three load cycles that are performed after the accelerated stress tests. So even if this mechanical load test does break cells, it is unlikely to result in significant power loss.

BP Solar has developed a test sequence for evaluation of cell breakage in PV modules. The test sequence incorporates a dynamic mechanical load test performed before the 50 thermal cycles/10 humidity freeze cycles of IEC 61215. The magnitude of the dynamic load test has been set at approximately 20 pounds per square foot, a level that causes cracks in already damaged cells to grow, but does not appear to crack undamaged cells. For the initial tests, modules were tested for increasing load cycles. Breakage appeared to saturate by 1000 cycles so this was chosen as the number of cycles in the sequence. Usually there is no significant power loss after the dynamic mechanical load testing. However, the subsequent thermal cycling opens up the cracks that propagated during the dynamic load test resulting in significant power loss. In addition to measuring output power, an IR camera is utilized to record the growth of cell cracks.

During this quarter the following thin cell reliability activities have been undertaken:

- Modules with 175 μm thick 125mm by 125mm cells were tested in thermal cycling, damp heat and humidity freeze. Included in this was the pre-conditioning of modules by dynamic loading. The module size for these tests was 1.25m^2, in a 12 x 6 cell configuration.
- Modules with 180 μm thick 156mm by 156mm cells were tested in thermal cycling, damp heat and humidity freeze testing. Included in this was the pre-conditioning of modules by dynamic loading. The module size for these tests was 1.667m^2, in a 10 x 6 cell configuration.
- Analysis and evaluation of modules returned from the field. These modules were inspected for cell breakage and then subjected to accelerated testing to predict end of life performance.

In all cases we have used both the standard post stress tests (IV, visual inspection and wet and dry high-pot) as well as infra red photography to illustrate and monitor changes in the inter-connect and cell integrity. The near infra red images (approx 1150nm) are particularly useful for illustrating cell breakage. The far infra-red (>2000nm) technique is useful to identify issues with over heating at inter-connects and bus bars.

Table 5.3 shows the change in electrical performance for the modules with 175μm thick multi-crystalline cells after accelerated testing. All of these modules have passed the test with less than 5% power loss. (Please note that the column for 10 humidity freeze cycles included 1000 mechanical load cycles and 50 thermal cycles before the 10 humidity freeze cycles).

Table 5.3: Electrical results for modules with 175 µm thick multi crystalline cells after accelerated stress testing

175 micron Multi Crystalline cells in 72 cell modules	20-Sep-07				11-Dec-07							
	Initial (After LID)				After 500 thermal cycles							
S/N	Voc V	Isc A	Pmax W	FF	Voc V	Change %	Isc A	Change %	Pmax W	Change %	FF	Change %
6246171 Sample 1	44.0	5.13	168.1	0.75	44.1	0.2%	5.02	-2.1%	163.8	-2.6%	0.74	-0.6%
6640293 Sample 2	43.9	5.11	168.5	0.75	44.0	0.2%	5.01	-2.0%	164.6	-2.3%	0.75	-0.5%
6640378 Sample 3	44.0	5.10	168.9	0.75	44.0	0.1%	5.02	-1.5%	164.4	-2.7%	0.74	-1.3%
	Initial (After LID)				After 10 humidity freeze cycles							
6640779 Sample 4	43.9	5.11	168.6	0.75	43.8	-0.3%	5.05	-1.1%	165.2	-2.0%	0.75	-0.6%
6653815 Sample 5	43.9	5.10	167.8	0.75	43.8	-0.3%	5.02	-1.5%	161.9	-3.5%	0.74	-1.8%
6660114 Sample 6	44.1	5.13	170.4	0.75	43.9	-0.5%	5.07	-1.2%	162.8	-4.5%	0.73	-2.9%

This does not mean that we are not seeing cracked cells caused by the accelerated testing. Figure 5.19 is a near NIR picture showing 15 cells within one of the modules made with 180 µm thick 156 mm by 156 mm cells. Figure 5.19a is before any accelerated testing. Figure 5.19b is after exposure to 1000 mechanical loading cycles. The loading has cracked one cell across the whole cell and broken a piece out of another cell without reducing the power significantly.

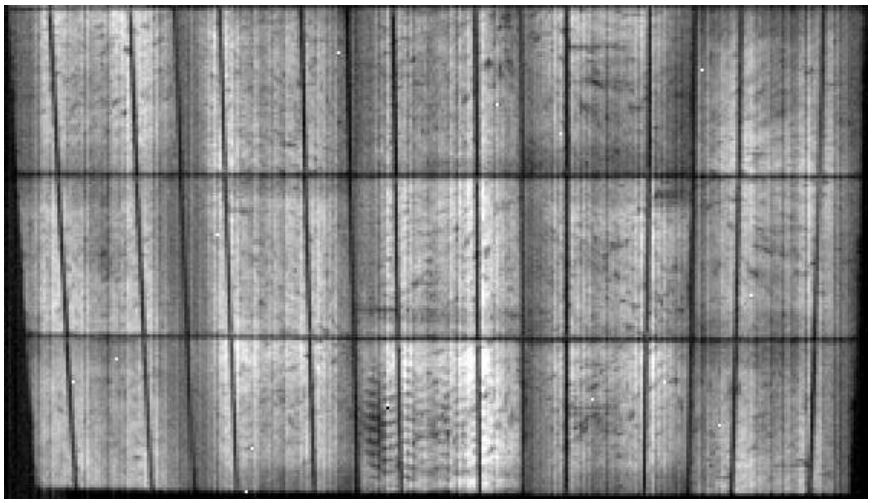

Figure 5.19a: 180 µm thick, 156 mm by 156 mm cells before accelerated testing

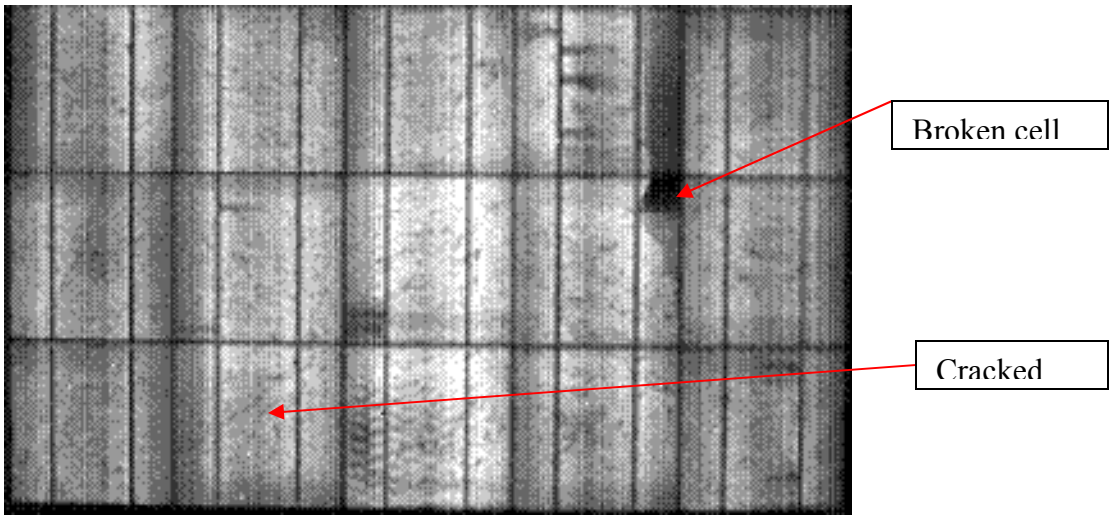

Figure 5.19b: 180 µm thick, 156 mm by 156 mm cells after dynamic loading

Samples of fielded modules are under investigation to determine long term stability. This is of interest and relevant to our program as they have known numbers of broken cells. The cells are single crystalline and the modules have been in the field for up to 4 years. Figure 5.20 shows the power loss suffered as the modules have been subjected to the accelerated testing consisting of 1000 mechanical load cycles followed by 50 thermal cycles. None of these modules have experienced more than 5% power loss, with most having less than 2% degradation.

Figure 5.20: Power change for previously fielded modules

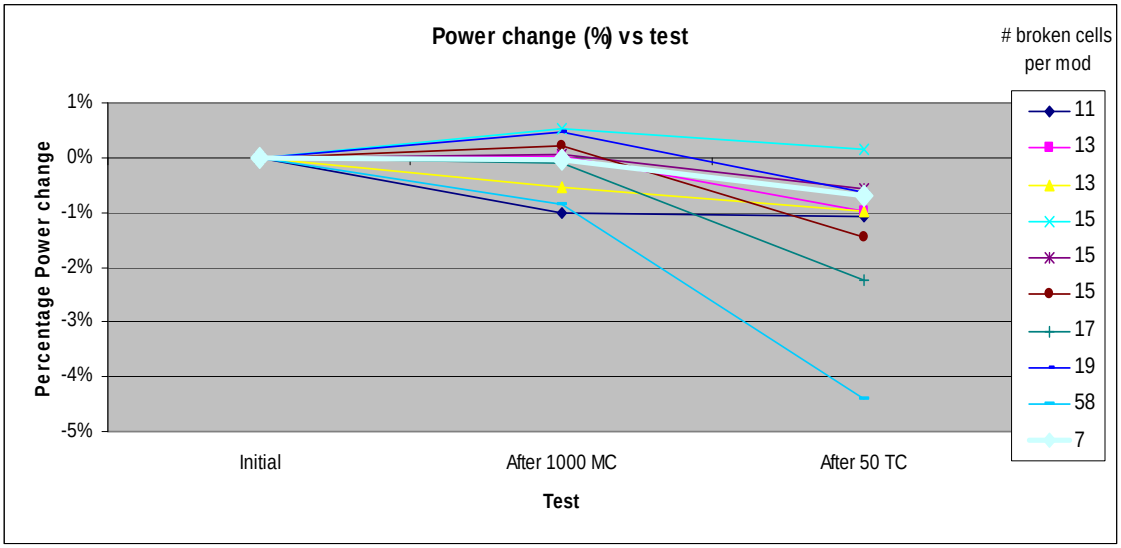

The pictures in Figure 5.21 show four rows of cells from a module that had been in the field for 3 years. The module was imaged using the NIR to identify cell breakages. The module was then subjected to 1000 mechanical cycles followed by 50 thermal cycles. The images show the progression of cell cracking through these sequences. The total power loss for this module was only -1% of its original power (i.e. 99% unchanged). This is a good example of the robustness of silicon modules against cell breakage.

Figure 5.21a: Field module: Initial image on return

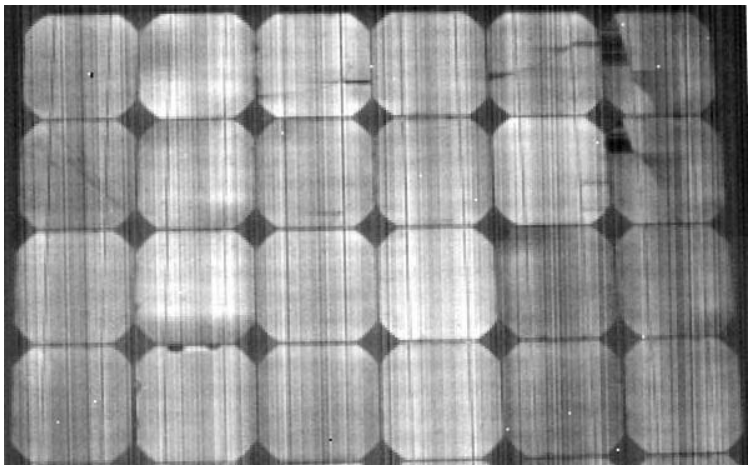

Figure 5.21b: Field module: After 1000 mechanical cycles

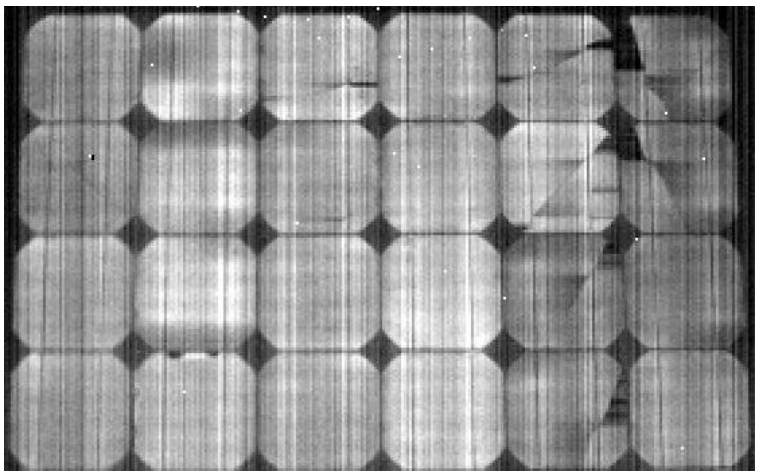

Figure 5.21c: Field module: After 1000 mechanical cycles and 50 thermal cycles

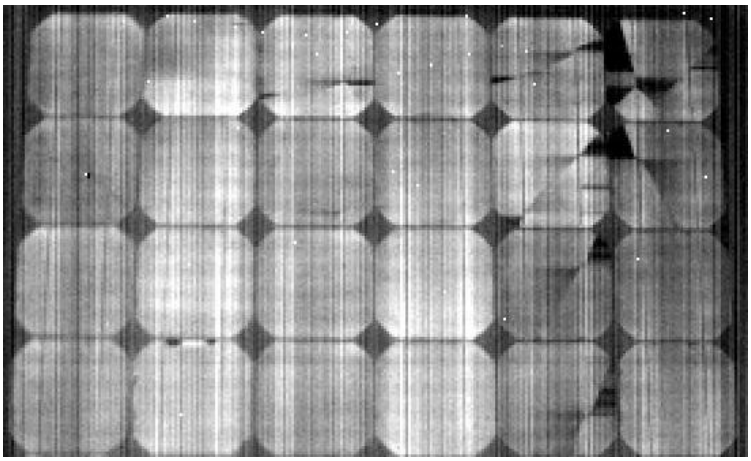

Module operation at high voltage: FSEC High Voltage Testing of Modules
Under the previous BP Solar Photovoltaic Manufacturing Technology Program (NREL Contract # ZAX-6-33628-11 entitled "Development of Large High-Voltage PV Modules With Improved Reliability and Lower Cost"), the Florida Solar Energy Center (FSEC) constructed and has been operating a high voltage test bed for evaluation of PV module performance. This effort was transferred to the TPP program.

The objective of this FSEC project was to carry out accelerated testing of PV modules deployed in hot and humid climate under very high voltage bias conditions so as to understand correlation, if any, between the leakage current and corrosion and subsequent power loss or dielectric breakdown. The system was populated with 4 modules, 2 of which are biased +1500 volts to ground and 2 that are biased -1500 volts to ground. Leakage current, back of module temperature and relative humidity are recorded during the course of each day. Figure 5.22 shows a typical plot for a sunny day. As the modules heat up during the day the leakage current decreases apparently because the sun induced heating drives the moisture out of the encapsulant.

Figure 5.22: Plot of leakage current and relative humidity for a sunny day

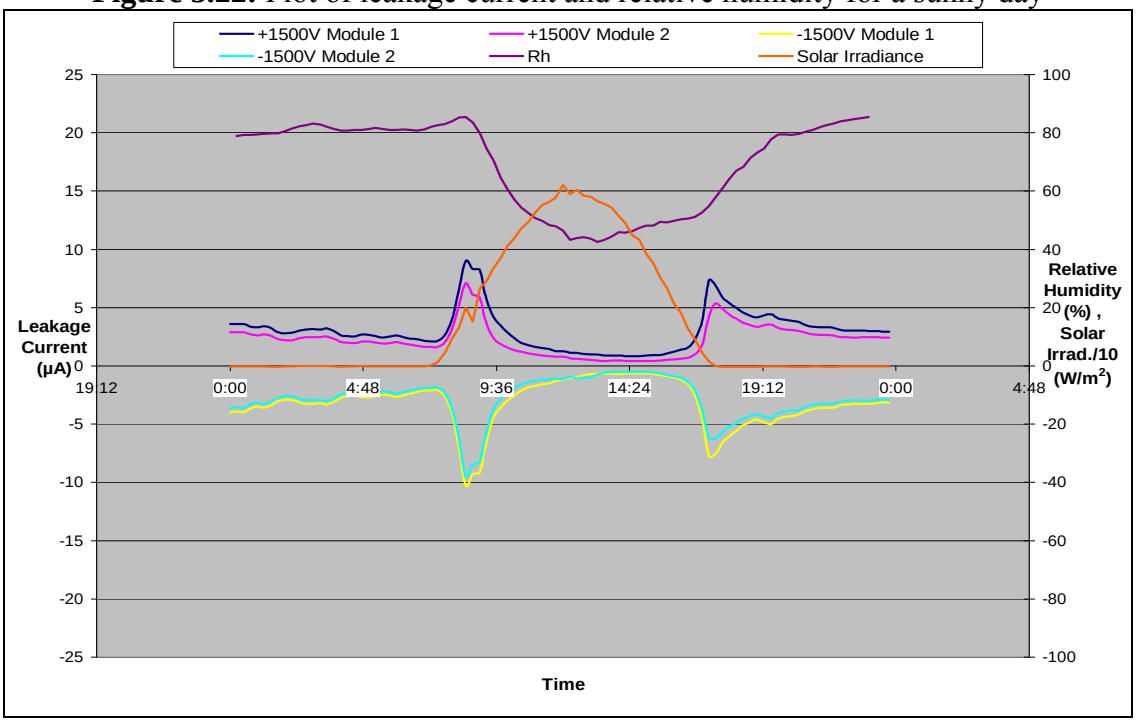

In addition, 3D graphs are plotted for each day with back of the module temperature, relative humidity and leakage current on the x, y and z axes respectively. Figure 5.23 shows the daily 3D plot of leakage current for one of the positively biased modules.

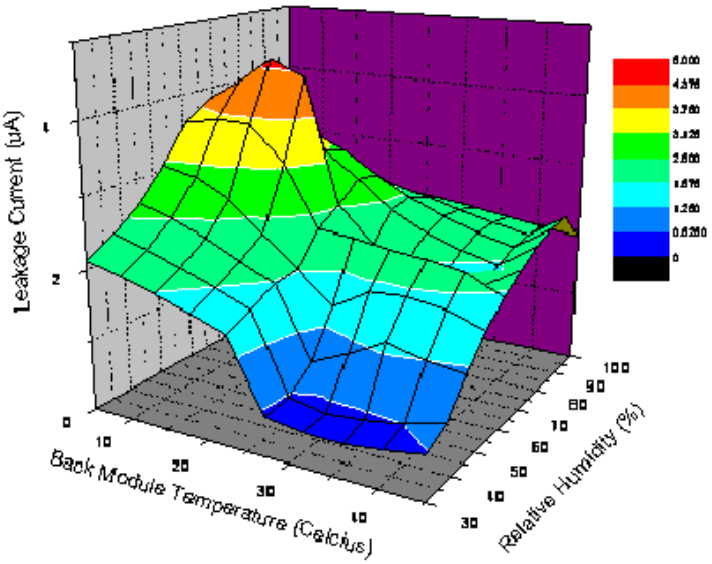

Figure 5.23: 3-D graph of leakage current versus back of module temperature and relative humidity for one +1500 V biased module on a sunny day

The high voltage test structure at FSEC was a very important tool to understand how

modules at high ground bias in humid conditions. As PV systems move to a Utility scale dimension in the US, the characteristics of the modules under these conditions will drive the choice of materials to ensure long term reliability.

Module frame performance studies under static loading.
The ability to mount a module in various climates and withstand loading is an important element of the capability of a PV module. While the frame (aluminum in most cases) is used to mount and support the module, the adhesive used with it has an important roll to play in the overall robustness. The adhesive acts to hold the laminate in the frame and transfer the stresses from wind load and, in worse case, snow load. The fundamental mechanical properties of adhesives can be determined by performing tests described in standards. One method that BP Solar used to determine mechanical strength is DIN 53504.

Using this method, BP Solar designed molds to make sample shapes for the test and then used a Zwick tensiometer to determine the mechanical properties. See Figure 5.24 for the geometry of the test samples, Figure 5.25 for the testing system and Figure 5.26 for the results).

Figure 5.24: Example of sample preparation for frame adhesives: DIN 53504.

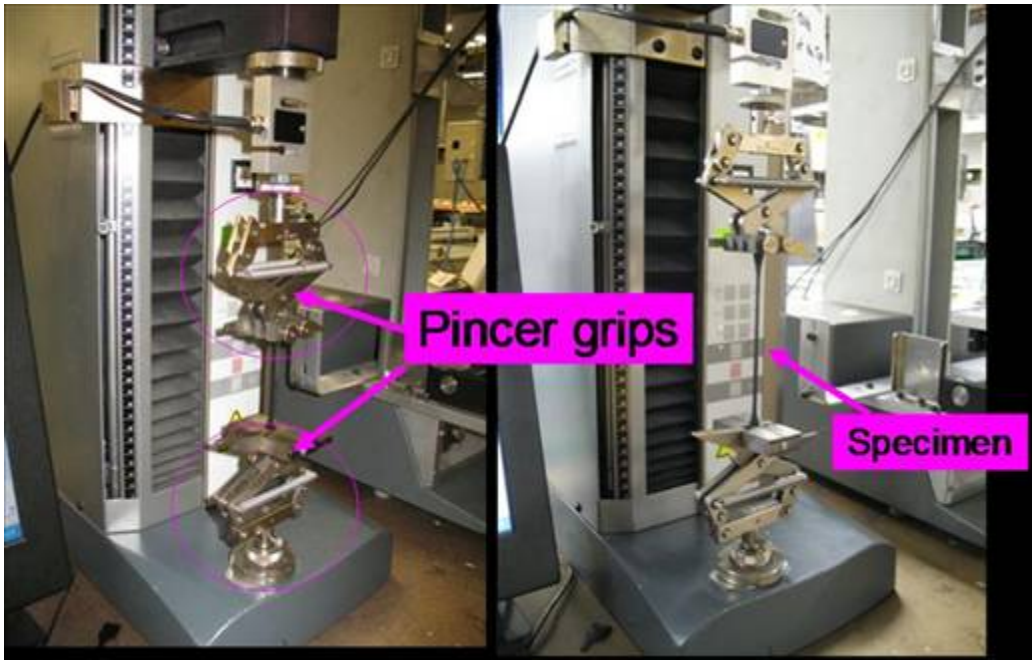

Figure 5.25: Samples under test (load) in the Zwick tensiometer (Model BDO-FB0.5TS)

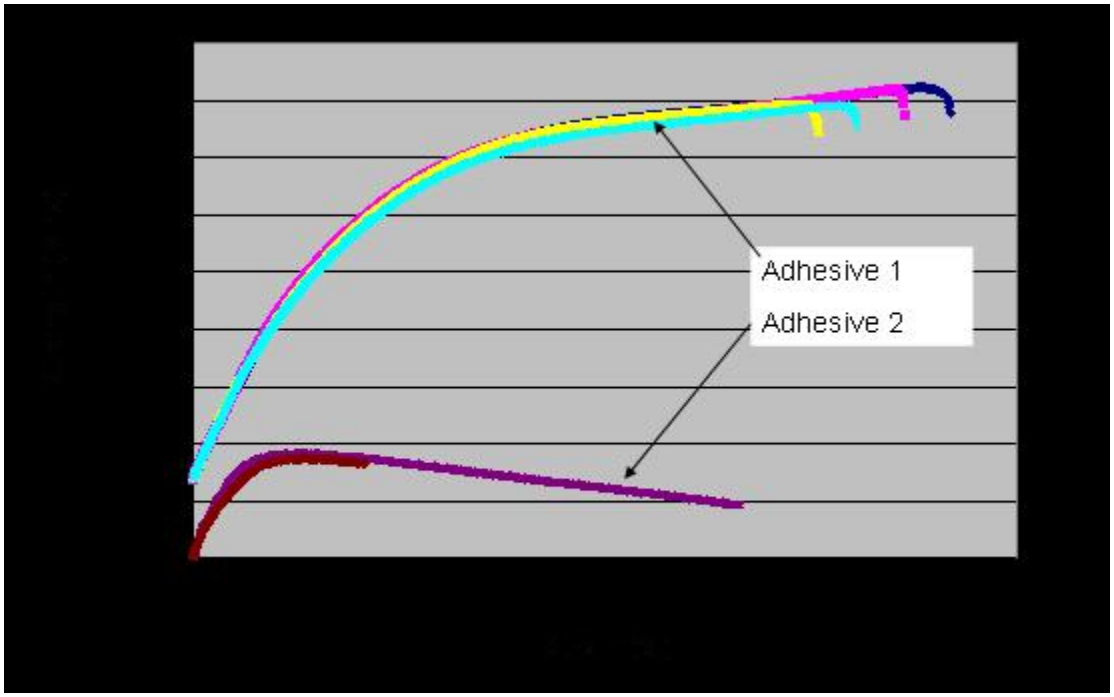

Figure 5.26: Example of two different frame adhesives and subsequent stress/strain curves generated in the procedure and apparatus described above.

BP Solar also designed a test to stress the module frame and measure deflection. This apparatus was designed to stress the module frame with a downward deflection, parallel to the glass laminate. This generated a bow deflection in the frame itself.

Some of the preliminary results are shown in Figure 5.27 for identical frames using the two different adhesives tested using the DIN standard. These results include both absolute tensile properties and deflection measurements from modules where two different types of adhesive were used.

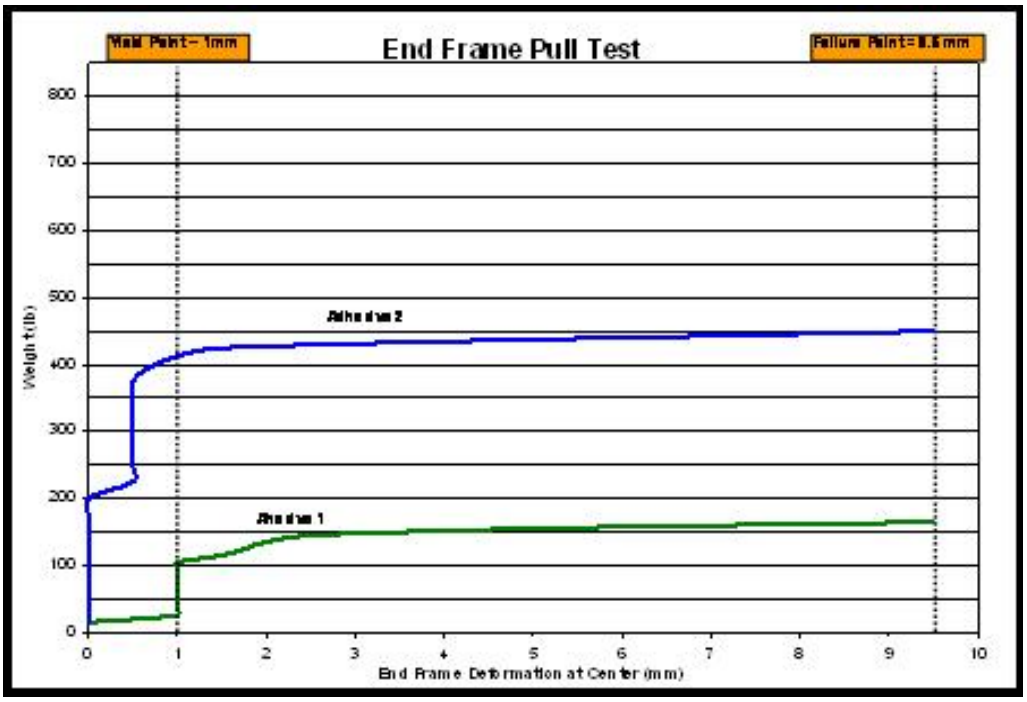

Figure 5.27: Adhesive 1 & 2 loaded in standard module configurations

It can be seen from the above graphs, that the correlation between the mechanical properties determined by the DIN method and the actual load test method on the frame correlate well. As a result, this method is being used to screen and select various frame adhesives.

Redesign of module for improved safety and reliability: Cable connections.
A new mechanical connector has been installed in the BP Solar product range as a result of activities funded by the DOE TPP project. The aim was to greatly improve contact reliability, making it fail safe and drive the design to a 6 sigma reliability goal. In 2.5 years through 2009, approx 0.25GW of product has been produced with this design and workmanship defects from the new connector have dropped to <10ppm from >50ppm for the previous design. The design is shown in Figure 5.28 and has been protected by a US and worldwide patent application.

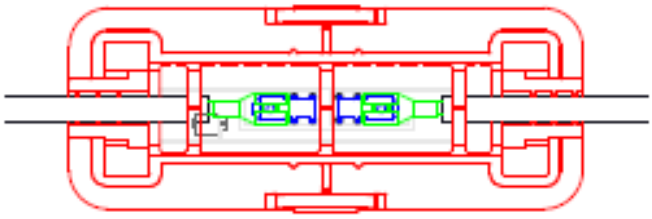

Figure 5.28: New junction box showing the clips (blue) and mating connectors (green)

The brass clip connector plating composition was changed to improve resistance to zinc diffusion, improve solder-ability and contact longevity. A thin Ni flash coating was added before tin solder plating. The XPS plot in Figure 5.29 shows plating composition after aging without the nickel barrier.

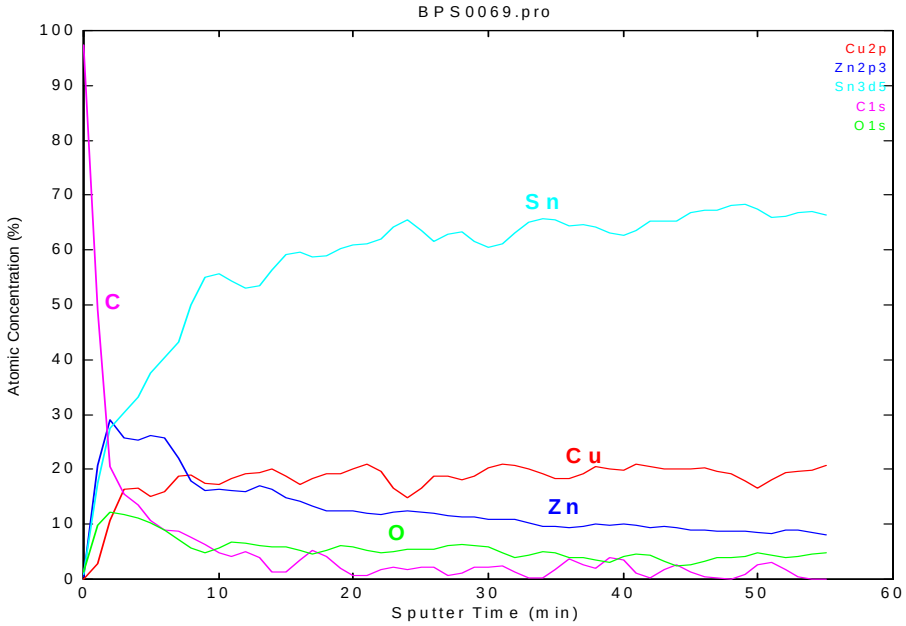

Figure 5.29: XPS plot of the plating composition of the clip made without Ni barrier after aging. Note the presence of copper.

In addition to the contact improvement, a silicone potant replaced the original epoxy potant. Silicone is non-flammable with a V0 UL fire rating. The contact cover/junction box material was also changed to increase its flammability resistance.

Module Encapsulants

EVA cure level method development

The PV industry has long been looking for a fast and reliable gel content test method to replace the traditional solvent extraction way. Differential Scanning Calorimetry (DSC) proved to be a very convenient way to measure EVA gel content. It can also provide the

onset curing temperature as well as the end of the curing temperature of EVA. Since the technique is based on monitoring the heat flux change of the sample, one can also detect the vinyl acetate content in EVA by DSC. Since it is so encouraging, BP Solar have purchased an DSC instrument as shown in Figure 5.30a. The DSC was used to measure STR fast cure EVA, yielding a nice correlation between extraction method and DSC as shown in Figure 5.30b. Data for samples from different BP Solar locations are also shown in Figure 5.31a through c.

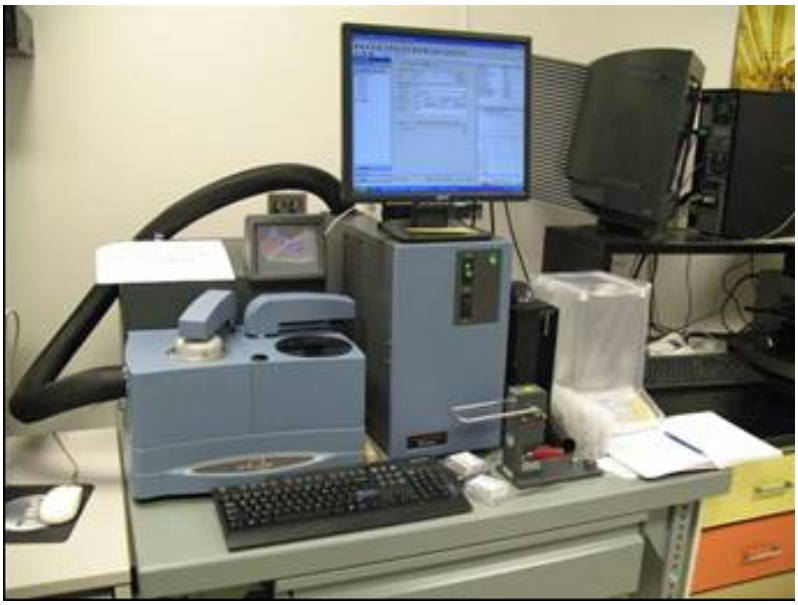

Figure 5.30a: Image of DSC Unit

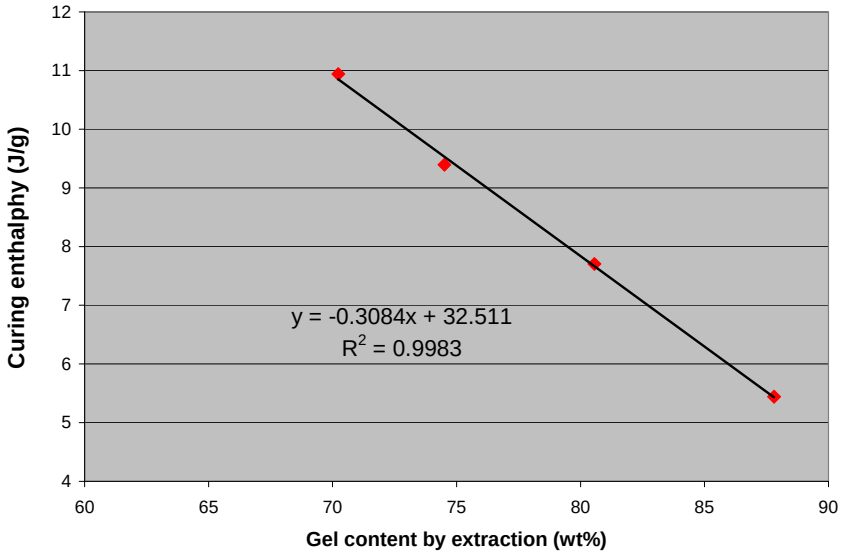

Figure 5.30b: Curing enthalpy vs. Solvent extraction gel content correlation study

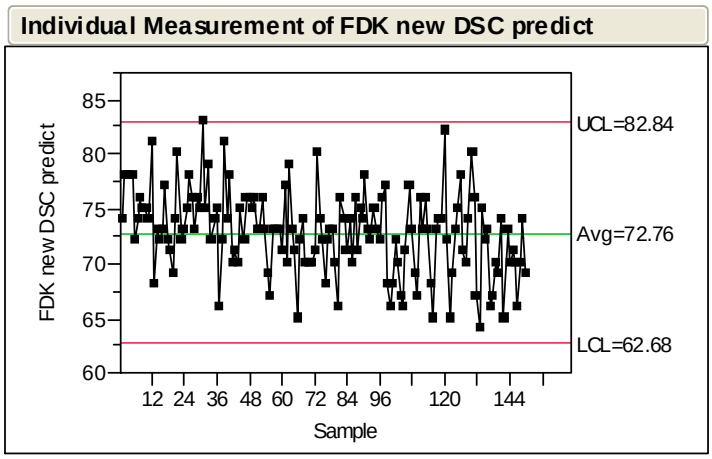

a) BP Solar Frederick

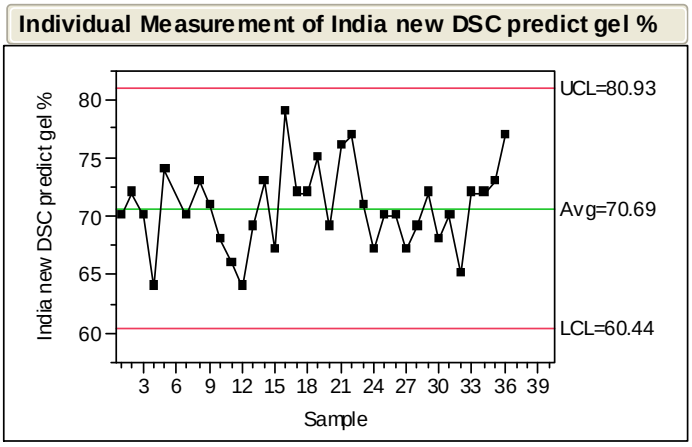

b) BP Solar India

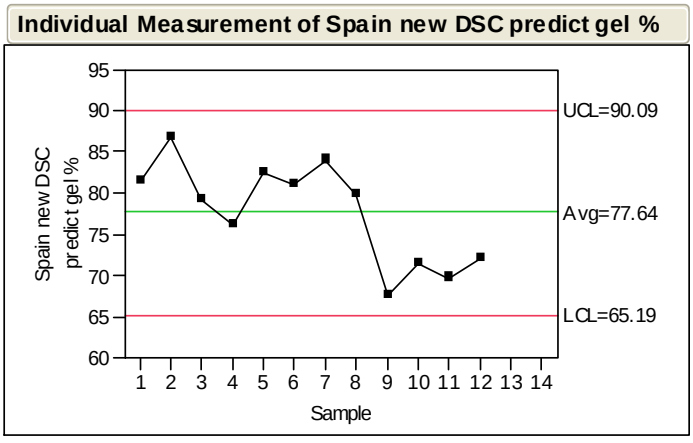

c) BP Solar Spain

Figure 5.31: DSC control limits for each location with a greater than 70% gel content by solvent

Compared with solvent extraction method, DSC can also provide lots of kinetics information. See the figure below, where onset, peak and end of cure temperature in EVA are clearly shown in Figure 5.32.

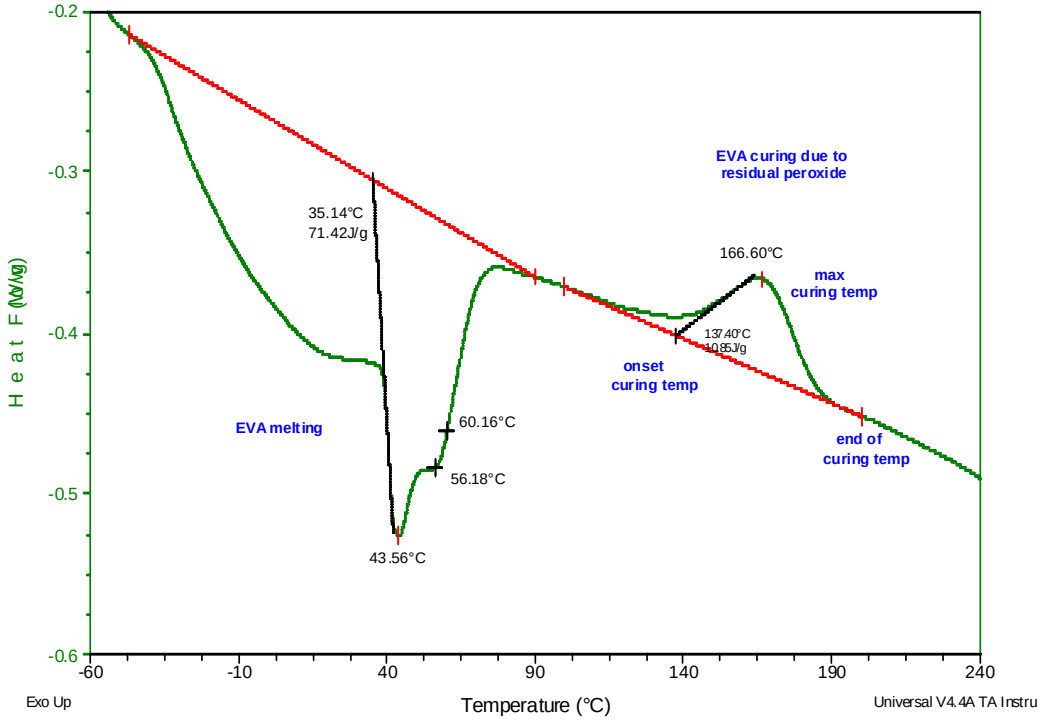

Figure 5.32. EVA curing kinetics by DSC

Table 5.4 below shows the comparison between DSCV and traditional solvent extraction.

Table 5.4: Comparison of DSC and solvent extraction for cure level testing

	DSC	Solvent extraction
Theory	*Rely on residual peroxide cure un-cured EVA*	*Rely on hot solvent dissolving uncured EVA*
Chemicals needed	*No*	*Yes, Toluene/BHT*
Turnaround	*about 1 hr per sample*	*24hrs at 60C just for dssolving plus sample prep and shipping*
Sample size	*~5mg*	*2" by 2" sheets*
Curing kinetics	*Onset of cure, max cure, end of cure Differentiate cure system*	*No*
	DSC	**Solvent extraction**
Pros	** Fast turnaround * Can provide cure kinectics * Phyiscal process * Can do in-house*	** More historic data * More direct than DSC * Widely used*
Cons	** Small sample size * Multiple runs needed * Rely on residual peroxide*	** Not true gel test, gel content include some EVA crystalline phase * Long turnaround * Rely on external lab for the test * High variations * Chemical process*

Sub-contractor STR ultra-fast cure EVA work

Significant progress was made on the ultra fast cure encapsulant during the TPP project. For EVA to be considered ultra fast cure, process times that afforded a gel content of >65% in less than 10 minutes (total process cycle time) were investigated. The goal for this development was to improve the curing kinetics and overall curing behavior of the 0140P formulation already qualified by BP Solar. In all candidate formulations tested during the project, the curing kinetics was faster than the 0140P formulation. In fact, all candidates, except one, registered cure speeds (measured as Peak Rate) at least 2X greater than 0140P; the one exception had a 37% higher peak curing rate than 0140P. Furthermore, all candidate faster-cure formulations were found to have a much greater crosslink network formation (increases of at least 50%) over the 0140P, as measured by oscillating die rheometry. All candidate formulations have been put into the Xenon-arc weather-o-meter (to determine UV stability) for at least 3 months. Additional optimization of one of the candidate formulations will be completed within the next week and then exposed for accelerated aging. STR faster formulation cures 18% faster, but also is 20% more expensive than standard samples.

Sub-contractor STR cell backside EVA

Formulation iterations of the cell backside encapsulant completed 500 hours damp-heat exposure and were measured for adhesion against glass. One formulation maintained 88% of its initial adhesion strength to glass at a moderate value of 32 lb per inch width of peel (lb/in). The second formulation appeared to have increased glass adhesion strength over the 500 hours to 56 lb/in from 50 lb/in initially. However, damp heat (85C/85%RH) testing showed bubble formation in these samples.

Sub-contractor STR Flame Retardant EVA Development

Flame-retardant (FR) encapsulant was investigated during the project too. During the trial, immediately after extrusion, the flame retardant encapsulant formed a tube-like shape when cut from the roll. This material behavior was exacerbated when the encapsulant had width dimensions greater than the scrim's, which is typical for BP specifications. However, after approximately 24 hours, the encapsulant sheet relaxed and was able to lay flat.

The higher-than-normal stress within the FR encapsulant appeared to be related to the base resin. According to the resin supplier, the observations of this "tubing" were consistent with the molecular structure of the resin. Lastly, during outdoor tests at BP Solar, the material was tested UL790 specification (burning brand, Class B). The STR formulation did not seem to reduce the flammability (Figure 5.33).

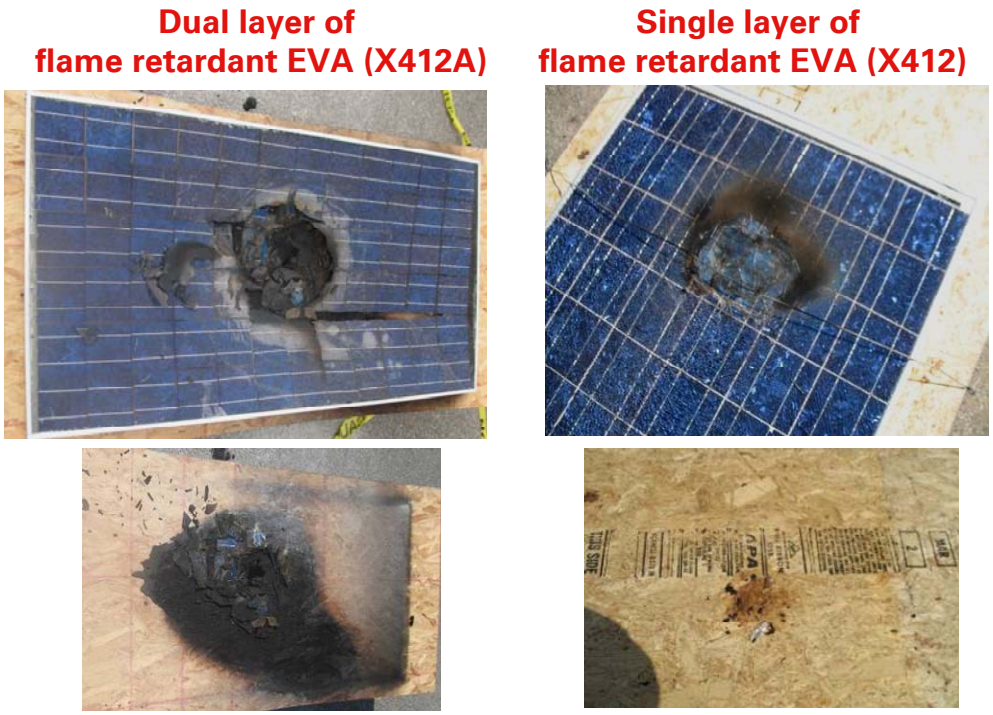

Figure 5.33. UL790 Burning brand test (Class B) for STR flame retardant EVA

Silicone Encapsulant Development

As part of development activities to identify a new and novel encapsulation material that would meet the industries growing needs for performance, safety, and longevity BP Solar evaluated silicone encapsulation system in collaboration with sub-contractor Dow Corning Corporation. The new Dow Corning system has the potential to reduce process time, improve module efficiency because of higher light transmission, and to reduce long term degradation of module performance. Efforts under the TPP program included module qualification and certification as well as quantification of improved energy collection in the field.

During the project efforts focused on the choice of suitable materials that could be used with the encapsulant. An example of the types of materials that needed to be modified for the BP Solar design included junction box potants, cables, and frame adhesives.

By the end of the program, the final bill of materials had been chosen and the process had been defined. This included a rework process in the event of module repair. Modules made to the final design were submitted for UL and IEC certification. The following summarizes the high points of the activity under TPP.

Standard BP Solar multi crystalline silicon cell matrices have been encapsulated by Dow Corning using the new silicone system. Resultant modules were then subjected to the BP Solar internal qualification sequence that includes:

- 500 thermal cycles from -40 °C to +85 °C,
- 1250 hours of damp heat at 85 °C and 85 % relative humidity

- 1000 mechanical load cycles, 50 thermal cycles and 10 humidity freeze cycles.

The silicone encapsulated modules passed all of these tests with minimum power loss as shown in Table 5.5. The percentage changes in this table are based on initial module measurements after the stabilization procedure (IEC 61215 outdoor exposure totaling 5kWh).

Samples	After 1000 Hr DH	After 1250 Hr DH
Damp Heat A	-0.8%	-0.9%
Damp Heat B	-0.8%	-1.5%
	After 200 TC	After 500 TC
Therm. Cycle A	-0.9%	-1.1%
Therm. Cycle B	-0.8%	-0.8%
	After MC/ 50TC	After MC/50TC/10HF
TC/HF A	-0.7%	-0.6%
TC/HF B	-1.0%	-0.1%

Table 5.5: Percent Power Loss of Silicone Encapsulated Modules after Qualification Testing

The initial wet insulation resistance of the silicone modules (measured at 1,000VDC) was 4 to 10 times higher than the wet insulation resistance measured for the standard EVA based modules. The wet insulation resistance of the silicone modules changed more during the damp heat test but still had approximately 1.5 times the insulation resistance after 1,250 hours of damp heat.

At this writing, BP Solar modules with Dow Corning silicone encapsulation are under external evaluation for third party certification to IEC 61215, IEC 61730 and UL 1703. All of the IEC tests have been successfully completed except for the TC50/HF10 sequence after UV preconditioning, which is in progress. All of the UL tests have been successfully completed. The silicone/back sheet structure received a partial discharge maximum permissible system voltage rating of approximately 1,300 volts for 225 µm of silicone encapsulant and a rating of almost 1,600 volts for 300 µm of silicone encapsulant. This test was performed as defined in IEC 60664-1.

Figure 5.34: Dow Corning test site in Freeland, Michigan

A pilot run was conducted to produce 5 kilowatts of silicone encapsulated modules for a demonstration array. In order to have a baseline with which to compare the results, BP Solar built 30 EVA laminated modules along with 30 matrices that were fabricated into silicone modules by Dow Corning using the same cell efficiencies. The silicone modules averaged 173.7W versus the EVA controls at 173.1W. Both arrays were installed at the Dow Corning site in Freeland, Michigan (Figure 5.34). They are being monitored separately to evaluate the energy performance of silicone versus EVA encapsulation. The results for the first 5 months of operation are shown in Table 5.6. The silicone modules produced approximately 0.5 % more energy during this time period.

EVA Total kWh	Silicone Total kWh	Difference kWh	Difference %
1976	1986	10	0.51

Table 5.6: Energy Collection from EVA and Silicone Arrays in Freeland, MI (Nov, 2009 to April, 2010)

Figure 5.35 shows three modules (one EVA control and two equivalent modules made with Dow Corning silicone encapsulant) deployed outdoors at BP Solar, Frederick where the maximum power point is measured every minute. From this data the specific energy yield was determined. Figure 5.35 shows the specific energy difference for the two groups. The differences (0.5 % and 0.7 %) are very similar to the energy yield difference seen on the large array at Freeland, Michigan**.**

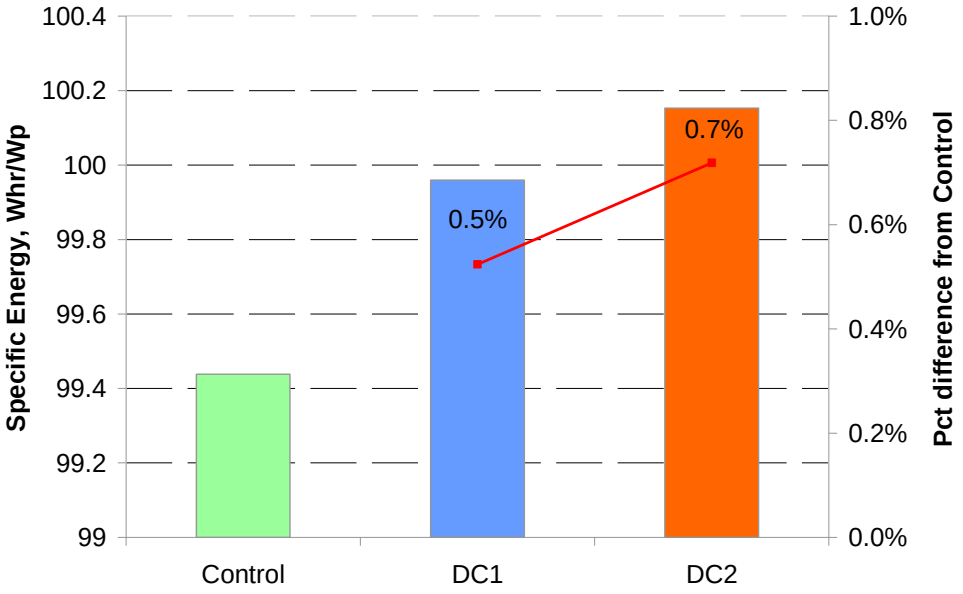

Figure 5.35: Specific Energy difference for an EVA module control vs. two equivalent modules made with Dow Corning silicone encapsulant

In summary, the Dow Corning silicone encapsulant looks a very interesting alternative to traditional EVA. Status in 2010 is that BP Solar is evaluating the economic benefit of replacing the current EVA encapsulant with the silicone encapsulant. This will include tool set change as well as materials cost.

Product Development

Roofing membrane integrated module

As part of the TPP project requirements to reduce the installed cost of PV, a significant activity to develop a large commercial project (LCP) product which would be compatible with large area flat roofs that required minimal roof penetration was undertaken. The approach taken by the BP Solar team looked at how to attach a PV laminate directly to the roofing membrane without the use of adhesives. The approached focused on developing a process to laminate a cell matrix directly to the roofing membrane using existing module and roof materials.

Throughout the project, the BP Solar Module Technology team performed a number of tests to figure out the correct form of roofing membrane that can be used for this application. In particular, the team attempted to laminate EVA onto ethylene propylene diene monomer (EPDM) and thermoplastic olefin (TPO) roofing membranes. Thermo-plastic polyolefin (TPO) single-ply roofing membranes provide exceptional resistance to ultraviolet, ozone and chemical exposure and are fast overtaking EPDM as the preferred roofing membrane in large commercial buildings in the US.

Through our research, it was found that EPDM generated significant delamination and bubbles on lamination. In addition, the adhesion between EVA and EPDM was low. In contrast, no bubbles were observed with TPO roofing membrane, and the adhesion

between TPO and EVA was very good (peel strength >110lbs/in). Figure 5.36 shows some pictures of the TPO laminate design.

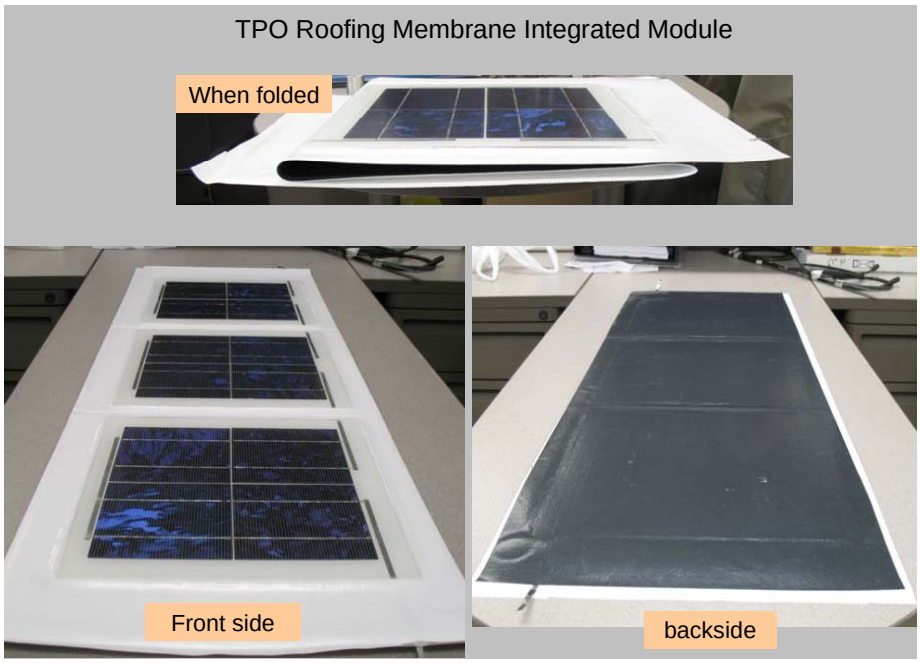

Figure 5.36: Samples laminated to TPO roofing membrane.

Also made 72 cell and 60 cell super modules each using TPO from a different manufacturer as the back sheet. The lamination process went well. Both samples were mounted onto the insulation foam boards typically utilized for installation of membrane roofing. Samples were exposed on the FDK outdoor testing site and weathering test. Figure 5.37 are the module for 7months outdoor test. BP Solar worked with the Carlisle Syn Tech of Carlisle PA on this project.

Figure 5.37: Outdoor exposed for 5months

The 60-cell super modules did not pass the BPS Q6000 reliability test due to leakage current test after damp heat exposure. The main area of failure (wet insulation failure) was at the point where the bus bar connection ran under the front cover glass. A number of potential solutions to this failure point were proposed and were ready for evaluation at the time the TPP project finished.

Roof Integrated PV Module

The goal of this subtask was to design a building integrated photovoltaic (BIPV) product for new construction that is compatible with S-shaped concrete tiles. The following document summarizes the development of this product over the two year contract.

To begin, a stage gate review was held to compare two separate design concepts and two material types. These options were benchmarked against an existing solution via a detailed selection matrix (comparing material reliability, cost, IP, HSSE, speed to market). Using this tool, a design (2 tile wide concept) and material type (aliphatic polyurethane processed via RIM – reaction injection molding) were selected. A subcontract with a known material supplier, Recticel, was then finalized. Finally, a preliminary design concept was sent to Recticel for mold feasibility analysis.

In parallel to investigating mold feasibility, residential concrete tile manufacturers were chosen based on volumes in the South Western US market. Many of these companies provided samples of Spanish S-type tiles, which were then laser scanned to get accurate models to design around.

After the initial mold feasibility study was completed, work began with a subcontractor to optimize a module clip design that would serve to secure the leading edge of the module to the roof tiles. A rapid prototype of a complete roof assembly was created at $1/12^{th}$ scale, including a roof, roof tiles, and solar module frames. This model allowed for greater visualization of the module concept and was useful in brainstorming activities when optimizing the design.

With the initial concept created, timelines were created with the subcontractor, and weekly teleconferences began. The subcontractor completed initial adhesion testing to verify the bond of polymer to the polyester laminate back sheet. Results were not optimal for single face adhesion, so an additional primer was needed.

In addition to the small scale roof assembly, full scale rapid prototypes of the module side frame sections were created to verify proper fit/form/function of the frame to the tiles. A digital image, shown below in figure 5.38, was also rendered to visualize the installed appearance of the module on a residential concrete tile roof. Finally, a roofing partner was chosen, MonierLifeTile, and a meeting was held to discuss the expected aesthetics and functionality of the design using the CAD renderings, images, and rapid prototype parts.

Figure 5.38: Digital Rendering of Module Concept on S-Type Tile Roof.

After initial design iterations and reviews, the first design solution was agreed upon that met all performance and functional requirements, and was feasible to mold. Specific areas of focus included aesthetics, mechanical strength, ease of installation, and proper rain water management. Likewise, several module clipping arrangements were explored for strength, cost effectiveness, and ease of installation. The selected clip was analyzed using FEA to validate the design against desired load requirements (Figure 5.39). The search for a primer that would improve adhesion also continued.

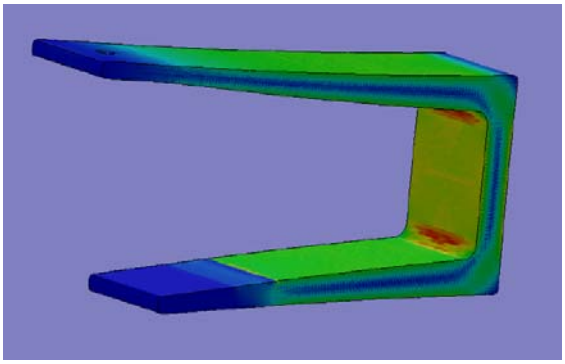

Figure 5.39: FEA of Initial Module Clip

A full scale rapid prototype of the proposed design was constructed to further visualize the final module design (Figures 5.40 to 5.41). The full scale prototype was installed on a test roof to validate fit, form, and function of the design before approving production of the prototype mold (Figure 5.41).

The CAD model was also finalized with the subcontractor to include the necessary mold draft angles and final details.

Figure 5.40: Full Scale Rapid Prototype Module (Bottom Isometric View)

Figure 5.41: Test Installation of Rapid Prototype Module on Small Roof

To complete the first year of development, molding dies were machined and the first generation modules were molded at Recticel in Belgium. To most effectively design this BIPV product, we decided to pursue a polyurethane framed module which is formed using the Reaction Injection Molding (RIM) process. Although polyurethane is a more expensive framing option than aluminum, the benefits gained offset the added cost. First, design flexibility and creativity are greatly enhanced using a moldable material. The extrusion process, typically used for aluminum frames, only produces set lengths of a 2-D cross sectional profile. A moldable material allows the designer to create 3-D contours at any location on the module creating potential for new module applications (Figure 5.42).

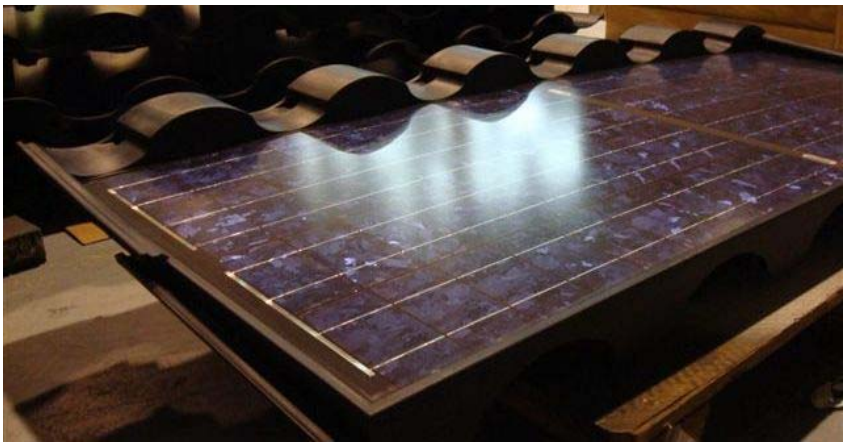

Figure 5.42: S-tile BIPV product (3-D contours)

Secondly, RIM is a low pressure and low temperature process which enables the frame to be molded directly around the laminate. This eliminates the need for frame adhesives, frame fasteners, and grounding hardware. This not only simplifies the module assembly process but also enhances module quality via better laminate adhesion and centering within the frame (Figure 5.43).

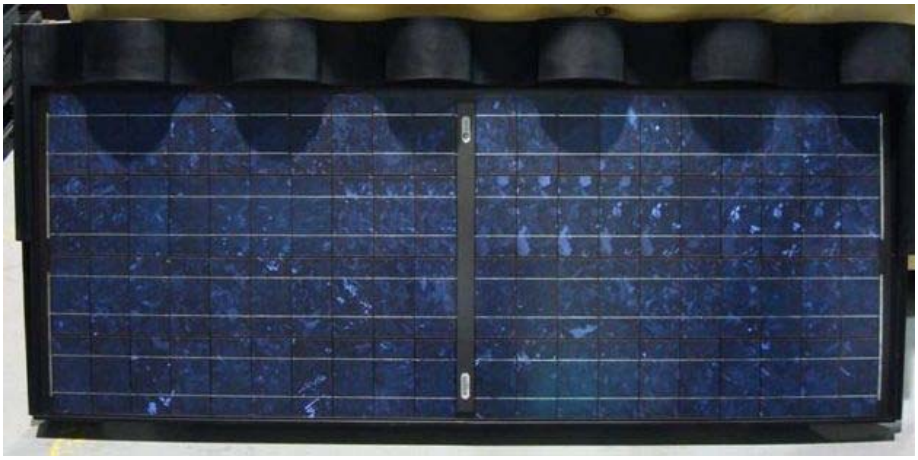

Figure 5.43: S-tile BIPV product (frame encapsulation around laminate)

Mounting devices such as fasteners, inserts, or clips can also be integrated into the frame using the RIM process.

The aesthetics of this module were greatly enhanced in comparison to the typical rectangular shaped modules which dominate the PV market. This aesthetic benefit, based on market surveys and response from our flat tile BIPV product, would open up a brand new customer base which currently views PV as an unacceptable home addition. Thirdly, this BIPV product lends itself to be installed by a roofing contractor instead of a traditional PV installer. This essentially combines the distribution and installation channels into one component which reduces overall product cost. Finally, due to the architectural benefits, home builders are more inclined to incorporate BIPV systems into new residential communities in comparison to traditional rack mounted systems. This

will allow the home buyer to offset the upfront cost of a PV system by distributing the cost into their mortgage payment. Unlike the recent decline in home sales due to the recent economic recession, new construction homes with PV are actually increasing in number in the western US.

The second year of development, also referred to as Phase 2, began with an installation and design review at Arizona State University. A team of graduate students, roofing experts, and local solar installers participated in a two day review of the first generation design. This included an installation (Figure 5.44) and several group discussions thereafter.

Figure 5.44: Gen 1. Installation at Arizona State University

Following the Gen. 1 installation review, several changes were made to the module design to improve its form, function, and performance. Aesthetics were upgraded with the addition of a tile-like lip to the leading edge of the module. This sweeping tile shape matches the profile of the concrete tiles, and will continue the feeling of tile across the PV array. Aesthetics were further enhanced by way of color matching the molded polyurethane frame with the concrete tile. A mock up using samples shot in the original mold illustrates the effect that the color-matched polyurethane has on blending the product with the roofing tiles (Figure 5.45).

Figure 5.45: Tile-like lip (left), and color-matching samples (right)

The greatest functional improvement to the design included a new clip system, or means of attaching the modules to the roof. The new clip system provides a more secure hold, attaching directly to the roof deck, as compared to the original design which attached to the concrete tiles themselves. The figure shown below illustrates the new clip (dark grey) located under the front end of the module, engaging an identical batten on the roof deck (light grey). This system also aids installers in leveling the modules on the roof deck, as the battens are installed first on a chalk line.

Other functional improvements include molded in "ruler lines" to aid installers with module alignment, and a cable hold for temporarily managing loose cables before they are connected on the roof deck. These features were born out of discussions with actual installers during the Gen. 1 installation review.

On the performance side, a major portion of Phase 2 was dedicated to testing the reliability and safety of the module. This included qualifying the polyurethane material against existing standards in the industry, including BP Solar's own reliability testing. Material performance testing included, but was not limited to: thermal cycling, damp heat, and UV aging. For load performance, module samples were mounted to a rigid structure and statically loaded on the front and back to simulate wind loads beyond 50psf (2400Pa). This in-house test provided confidence in the new clip system, which will be tested to UL1987, "Uplift Tests for Roof Covering Systems".

Effort was dedicated to improving the fire resistance of the module when installed on a roof. More specifically, we focused on improving the spread of flame performance as measured by UL790, "Standard Test Methods for Fire Tests of Roof Coverings". Three developmental tests at the Underwriters Laboratories (UL) in Deerfield, IL, allowed for iterative improvements to be made to prototype modules. Such improvements came in the form of material changes, and the refinement of the clip attachment system, which allowed it to effectively double as a fire wall. As can be seen below (Table 5.7), this iterative testing resulted in increased resistance to the spread of flame vertically, up the array, and has brought the design very close to achieving the necessary 10:00 minute minimum required for a Class "A" certification.

Table 5.7: Observed Time to Failure. Spread of Flame Testing.

	UL Recorded Time to Failure (min)	
Test Iteration	**Lateral Spread of Flame (40in)**	**Vertical Spread of Flame (6ft)**
1	**N/A***	**6:36**
2	**N/A***	**6:54**
3	**8:43**	**9:28**

*Note: Failure via lateral spread of flame in test iterations 1 and 2 was certain, however, the time was not recorded by UL staff.

Continued efforts since the last spread of flame test included: reducing the volume of polyurethane per module by 15%, and screening potential fire resistive materials for use as an additional fire barrier. This test proved to be one of the most challenging obstacles in Phase 2.

To fully realize the advantages of the many design changes that have been proposed and tested throughout Phase 2, a new mold was finalized in November, and mold dies were ordered. The new mold dies (Figure 5.46) were also upgraded to machined aluminum for increased life, as compared to the original mold dies which were made of epoxy. This will ensure that the mold dies can provide an adequate number of samples necessary for certification testing.

Figure 5.46: Machined Aluminum Die for 2nd Generation Mold

The final quarter of this project began with the manufacture of the Gen. 2 design. As can be seen below (Figure 5.47), this design incorporated all of the changes mentioned above into a very attractive package.

Figure 5.47: Isometric View of Gen 2 Module

The 150 Watt module was named the "S-Tile HP" for its higher power half cell laminate. Finally, certification testing was initiated for UL 1703, and AC365, which is ICC's requirement for building integrated PV.

Task 6: Manufacturing

The objectives of Task 6 are broadly defined as implementation of continuous improvement activities for equipment, process, and quality control. Critical areas that were defined by the Frederick manufacturing team were process monitoring and control, Komax equipment improvement, and improvement in the manufacturing indices at wafering, cell, and module assembly for wafer thicknesses <200um.

Monitoring and Control

Factory process control improvement was identified early on as a major focus for Task 6. Key focus areas were on improved measurement tools, control procedures, and data tracking/reporting.

Critical controls that were identified and implemented to improve module assembly process:

1. Measurement of anti-reflective coated glass light transmission with BYK-Gardner HazeGard tool. The primary value of ARC glass is that the increase in power at STC and in energy generation over time provides a return on the higher cost of the glass. A key method for non-destructive evaluation of ARC glass is to quantify and compare light transmission of the glass.
2. 180' tab pull tester setup for improved destructive testing of solder joints at tabbing/stringing process. Previous manual tester pulled interconnects at 45^{o} relative to the plane of the cell but frequently broke the cell during the test, which became a more frequent problem with thinner cells. A 180^{o} semi-auto pull tester removed the influence of the operator on the test, directs the force onto the interconnect instead of the silicon, and was proven to be a more reliable test method and more indicative of the solder joint quality.
3. Development and implementation of improved process control plans for soldering, lamination, and flash test.

The cell line also received considerable attention for improvements in process control:

1. Front grid pattern line width and height inspection. Cell gridline control is one key to optimizing the metallization process between the trade-off of increasing I_{sc} and reducing R_s. A non-contact measurement tool was developed and implemented in production for calculation of an average gridline width and height based on measurement of multiple points on the cell grid.
2. Emitter sheet resistance control. An improved 4-point resistance measurement tool was developed and implemented to measure and monitor the diffusion process.
3. Cell test calibration and control. Development of a Gauge R&R technique which was applied to all cell testers for improvement in the regular calibration and correlation methodology.
4. SiN thickness and refractive index (RI) measurement. Industry-standard method for monitoring SiN process was to process a polished Czochralski wafer and

correlate the results to production multi-crystalline wafer. The challenge for existing measurement tools was the diffusion of light due to the changes in reflectivity of the various grains in the measurement area. A new ellipsometer from Sentech was tested and implemented which is capable of measuring layer thickness and RI directly on the multi-crystalline wafer, providing nearly real-time results on the quality of the SiN PECVD process.

Factory data collection

In addition to improvement of controls and measurement tools, focus was given to improving data collection and reporting on the factory floor to enable better process data collection and analysis, and drive process improvement.

Key improvement items were implemented at all points in the process flow:

Equipment – all major production tools were linked to an operations dashboard displaying real-time equipment status to line personnel and operations managers.

Casting/Sizing

a. new brick ID system and MES code for brick-level labeling and tracking
b. system upgrades to Casting MES for ingot tracking

Wafering/Cell/Module

a. adding cassetting/cleaning station to MES for improved materials tracking
b. implementation of SPC reporting for new measurement tools at Wafer outgoing, Diffusion, SiN, and Metallization
c. development and implementation of reaction plans for out-of-control process events

Komax Sub-contract

A major sub-contract was awarded to Komax for joint development of improved screen print equipment and an improved tabber-stringer. BP Solar has a long history with Komax production tools and has been a partner with them for development of new equipment and continuous improvement.

Screen print improvements:

1. Reduced cell breakage: A robot design was incorporated into the current machine for better pick-and-place control and softer handling of the cell. This design also includes a cell inspection that allows fewer handling steps.
2. Glass chuck heaters change: The chuck holders were redesigned for faster removal of the chuck heaters and easier installation of replacements
3. Excess paste detection: The vision system for excess paste on the glass work holder did not have the ability to detect paste without a
   UV phosphorescent maker, so capability was added to detect standard paste for more flexibility.

Tabber/stringer improvements:

1. Improved measurement and control of solder temperature: Developed and implemented an upgraded closed loop solder control for real time temperature measurements. Temperature control is within ± 2°C. This control is now being done without the need for disposable tooling.
2. Evaluate parameters that influence quality of solder bonds: Have optimized the thermal gradients to reduce thermal stress
3. Increase understanding of soldering process: Continue to test and develop recipes for different cell types and thicknesses. Have developed a design that allows for spot or continuous soldering bonds on most silicon cell designs up to 160mm.

Process optimization

Continuous improvement in module cost reduction requires balancing a thinner wafer for reduced silicon usage with a realistic assessment of the capability of the equipment and process available in the industry. Although some manufacturers have shifted to 180+/-20um, due to concerns on lower yield and Efficiency, the typical wafer thicknesses are 200+/-20um.

These industry-standard thicknesses require process capability <200um, so in addition to the Komax tabber/stringer developments, a concerted effort was made to improve equipment and process in wafering and cell lines.

Examples of process improvements that were delivered as a result of TPP support:

1. Total thickness variation (TTV) – reduced defect from 3.6% level in Q1'09 to <1.5% at end of Q2'09. Primary corrective actions were to fix persistent equipment problems, reduce load size on certain saws, improve installation method for wire saw wire guides, and setting up SPC charts and associated reaction plans for identifying and reacting when a saw has high TTV defect.
2. Wire break – loss of material due to wire breaks reduced from ~3% at beginning of Q2'09 to ~1.5% at end of quarter. Primary fix was reducing load size on certain saws and optimizing table speed on others.
3. Saw mark – specific saws were found to have high level of saw stop rates. Frequent stops are found to cause hard line saw marks. Improvements made to these saws in September '09 resulted in ~1% defect reduction.
4. Qualification of new slurry recycler to improve variation in slurry grit size and quality
5. Development of new wire guide coating and grooving spec
6. Improvement in bare cell FF due to Co-fire optimization
7. Cell stain improvement from ~2% to <0.8% due to improved handling procedures implemented for thinner wafers.

Task 7: Inverter System Development

Xantrex Charge Controller

Xantrex efforts during this quarter involved the testing of the prototype design (B model). Testing of the functional circuit blocks (auxiliary supply, power converter stage, communication link, digital controller etc.) was completed on several of the prototype units, allowing the full DVT (Design Verification Testing) to get underway.

The DVT initially focused on the overall electrical specifications and efficiency of the design to ensure this latest configuration would adequately achieve all target specifications. This was successful, so the full thermal testing cycle was begun, using an extensive array of thermocouple sensors on all key components while operating the test unit under a range of conditions at the maximum rated ambient temperature. Typical results are shown in Figure 19. Temperatures showed thermal margins well within design specifications under all conditions, validating the thermal management system design.

Testing for compliance with FCC part 15 class B EMC (Electromagnetic Compatibility) limits is a critical step with all high frequency switching devices like this product. A significant amount of time during this period was spent performing this testing. Unfortunately the initial results were significantly over the maximum allowable level. Several rounds of modifications have been made to the circuit (noise sources and filters) to bring these levels down. Additional work will be required in the next quarter to ensure the class B limits are met.

The main power circuit board will have to be revised to incorporate the changes required to meet the noise limits (above) and then the full DVT plan will be re-run on the revised product as a final verification of the design. This will lead to the next prototype build in early 2010, done at the manufacturing facility of the proposed contract manufacturer.

ASU Inverter Work

During this quarter, ASU:

- Implemented the active/reactive control, voltage and frequency control techniques in a Simulink model of a universal power management system (UPMS), and verified UPMS's multi-functionalities through simulations.
- Created a Simulink/SimPowerSystems test-bed and tested the developed control techniques and UPMS's functionalities in a micro-grid with multiple UPMSs, in both grid-connected and islanded modes.
- Completed the digital control design for the basic control functions for the two-stage PV inverter

Micro Inverters

Environmental testing of 10 micro inverters and/or DC to DC converters, continued this quarter. New devices obtained in the last few months are working well and the tests have been proceeding without any additional failures. We are planning to install, up to ten AC micro inverters, from several vendors, on our outside test array. Hardware has been purchased for the installation and the electrical box with appropriate ac circuits and network connection has been installed. Twenty new 175 – 180 watt solar are to be installed. Two 15 kva isolation transformers have been purchased for installation behind the array and will provide appropriate voltage for connection of the micro inverters.

All above efforts stopped with partners.

Task 8: Monitoring and BOS

Monitoring – SMUD House of the Future

Energy dispatch testing has been all but been completed on the House of the Future. Our agreement with the home owner ends Jan 1st 2010. Several issues such as poor communications reliability and data accuracy have been addressed. Some obstacles out of our control also limited the amount of testing we were able to perform. During the testing period from May through August there were unusually cool temperatures, making the need for peek power dispatching unnecessary for many of the test days. SMUD also restructured their peek energy costs and along with the fact the home owner appeared to be very frugal with his energy usage, the cost effectiveness of dispatching from the batteries could not be validated. During the quarter 25 dispatch tests were performed. The data from these tests will be analyzed during the next quarter. We are hoping to compare data from NREL monitoring of the household loads (air conditioning, Inside Temperature, Solar Hot Water, etc.) with our own data providing an overall picture of the homes operation.

Based on the experiences with the first house, the software and hardware are being redesigned. Specific activity includes:

- New inverter settings for both inverter and charge controller have been implemented to better utilize battery storage.
- Automated web control of dispatch function developed and deployed
- Limited control of dispatch functions handed off to SMUD and worked well during testing, although these tests were limited due to low summer temperatures.
- New internet line has been run into BP Solar to better facilitate House of the Future web site. Web site has been moved.
- Cellular connections are not reliable enough for use with real time or near real time control. A dedicated hard wire internet connection is to be used on future test sites.
- Battery charge and discharge profiles have a large effect on both long term and short turn battery capacity. Better remote capabilities will be provided allowing us to modify more charge and discharge parameters remotely.

Combiner boxes

We have received several combiner boxes and are expecting delivery of several more boxes for evaluation. Some of these combiner boxes include string monitoring of current with either digital or analog communications. All of the boxes require external power and some sort of wired communications. We are also in the process of developing a combiner box design in house which would be powered from one or more of the strings and would monitor both current and voltage, these boxes will be able to communicate both wirelessly (ZigBee) or through isolated RS485 network. We have initiated discussions with an electrical equipment manufacture about their combiner boxes and the possibility of incorporating monitoring and arc suppression within the box.

DC Arc Suppression
We have identified an electrical equipment manufacturer who has a prototype design of an arc suppression unit that would fit within their combiner box. They demonstrated arc suppression using input from a 2400 watt 360 volt array. A series arc was initiated and the device extinguished the arc very quickly.

An array with new S-tiles was planned for installation at Monier Lifetile in California, modules were sent but all efforts stopped at this point.
SMUD house of the future still operating but data is not logged by BP Solar.

Task 9: System Engineering

Residential roof integrated PV Array
Color matching S-tile modules installed on a mock test roof confirmed the sagging issue with the original mold (Generations 1-3) due to the weight of the laminate not being properly supported by the polyurethane frame. This issue has been addressed in the Generation 4 model, and will be present in the 2nd mold. We will look into potentially pursuing some of that effort.

Membrane roofing product
An NDA was completed with a large roofing membrane manufacturer. An MOU covering technology collaboration is under development. Discussions to determine the cause of discoloration of the EVA/TPO laminate were held at the manufacturers in September.
No further development.

Ground Mounted Tracker
Commercially available tracker will be tested separately by BP Solar at ASU for decision on the most reliable design in the next year.

Task 10: System Installation and Maintenance

Residential System
Work continued in support of the S-tile residential roof tile. Mounting and installation of the S-tile are important factors in its ability to pass the spread of flame test. The mounting brackets are being utilized to provide a fire break on the underside of the modules. Effort on hold.

Commercial Membrane System
We met with Carlisle to discuss the installation requirements for the membrane system. One of their recommendations was to limit the design to 3 modules on a piece of TPO so that the TPO does not have to be folded. It appears that a super-module of this size (~ 500 to 600 watts) would be large enough to take advantage of reduced cost, but small enough to be handled by the same equipment they already use to handle the rolls of TPO.
Carlisle also recommended that we use their TPO tape for covering the glass edges and interconnects as this material is already used in conjunction with TPO roofing

membranes and so has a long history of survival on the roof. All efforts stopped at this point.

Task 11: Deployment and Testing

Most deployment activity was due to be undertaken during the final phase of the project. Unfortunately, as the project was terminated (February 2010) before the final phase, no large scale deployment funded by TPP occurred. What is described in this section is the very successful and valuable, small scale, outdoor test system that BP Solar used to evaluate new technologies at the module level during the project. The following section describes the design and functionality of this system.

Figure 11.1: Roof top test array

Figure 11.2: Ground mount test array

BP Solar at Frederick have installed test arrays on the roof top (Figure 11.1) and at ground level (Figure 11.2) for the purpose of measuring the performance of single samples and small arrays of PV modules.
Both test arrays can accommodate a wide variety of PV module sizes and technologies. Sample modules are installed on a fixed tilt rack facing due south and are connected to the measurement channels of a Daystar multi-tracer instrument, which is installed indoors. "Multi" in multi-tracer means that all of the measurement channels are operated independently in two basic measurement modes:

1. Continuous maximum power point tracking (MPPT) operation, simulating "grid-tied" operation for energy generation measurement.
2. "Snapshot" I-V characteristic curve measurement at designated intervals throughout the day.

These modes operate nearly simultaneously and independently.

Separate current and voltage sense leads are carried from the multi-tracer as close to the module terminals as practical to minimize the measurement errors associated with I^2R voltage losses (Figure 11.3). Auxiliary measurement channels of the multi-tracer enable environmental measurements e.g. irradiance, ambient temperature, etc.

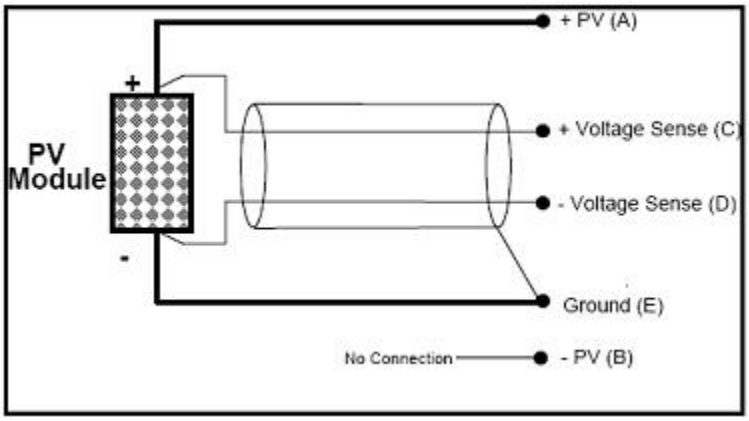

Figure 11.3: Wiring schematic

Modules connected to each channel are operated using electronic loads, not inverters. Each channel makes three basic measurements: module current, module voltage and module temperature. Analysis of the collected data is performed off-line.
BP Solar uses these test arrays to accomplish a variety of experimental measurements including:

- Side-by-side comparison of prototype modules to assess the impact of design improvements on energy generation, performance at low irradiance, thermal dissipation, etc.
- Verification of indoor performance test measurements.
- Competitor sample performance evaluations.
- Determination of PV module performance characteristics for use in energy modeling.

- Testing of 3rd party, OEM supplier modules.
- Exploration of shading tolerance characteristics.
- Long-term performance degradation measurement.

As an illustration of the usefulness of the outdoor test system the follow describes a study performed between a thin film module and a crystalline silicon module.
The objective of the study was to highlight the difference between the real world outdoor performance and the predicted performance from a modeling program. The results are shown in Figure 11.4 and 11.5. Figure 11.4 shows the Performance Factor versus daily solar insolation (Sun hours at 1000W.m^{-2}) for a thin film module and a crystalline silicon module. The data for this graph was gathered from a test array at BP Solar, Frederick Maryland. The performance factor for the crystalline silicon module is higher than the thin film module except at low irradiances or low sunlight periods. This means the silicon module generates more kWh per rated kWp per unit time than the thin film module. When the performance of the same two modules are modeled using one of the commercially available sizing programs, the performance is very different, as show in Figure 11.5. In this case, the thin film module outperforms the silicon module at all both high and low light levels. Also, both modules appear to decrease in performance as the light intensity reduces over a high to medium range (8 sun hours to 4 sun hours). This is unusual for modules whose performance is series resistance limited.

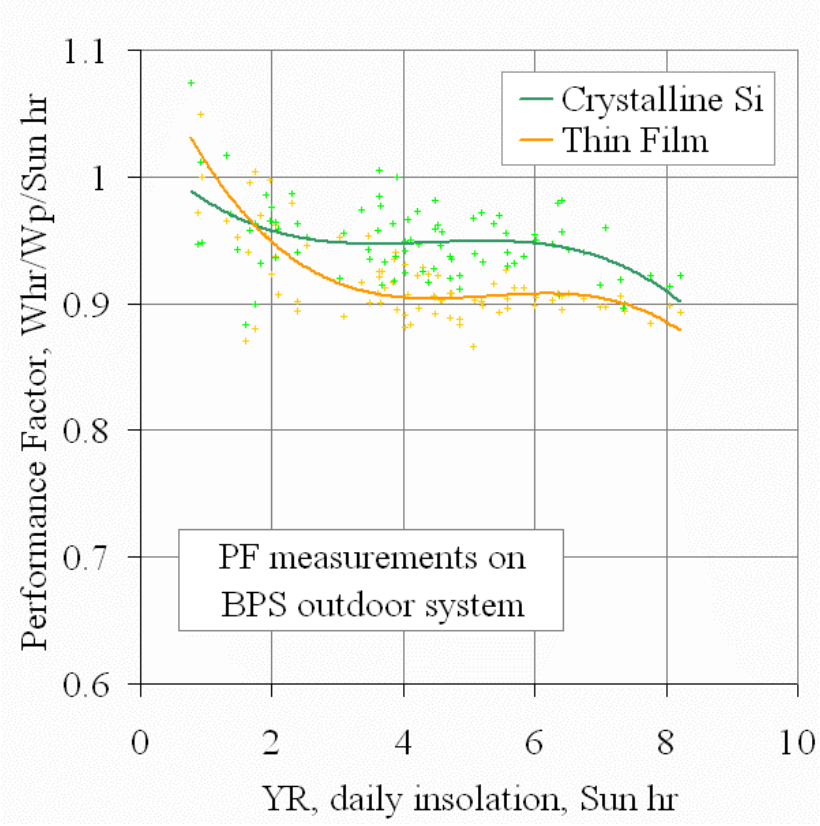

Figure 11.4: Performance Factor vs. daily insolation determined from actual measurements

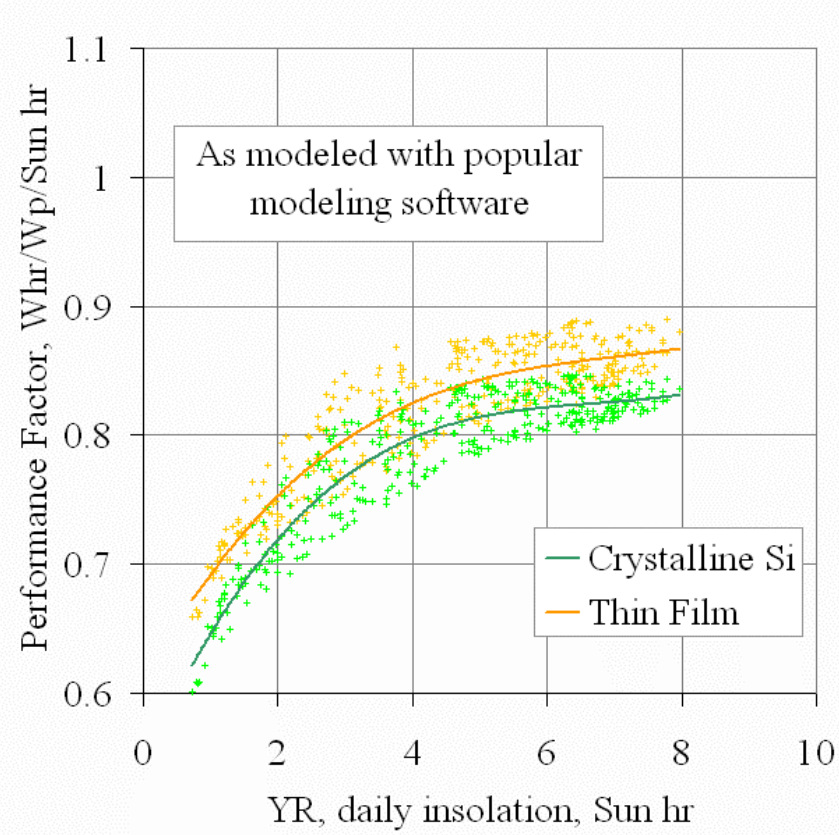

Figure 11.5: Performance Factor vs. daily insolation determined by a commercially available sizing program.

Task 12: Collaboration

Arc Faults in PV Modules: External Collaboration

Over the past several years, there have been increasing numbers of PV module failures related to arc faults. The majority of these have been located at the connection between the module's output cable and the internal bus bars. We spent a good deal of effort under the PVMaT contract to develop a much more reliable method for connecting the cables, which incorporated a mechanical connection as well as a solder joint. This construction should greatly reduce the number of arc-related failures at the cables, but it leads us to consider how current module designs will eventually die. It might be a bus ribbon or cell interconnect which eventually arcs, resulting in the same type of shock and fire hazard that has been observed with cable failures.

Arc fault protection has been studied extensively, particularly with regard to high-voltage ac equipment. It is well established in the literature that there are three basic methods to reduce the risk of arc hazards:

- Increase the working distance between conductive components
- Reduce the available arcing current
- Reduce the time to clear the arc fault once it occurs

The most likely scenario for arcs in a PV module occurs when solder connections come apart or the conductors themselves break. In this case, the "working distance" is near zero, and the components are held in close proximity by encapsulating or sealing materials; so it would be difficult if not impossible to increase the physical distance.

We can limit the current available to an arc fault through system design and cell size; but since we already know that arcs occur in module strings with ~5A of current, it doesn't appear promising that we can reduce the current enough to significantly improve the situation. Therefore, we believe that our efforts should be directed toward detecting and clearing any arc faults as quickly as possible.

Solar ABCs Activities

In response to recent increases in PV module field failures due to over-temperature and arcing within high voltage PV systems, the Product Safety Panel of the Solar America Board for Codes and Standards (Solar ABCs) has identified development of an arc fault interrupter (AFCI) as a technology research area that may lead to improved reliability and reduced costs for PV systems.

In October 2007, there was an IEC workshop on PV arcing issues and potential protection means. Tim Zgonena of UL made a presentation on UL experience and information gathered to date on the topic. He concluded that a PV AFCI product would mitigate many of the potential PV fire hazards that the industry is starting to encounter.

A significant portion of the attendees and some of the other presenters were supporting a means to minimize the arc fault hazard by increasing the quality and reliability of the existing PV systems components. Unfortunately, while this method will potentially reduce the number of failures, it does not mitigate the hazard when it does occur. The IEC group is very interested in the results of the Product Safety Panel AFCI research and intends to develop IEC PV AFCI requirements starting in 2008. The Product Safety Panel also hosted a conference call meeting in December 2007 to further discuss this and other issues.

Existing Devices

There are many arc protection devices commercially available, although most have been designed for ac systems. Arc flash detection relays can use a combination of light, sound, pressure or current rate-of-rise as the trigger to interrupt the circuit. Many rely on optical sensors to detect a rapid increase in light intensity associated with an arc. One approach is to use optical fiber as the sensor, feeding it through all the junction boxes in the circuit. Fiber loops are typically 60 meters long, but up to 20 can be daisy-chained as needed to cover the whole system. The continuity of the fiber can be monitored by sending a periodic test pulse that activates an alarm if not returned as expected. Usually, fiber-optic sensors are combined with current sensing relays to prevent false trips. The backup current protection can be instantaneous (ANSI device 50) or time over current (ANSI device 51).

Once detected, an arc can be stopped by tripping an upstream breaker, or creating intentional fault by energizing a high-speed grounding switch. A grounding switch is typically faster but adds cost. A "reverse interlocking scheme" is often used as a compromise between economical and performance considerations. Zone selective

interlocking (ZSI) uses communication signals between protection zones to activate the appropriate breakers. "Bus differential" protection is faster than ZSI and can be retrofit, but is expensive due to the number of current transformers. The biggest obstacle in any of these solutions is the additional wiring required between relays; a newer approach is relay to relay communication through wireless transceivers ("motes") incorporated into the device.

Many of the more advanced systems incorporate microprocessors with complex logic to differentiate between load current and fault current. When used in large ac power applications, these calculate "sequence components" which compare current and voltage in different parts of the system and then initiate a pre-programmed response. It is not immediately obvious whether these would work in a dc system; this will be one area of our investigation.

Suitability for PV

We reviewed the available commercial products with regard to their application in PV systems. Fiber-optic sensors which trip a circuit breaker when bright light is detected are quite likely to work if they are embedded in the j-box of each module. However, they would probably be too expensive to install them on each module; either integrated with the output cables or as a separate set of cables. They could potentially be included as part of the system installation, if we provided a means of attaching them to the j-boxes, but again this would be an added cost. But even if we could make fiber optics work to detect arcs inside the j-box, they would still not be helpful for arcs that might occur elsewhere in the module (e.g., interconnect ribbons).

Another possible concept is to use the heat generated by an arc to open a sensor circuit and trip a disconnecting relay. A small wire running through each module's j-box could be designed to melt at temperatures above the expected operating range, perhaps around 160 degrees C. This approach would have the same obstacles of cost and complexity as the fiber optics; and it is difficult to envision how such a design could be assembled cost-effectively in the factory.

DC Arc Suppression

BP Solar has continued its efforts to evaluate arcs in PV systems and to search for possible solutions. From our laboratory and field data, arcs have now been demonstrated in cable connections, diodes (terminal and board mount), interconnect ribbons and cell edges. Arcs can start at less than 300 volts and 5 Amp. Due to carbonization, arcs can resume on subsequent days of operation.

UL has begun an effort in the arcing area, announcing the formation of a UL Ad Hoc Working group. George Kelly of BP Solar has joined this group.

The one area where arc detection has been utilized is the aerospace industry. These designs are typically small solid-state devices that could easily be incorporated into a combiner box in a PV system. These devices perform a similar function as a circuit breaker, and are designed to deal with both series and parallel arcs. The next generation will incorporate the ability to detect the location of the arc. There is no cost data available yet on these devices.

Appendices

Appendix 1: Patent Applications

The following is a list of patent applications which were filed as a result of the work performed during the TPP project. The applications are listed in Table A1.1.

Table A1.1 Patent Applications

TITLE	INVENTORS	DATE REPORTED	DOE "S" N^{o}
Thermoplastics Roofing Membrane Integrated Photovoltaic Modules	Z. Xia, D. Cunningham, J. Wohlgemuth	6/19/2008	S-117,112
Apparatus and method for direct electric melting	N. Stoddard, P. Von Dollen	9/19/2008	S-117,415
System for Liquid Silicon Containment Employing Carbon-Carbon Composite Materials	J. Cliber, R. Clark, N. Stoddard, P. Von Dollen	9/19/2008	S-117,416
System for Large Ceramic Member Support and Manipulation at Elevated Temperatures in Non-Oxidizing Atmospheres Using Carbon-Carbon Composite Materials	J. Cliber, R. Clark, N. Stoddard, P. Von Dollen	9/19/2008	S-117,417
Local Catalytic Reaction-Based Heat Removal to Enhance Directional Solidification of Silicon Ingots	P. Von Dollen	9/19/2008	S-117,418
Method and Materials for High Temperature Impact Cushioning for Silicon Loading and Melting	N. Stoddard, P. Von Dollen	6/2/2009	S-119,331
A Non-woven polymer matt for improving the reliability of c-PV modules	Z. Xia, D. Cunningham, J. Wohlgemuth	5/1/2009	S-119,159
Ceramic Coated Carbon-Carbon Composite Materials for Silicon Casting	P. Von Dollen	5/1/2009	S-119,769

Table A1.1 Patent Applications (continued)

TITLE	INVENTORS	DATE REPORTED	DOE "S" N^{o}
Formation of selectively doped areas on a wafer using printed dopant sources and printed dielectric barrier material to protect the wafer surface from auto-doping effects during curing and/or diffusion in a furnace.	R. Sidhu, J. Zahler, M. Bennett, D. Carlson	10/30/2009	S-119,767
Light management in PV modules	Z. Xia, J. Wohlgemuth, D. Cunningham	10/30/2009	S-119,768
Use of a compliance layer to prevent the breakage of a seed layer	N. Stoddard	3/17/2010	S-122,316
Attachment Method For Building Integrated Photovoltaic (BIPV) Product	M. Hering, D. Amin	10/6/2010	
Integrated Materials for Silicon Casting	P. Von Dollen	10/6/2010	
Functionally Graded Ceramics for Silicon Casting	P. Von Dollen	10/6/2010	

Appendix 2: Publications

1) Casting Single Crystal Silicon: Novel Defect Profiles from BP Solar's Mono^{2} ™ Wafer. *Nathan Stoddard, Bei Wu, Ian Witting, Magnus Wagener, Yongkook Park, George Rozgonyi and Roger Clark.* Solid State Phenomena Vols 131-133 (2008) p. 1-8.

2) Reaching Grid Parity Using BP Solar Crystalline Silicon Technology. *John Wohlgemuth, Roger Clark, Jean Posbic and Daniel W. Cunningham.* 33rd IEEE Photovoltaic Specialist Conference, San Diego, May 2008

3) The Effect of Cell Thickness On Module Reliability. *John Wohlgemuth, Daniel W. Cunningham, Neil Placer, George Kelly and Andy M. Nguyen*. 33rd IEEE Photovoltaic Specialist Conference, San Diego, May 2008

4) Using Accelerated Tests and Field Data to Module Reliability and Lifetime. *John Wohlgemuth, Daniel W. Cunningham, D Amin, J Shaner, Z Xia and J Miller*. Proceedings of 23rd European Photovoltaic Solar Energy Conference, Valencia, 2008.

5) Performance Comparison between BP Solar Mono^{2TM} and Traditional Multi-Crystalline Modules. *Daniel W. Cunningham, A. Parr, J. Posbic and W. Poulin.* Proceedings of 23rd European Photovoltaic Solar Energy Conference, Valencia, 2008.

6) Reliability of PV Systems. *John H. Wohlgemuth.* Proceeding of SPIE Conference on Optics & Photonics, Solar Energy + Applications", San Diego, 2008

7) The Leading Edge of Silicon Casting Technology and BP Solar's Mono^2 Wafers. *NG Stoddard, B Wu, L Maisano, R Russell, J Creager, R Clark and JM Fernandez.* 8th Workshop on Crystalline Silicon Solar Cells and Modules, Vail, CO, 2008

8) Reaching Grid Parity Using BP SOLAR Crystalline Silicon Technology. *John Wohlgemuth, Roger Clark, Jean Posbic, James Zahler, Mark Gleaton, Dave Carlson and Daniel W. Cunningham.* IEEE PV Specialist Conference, Philadelphia, June 2009.

9) A Non-solvent Extraction Method for Measuring the Gel Content of Ethylene Vinyl Acetate as PV Encapsulant. *Zhiyong Xia, Daniel W. Cunningham and John Wohlgemuth.* IEEE PV Specialist Conference, Philadelphia, June 2009.

10) Lifetime Prediction of PV Encapsulant and Back sheet via Time Temperature Superposition Principle. *Zhiyong Xia, John H. Wohlgemuth and Daniel W. Cunningham.* IEEE PV Specialist Conference, Philadelphia, June 2009.

11) A Semi-empirical Method of Predicting the Lifetime of EVA Encapsulant and Polyester Based Back sheet Materials. *Zhiyong Xia, John H. Wohlgemuth and Daniel W. Cunningham.* SPIE Solar Energy and Technology Conference, August, 2009.

12) Key Aspects of Module Design that Influence Energy Generation. *Daniel W. Cunningham, Dinesh Amin, A Nguyen, Jay Miller, Zhiyong Xia, and John Wohlgemuth*. Proceedings of 24th European Photovoltaic Solar Energy Conference, Hamburg, 2009

13) A Semi-Empirical Method of Predicting the Lifetime of EVA Encapsulant and Polyester Based Back Sheet Materials. *Z. Xia; J. Wohlgemuth and D W. Cunningham*. SPIE Conference on Module Reliability in August, 2009

14) A New Method for Measuring the Cross-link Density in Ethylene Vinyl Acetate Based Encapsulant. *Z. Xia, D W. Cunningham and J. Wohlgemuth.* PV International Magazine, 5th edition, 2009.